Energinet Eltransmission A/S

Kattegat Offshore Wind Farm

Sea Ice Site Condition Assessment

REPORT

Date: 2024-10-21
Doc. No: 24021-04-03
Revision: 3

C2WIND

Document information and change log

Revision	Date	Status / Reason for Issue	Author	Checker
0	2024-09-10	Issued for internal review	JLW/CFN	LAH
1	2024-09-20	Issued for Client	JLW/CFN	CBM
2	2024-10-14	Revised based on Client’s comments	CFN	JLW
3	2024-10-21	Final version to Client	CFN	JLW

Section	Summary of Changes (latest revision only)

Changes made in the most recent revision, are marked with yellow highlighting. For figures and tables, this means that the first part of the caption, i.e. the word “Figure” or “Table”, has been highlighted.

Table of Contents

List of abbreviations and parameter descriptions

Abbreviations	
AME	Absolute Mean Error
AMOC	Atlantic Meridional Overturning Circulation
BACC	BALTEX Assessment of Climate Change for the Baltic Sea basin
BSPR	Baltic Sea Physics Reanalysis
CC	Correlation Coefficient
CMEMS	Copernicus Marine Environment Monitoring Service
COD	Commercial Operation Date
COV	Coefficient of Variation
DJF	December-January-February
DLC	Design Load Case
DMI	Danish Meteorological Institute
DVR90	Dansk Vertikal Reference 1990 (Danish Vertical Reference 1990)
EE	Energinet Eltransmission A/S
ELIE	Extreme Level Ice Event
EVA	Extreme Value Analysis
EWS	Early Warning Signals
FEED	Front-End Engineering Design
FLS	Fatigue Limit State
IPCC	Intergovernmental Panel on Climate Change
ibid.	From Latin ibidem (“in the same place”), it is used to save space in textual references to a quoted work that has been mentioned in a previous reference
ILA	Integrated Load Analysis
KG	Kattegat
MSL	Mean Sea Level
NC	Non-compliant
OWF	Offshore Wind Farm
ppm	Parts per million
ppt	Parts per thousand
QQ	Quantile-Quantile
RCP	Representative Concentration Pathways
RMSE	Root Mean Squarre Error
SSP	Shared Socioeconomic Pathways
SST	Sea Surface Temperature
SMHI	Sveriges Meteorologiska och Hydrologiska Institut
SWL	Still Water Level
ULS	Ultimate Limit State
WTG	Wind Turbine Generator

Latin parameters	
A	Weibull scale parameter
C_c	Current drag coefficient
C_R	Crushing ice strength coefficient
$C_\mathrm{R,1,NC}$	1-year crushing ice strength coefficient for noncompliant support structures
$C_\mathrm{R,50,NC}$	50-year crushing ice strength coefficient for noncompliant support structures
$C_\mathrm{R,1,C}$	1-year crushing ice strength coefficient for compliant support structures
$C_\mathrm{R,A,NC}$	Average ice strength coefficient for noncompliant support structures
CS_surface	Surface current speed
C_w	Wind drag coefficient
D	Diameter at ice action elevation
D_bin	Days in the h_bin bin
$D_\mathrm{bin,lifetime}$	Days of occurrence for each ice thickness bin in the lifetime of the wind farm

$D_{\mathrm{int},0-15}$	Days of ice thickness interval, for interval [0-15[cm
$D_{\mathrm{int},15-30}$	Days of ice thickness interval, for interval [15-30[cm
$D_{\mathrm{int},30-50}$	Days of ice thickness interval, for interval [30-50] cm
D_{int}	Days of thickness interval
E_{f}	Young's modulus of the ice sheet
$\vec{F}_{\mathrm{c}}$	Vector of the drag force on the ice, caused by current, per unit horizontal area, acting horizontally on the ice
$\vec{F}_{\mathrm{drag}}$	Vector of the drag force on the ice, per unit horizontal area, acting horizontally on the ice
F_{G}	Global ice force
$\vec{F}_{\mathrm{w}}$	Vector of the drag force on the ice, caused by wind, per unit horizontal area, acting horizontally on the ice
H_{k}	Keel depth
H_{s}	Sail height
L_{design}	Design lifetime of the wind farm
L_{f}	Latent heat of melting for ice
N	Number of points
$\overrightarrow{PL}$	Pack ice force vector
P_{G}	Global ice pressure
$R_{c,50}$	50-year consolidated layer thickness ratio to sheet ice thickness
S_{f}	Cumulative freezing degree days
T_a	Air temperature
T_{f}	Freezing temperature of saline water
$T_{\mathrm{f,lim}}$	Upper SST limit for thermal ice growth
T_{w}	Sea surface temperature
T_{year}	Total number of days with mobile ice per year
U_i	Ice speed
$U_{\mathrm{i,mean}}$	Mean ice drift velocity of mobile ice
$\vec{U}_{\mathrm{c}}$	Current speed vector
$\vec{U}_{\mathrm{W}}$	Wind speed vector
V	Vertical force from sea ice
V_{b}	Ice bending vertical force
V_{τ}	Adhesive vertical force
c	Apparent keel cohesion
e	Porosity of ice rubble
f_{AR}	Empirical term for ice pressure
g	Acceleration of gravity
h	Sheet ice thickness
h_{50}	50-year sheet ice thickness
h_{bin}	Ice thickness bin
$h_{\mathrm{c},50}$	50-year consolidated layer thickness
h_{c}	Consolidated layer thickness
$h_{\mathrm{c,max}}$	Maximum consolidated layer thickness
h_{max}	Maximum sheet ice thickness
h_{Hub}	Hub height
h_{k}	Distance between the base of the consolidated layer bottom and the base of the keel
h_{max}	Maximum ice thickness in winter
h_1	Reference thickness
k	Weibull shape parameter
m	Empirical exponent
n	A number which depends on the ice thickness
t	Time
w	Projected width of the support structure

Δz	SWL range for ULS DLCs
Greek parameters	
θ_{ice}	Ice direction (coming from direction)
θ_{w}	Wind direction (coming from direction)
ρ_{ice}	Density of ice
ρ_{w}	Density of water
ρ_a	Density of air
σ_{f}	Flexural strength of the ice sheet
β	Thermal conductivity factor
κ	Thermal conductivity of ice
τ	Adhesive strength
ϕ	Angle of internal friction
ν	Poisson’s ratio for ice sheet
μ_{ic}	Coefficient of kinetic friction, ice-concrete
μ_{ii}	Coefficient of kinetic friction, ice-ice

Executive summary

The present section contains a summary of the sea ice-related site conditions, including references to where in the present report the information is taken from.

Sea ice parameters		Reference
50-year sheet ice thickness, h_{50}.	h_{50} = 38 cm	Section 6.3
1-year ice (crushing) strength coefficient for non-compliant structures and/or large relative velocity between support structure and ice, $C_{\mathrm{R,1,NC}}$.	$C_{\mathrm{R,1,NC}}$ = 0.99 MPa	Section 8.1
1-year ice (crushing) strength coefficient for compliant structures and/or small relative velocity between support structure and ice, $C_{\mathrm{R,1,C}}$.	$C_{\mathrm{R,1,C}}$: Not established. To be determined as a part of an Integrated Load Analysis.	Further detailed in Section 8.1
50-year ice (crushing) strength coefficient for non-compliant structures and/or large relative velocity between support structure and ice, $C_{\mathrm{R,50,NC}}$.	$C_{\mathrm{R,50,NC}}$: Not established.	See footnote [1]
Average ice (crushing) strength coefficient for non-compliant structures and the large relative velocity between support structure and ice, $C_{\mathrm{R,A,NC}}$.	$C_{\mathrm{R,A,NC}}$ = 0.65 MPa	Section 8.2
50-year design ice ridge geometry.	Table 7-1	Section 7
Ice velocity.	Table 11-1	Sections 11.1 and 11.2
Sheet ice thickness distribution.	Table 6-6	Section 6.4
Wind-ice drift directional misalignment and occurrence frequencies.	Table 10-2	Section 10
Mobile ice duration.	100 % of observed days	Section 6.4.1
Parameters for flexural failure.	Table 9-1	Section 9
Wind-ice drift coming directional misalignment values, and their combination with hub height wind speeds, with wind directions, with ice action speeds, and the durations of these combinations.	See the text in bold in Section 11.3	Section 11.3
Wind-ice drift coming directional misalignment values, and their combination with hub height wind speeds, and with ice action speeds.	See the text in bold in Section 11.4	Section 11.4

---

[1] The 50-year ice crushing strength is only to be used if the 1-year ice thickness is greater than 0 according to [ISO19906], which is not the case for the evaluated site.

1. Introduction

Energinet Eltransmission A/S (EE, or "the Client") has appointed C2Wind ApS (C2Wind) to carry out Site Ice Conditions Assessment for the Kattegat Offshore Wind Farm (KG) project, located in Kattegat. The purpose of this document is to serve as documentation of the sea ice conditions to be used as front-end engineering design (FEED) of Wind Turbine Generators (WTGs) including the substructure and foundation. It contains sea ice parameters for support structures with or without, an ice cone. In contrast, it does not deal with input to the design of potential Offshore Substation(s) and cables.

In general, this report cannot be used as a basis for the design of an offshore substation or cable design. This is mainly due to the derived parameters in this report which target the design load cases for WTGs. However, some parameters can still be used for the design of other structures than WTGs.

The design sea ice conditions at the site are established based on:

- Observations of sea ice- and navigational conditions, are summarised in Appendix A.
- Air- and sea surface temperatures (SST) from measurements or model data.
- Hindcast model data for the site in [HCWWDATA] and [HCCUDATA].
- Wind statistics data from [WA], which also forms input to the SCA for the site.
- National and international standards.
- Journal papers, reports, and other publicly available sources.

The data sources used to determine the sea ice conditions are described in more detail in Section 4.

1.1 Geographical location

The KG area for investigation is located to the east of the city of Grenå in Jutland, Denmark, see Figure 1-1.

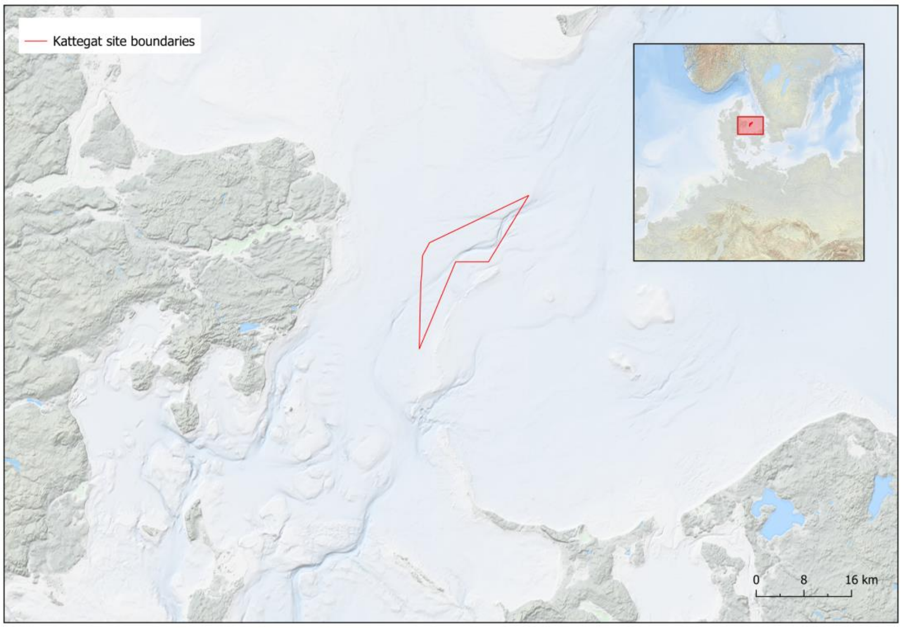

Figure 1-1: Overview of the KG site.

2. General considerations

2.1 Vertical reference

All elevations specified in this report are in the DVR90 elevation system unless otherwise noted. 0 mDVR90 is taken as being equal to 0 mMSL. Nevertheless, this simplification does not introduce a significant bias as the applicable vertical reference, DVR90, is approximately equal to MSL at the site.

2.2 Assumed hub height

In accordance with the caption text of Table 1 of [WA], the WTG hub height is assumed to be:

h_{Hub} = 150.0 mDVR90.

Where relevant, atmospheric parameters have been extrapolated to this elevation.

The results in the present report are assessed to be applicable without change for a hub height interval of ± 5 m about h_{Hub} stated immediately above.

2.3 Conventions

Unless noted otherwise, the following conventions are used throughout the report.

- Elevations are given as distances above DVR90 in metres (mDVR90).
- Directions are relative to North (0°) with clockwise direction as positive when seen from above (e.g. East is 90°),
  - Wind: °N coming from.
  - Current: °N going towards.
  - Ice drift coming: °N coming from.
  - Directional bins of 30°: See Table 2-1.

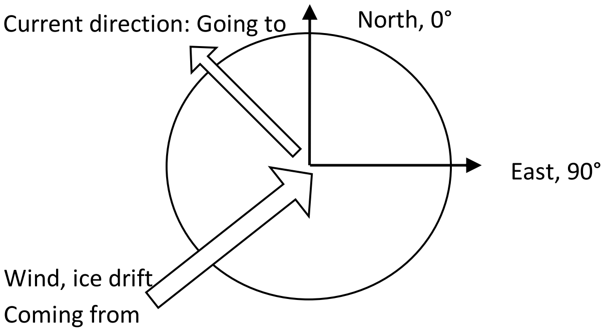

Figure 2-1: Compass directions and directional convention.

Directional bin centre	Directional bin interval
[°N]	[°N]
0	$345 \leq \theta < 15$
30	$15 \leq \theta < 45$
60	$45 \leq \theta < 75$
90	$75 \leq \theta < 105$
120	$105 \leq \theta < 135$
150	$135 \leq \theta < 165$
180	$165 \leq \theta < 195$
210	$195 \leq \theta < 225$
240	$225 \leq \theta < 255$
270	$255 \leq \theta < 285$
300	$285 \leq \theta < 315$
330	$315 \leq \theta < 345$

Table 2-1: Directional bin definitions.

Density (scatter) plots throughout this report will show normalised densities according to the colour bar in Figure 2-2, where the normalisation is so that the maximum point density in each figure is unity.

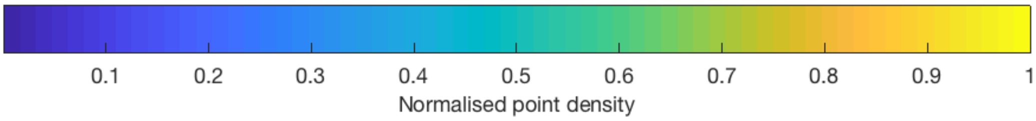

Figure 2-2: Colour bar showing the density of points in density (scatter) plots throughout the present report. Please note that the scatter point densities are normalised so that the maximum density is unity.

Intervals of numbers are denoted according to Item 2-7.7 of [ISO800002] for closed intervals, and the optional notation of Items 2-7.8 through 2-7.10 of ibid. for half-open and open intervals[2]. For example, the interval from 0 to 1 is denoted:

- [0;1] if both endpoints are included in the interval.
- [0;1[if 0 is included in the interval, but 1 is not.
-]0;1] if 0 is not included in the interval, but 1 is.
-]0;1[if neither end point is included in the interval.

2.4 Terms and definitions

Throughout this report, some key terms are used and are defined in the following list:

- **Danish Sea ice code:** The sea ice registration method before 1983 when the method was switched to the Baltic Sea ice code.

- **Baltic Sea ice code:** General sea ice registration method used by several countries around the Baltic Sea. Adopted by Denmark in 1983.

---

[2] That is, the notation used for intervals of numbers is the second option here: https://en.wikipedia.org/wiki/Interval_(mathematics)#Including_or_excluding_endpoints, using semicolon as separator of endpoints as allowed by: https://en.wikipedia.org/wiki/Interval_(mathematics)#Notations_for_intervals.

- **Competent ice:** Sea ice types that are competent of inducing non-negligible loads to the support structure and furthermore have not been rafted, compacted, or broken up and then refrozen. This is further explained in Section 5.1.3.

- **Ice winter**: Winter with at least 1 day of competent ice.

- **Mobile sea ice:** Sea ice that is movable (e.g. not frozen in place).

- **Immobile sea ice:** Sea ice that is not movable (e.g. frozen in place).

- **Ice-induced vibrations:** In the present report, no clear distinction of the individual phenomena potentially leading to ice-induced vibrations is made; all are simply referred to as ice-induced vibrations as long as they can induce significant dynamic ice load effects on the WTG support structures.

- **Compliant structures:** Structures that will deform significantly during ice interaction meaning that the relative velocity between the structure and the sea ice is reduced.

- **Non-compliant structures:** Structures that will deform slightly during ice interaction meaning that the relative velocity between the structure and the sea ice is almost equal to the ice drift velocity.

3. Applied standards and guidelines

The present document is made in accordance with the following design standards and guidelines:

[IEC6131]	IEC 61400-3-1 Ed. 1: Wind energy generation systems - Part 3-1: Design requirements for fixed offshore wind turbines, (2019-04-05).
[ISO19906]	ISO 19906:2019(E): Petroleum and natural gas industries - Arctic offshore structures, (2019).
[DNV0437]	DNV-ST-0437 - Loads and site conditions for wind turbines, (Edition May 2024).

In case of discrepancy between the standards and guidelines above, the hierarchy of standards and guidelines is so that documents high on the list overrule documents lower on the list.

3.1 Design load cases

Following the standards and guidelines outlined above, the Design Load Cases (DLCs) where sea ice inputs are relevant are outlined in Table 3-1. Two sets of DLCs are shown:

- D3 to D8 are references to the DLCs outlined in Table 3 of [IEC6131].
- SeIc.1 to SeIc.6 are references to the DLCs outlined in Table 9-3 of [DNV0437].

The individual DLCs from [IEC6131] and [DNV0437] are in Table 3-1 shown in two different rows. Where a DLC is shown from both sources, the inputs to the DLC are the same. For example, DLC D3 equals DLC SeIc.1.

According to the hierarchical order of the standards, the DLCs to consider in the design of the WTG support structure are those from [IEC6131] since this is the governing standard in Denmark according to [BEK1773] and its normative requirements. This means that the DLCs from [DNV0437] are optional but not a requirement to obtain a certification according to [IECRE502]. The reason for including the [DNV0437] DLCs in Table 3-1 as well, is that the required inputs to the DLCs in [DNV0437] have a higher level of detail outlined compared to the inputs to the DLCs from [IEC6131] that require additional interpretation.

It must be noted that from [IEC6131] no DLC corresponds to the [DNV0437] SeIc.3 DLC is found. The SeIc.3 DLC is a DLC which combines power production with an ice ridge event. Since the WTG is expected to be in the power production condition far more often than the parked condition, the probability of an event with power production combined with the loads from an ice ridge is higher than the probability of an ice ridge exposure combined with parked WTG condition as covered by DLC D6/SeIc.6. Therefore, it is the recommendation from C2Wind that DLC SeIc.3 is included in the load basis for design of the WTG support structure. Due to this, necessary sea-ice inputs to SeIc.3 are included in this report.

The reason for not including DLC D1 and D2 in Table 3-1 is that they require no environmental inputs. In addition, it is argued in Sections 12.1 and 12.2 that these DLCs are negligible.

Please be aware that the ice crushing strength coefficient, C_{R}, is only necessary for vertical structural geometry in the ice-structure interaction zone (no ice-cone) and the flexural failure mode parameters are only necessary for sloping structural geometry in the ice-structure interaction zone (with ice-cone). All other parameters are independent of the ice-structure interaction geometry.

Sea ice parameter	Reference	D3	D4	D5	D6	-	D7	D8
		Selc.1	Selc.2	-	Selc.6	Selc.3	Selc.5	Selc.4
50-year sheet ice thickness, h_{50}	Section 6.3	x		x				x
1-year ice crushing strength coefficient, $C_{\mathrm{R,1}}$	Section 8.1	x						x
Average ice crushing strength coefficient, $C_{\mathrm{R,A}}$	Section 8.2		x		x	x	x	
50-year ice ridge geometry	Section 7				x	x		
Ice velocity	Sections 11.1 and 11.2	x	x				x	x
Sheet ice thickness distribution	Section 6.4		x				x	
Wind-ice drift directional misalignment and occurrence frequencies	Section 10		x				x	
Mobile ice duration	Section 6.4.1		x				x	
Flexural failure mode parameters	Section 9	x	x	x	x	x	x	x

Table 3-1: Overview of primary sea ice related parameters necessary for each DLC. The DLCs denoted D3 to D8 are according to Table 3 of [IEC6131] whereas the DLCs denoted Selc.1 to Selc.6 are according to Table 9-3 of [DNV0437].

4. Overview of data sources

In order to obtain the necessary environmental parameters outlined in Table 3-1, a range of different data sources are used. The data sources are a mixture of e.g. historical sea ice observations, historical temperature measurements, and hindcast model data. The sea ice observations are primarily recordings of the number of days where a specific type of sea ice has been observed at stations across Denmark hosted by the Danish authority Istjenesten. The historical temperature measurements are either air- or sea surface temperatures (SSTs), where the air temperatures are from DMI, and the SSTs are from various sources. The primary environmental data applied to determine each sea ice parameter is outlined in the overview of Table 4-1.

Sea ice parameter	Sea ice observations	Air temperature	Sea surface temperature	Salinity	Current	Wind
50-year sheet ice thickness, h_{50}	x	x	x	x		
1-year ice crushing strength coefficient, $C_{\mathrm{R},1}$	x					
Average ice crushing strength coefficient, $C_{\mathrm{R,A}}$						
50-year ice ridge geometry	x	x	x	x		
Ice velocity					x	x
Sheet ice thickness distribution	x					
Wind-ice drift directional misalignment and occurrence frequencies					x	x
Mobile ice duration					x	x
Flexural failure mode parameters						

Table 4-1: Overview of primary data types used as input to calculate and justify the sea ice parameters. The empty rows denote sea ice parameters which are independent of site-specific environmental inputs.

The source of each of the environmental datasets applied in the present study is summarised in Table 4-2.

Primary data type	Detailed description	Reference
Sea ice observations	Section 4.1	[ISBES], [SMHIAT]
Air temperature	Section 4.2	[DMIMET]
Sea surface temperatures	Section 4.3	[DMIOCE], [SMHIOCE], [SPARRE], [MADSEN], [CMEMS]
Salinity	Section 4.4	[CMEMS]
Current	Section 4.5	[HCCUDATA]
Wind		[HCWWDATA]

Table 4-2: Brief overview of the sources used in the present report. Further elaborations on the data are provided in the outlined sections.

The locations of the meteorological-, oceanographic-, and sea ice observation stations from which historical data records are collected for use in the present study, are shown in Figure 4-1.

In addition to a detailed description of each data source, the availability of each individual data source, for the winters selected for detailed analysis in this report, is outlined in Section 4.6.

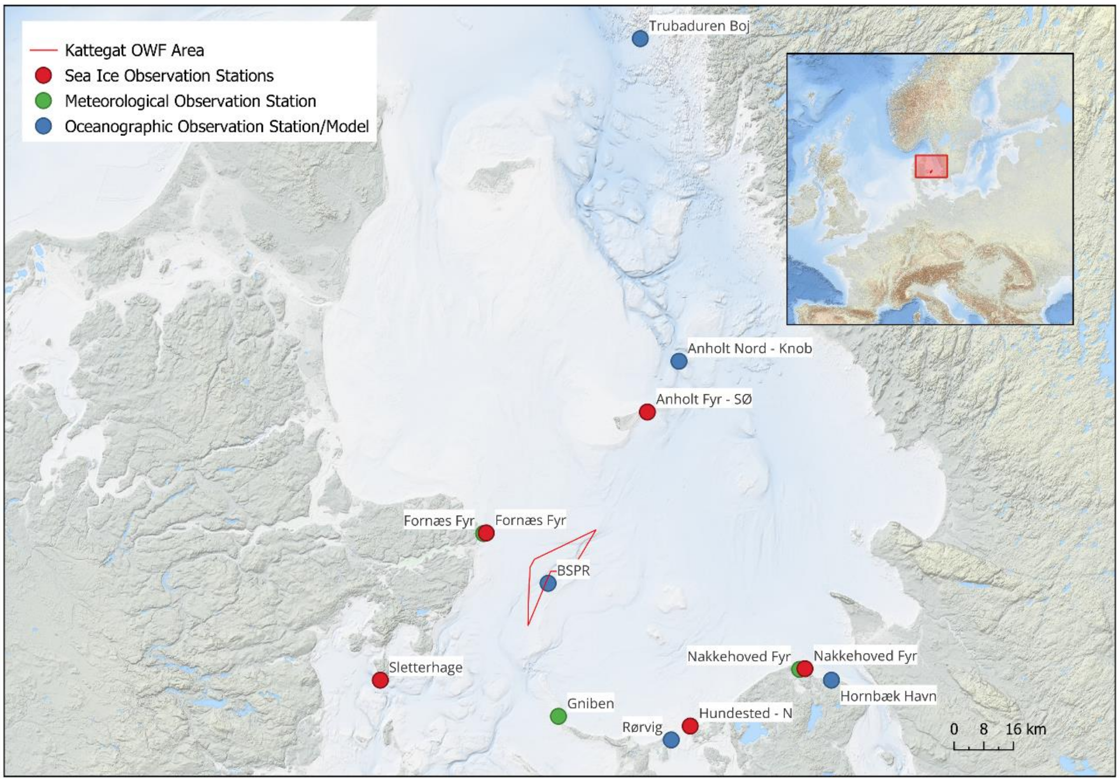

Figure 4-1: Overview of the location and type of the primary data sources used for the sea ice assessment. Included are: The location of the sea ice observation stations, the meteorological stations measuring the air temperature, and the oceanographic stations or models providing the sea surface temperature (SST) and salinity.

4.1 Sea ice observations

The sea ice observations are taken from [ISBES] supplemented with ice atlases from [SMHIAT] where the observation stations shown in Figure 4-2 are chosen as representatives for the KG site. An overview of the sea ice observations from the stations is shown in Appendix A where a brief introduction to the data is outlined as well. The sea ice observations provide key inputs to define the start- and end dates of the winter period in which the sea ice is modelled using the thermal ice growth model.

Figure 4-2: Overview of the sea ice observation stations from [ISBES] that are chosen to be representative of the KG site.

4.2 Air temperature

The air temperature, T_a, is another primary input needed for the thermal ice growth model. Historical recordings of the air temperature are available in the datasets provided through the open-data service of [DMIMET] for several observation stations; these are referred to as DMI stations in the following. The closest observation station to the KG site is '*Fornæs Fyr'* which is located approximately 20 km East of the KG site as seen in Figure 4-3. It is noted, that the measuring of air temperature at '*Fornæs Fyr'* was discontinued the 1st of January 2000, why the air temperature measurements after this date are from the '*Gniben'* meteorological observation station, located approximately 30 km South of the evaluated site (see Figure 4-3). The historical availability of the air temperature data is discussed in Section 4.6. The air temperature measurements from the aforementioned DMI stations are assessed to be representative of the air temperature at the evaluated KG site since both are located within proximity to the site and mostly surrounded by seawater. The '*Nakkehoved Fyr'* meteorological observation station is used for the air temperature validation performed in Section 5.2 and thus depicted in Figure 4-1 and Figure 4-3 as well.

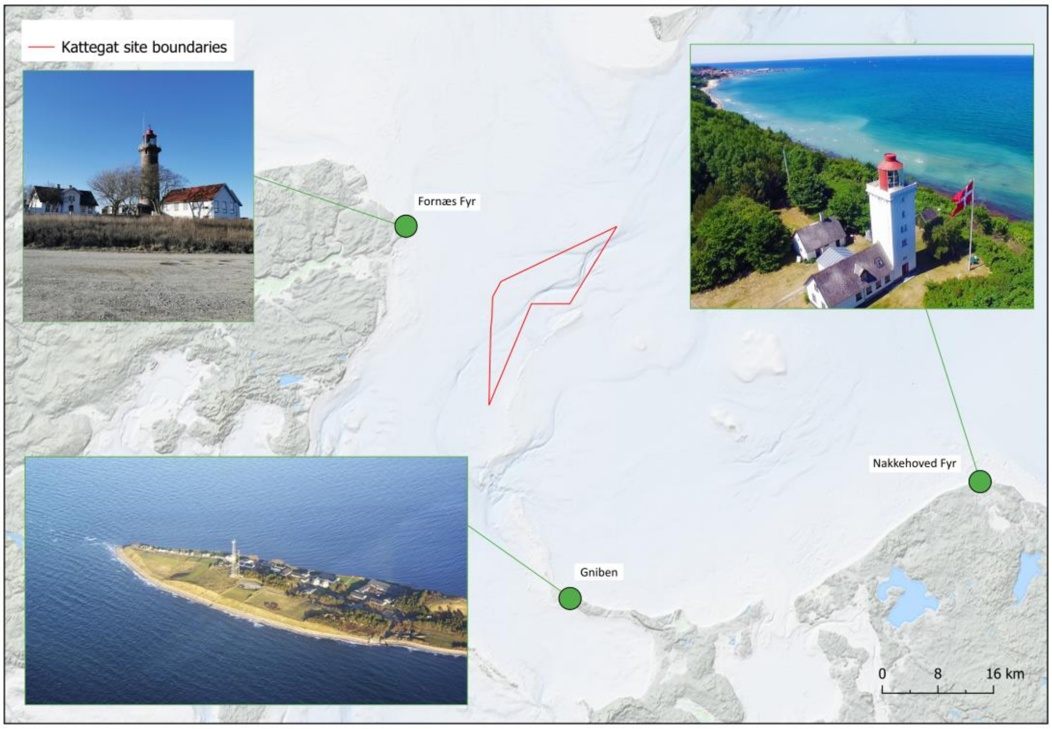

Figure 4-3: Overview of the meteorological observation stations from which datasets are extracted from [DMIMET] and applied as input to the thermal ice growth model.

4.3 Sea surface temperature

In the thermal ice growth model, the sea surface temperature (SST), T_w, is used to limit the timestamps where the ice can thermally grow. Historical measurements of the SST with sufficiently high quality are scarce. However, recordings of the SST are available in the datasets of [DMIOCE] and [SMHIOCE] for the '*Hornbæk Havn*' and *'Trubaduren Boj'* respectively, see Figure 4-1. In addition, SST measurements from the '*Anholt Nord – Knob'* lightship are available for the early winters, cf. [MADSEN] and [SPARRE]. The historical availability of the SST data is discussed in Section 4.6.

The SST measurements from '*Hornbæk Havn'* are applied to the winters of 2009/2010 and 2010/2011, whereas the SST measurements from '*Trubaduren Boj'* are used for the winters of 1978/1979 and 1984/1985. The measurements from the '*Anholt Nord – Knob'* lightship are used for the evaluation of the winters 1962/1963, 1965/1966, 1969/1970, and 1981/1982. Note however, that the SST data from the '*Anholt Nord – Knob'* lightship in the aforementioned winters is limited due to the common practice of retracting lightships to their harbours for periods of present sea ice, applied at the time. The validity of the SST measurements for use in the thermal ice growth model is examined in detail in Section 5.3 where the modelled SST data from the Baltic Sea Physics Reanalysis (BSPR) product of [CMEMS] is used to assess if the various SST measurements are applicable at the site.

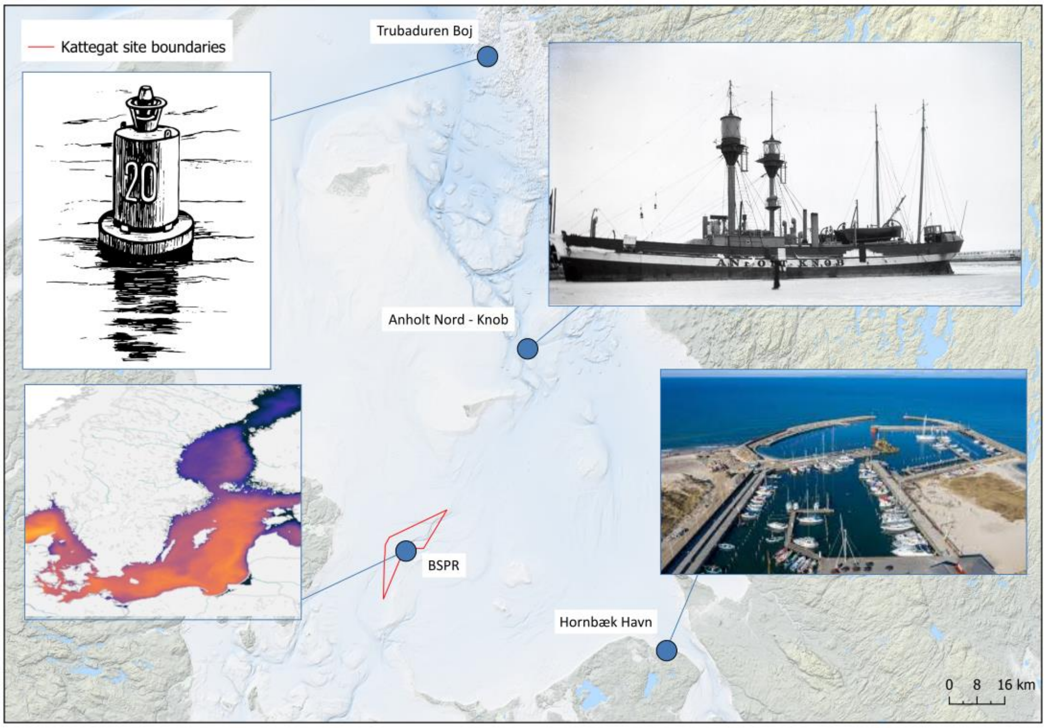

Figure 4-4: Overview of the oceanographic observation stations from which datasets are extracted from [DMIOCE], [SPARRE], and [MADSEN]. The SST has also been extracted from the Baltic Sea Physics Reanalysis model (BSPR) in [CMEMS] where the location of the extraction point is shown in the figure as well. All SST measurements are applied as input to the thermal ice growth model.

4.4 Salinity and freezing temperature

The thermal ice growth model is highly dependent on the freezing temperature of the saline water, T_f. The freezing temperature of the saline water will however vary based on the salinity of the sea water. In the inner Danish waters, the salinity of the seawater varies with the eastbound inflow of saline water from the North Sea and the westbound outflow of less saline water from the Baltic Sea. As this flow is to some extent affected by the changing seasons, the freezing temperature for the saline water is determined by the use of data from the winter periods only. The salinity at the KG site is available in the hindcast data of [HCCUDATA]. However, this data suggests a salinity level significantly higher than other sources, which for the purpose of establishing the freezing temperature for saline water, will be non-conservative. Instead, the modelled salinity included in the dataset of [CMEMS] is used. The modelled salinity between 2006 and 2016 from this dataset is depicted in Figure 4-5.

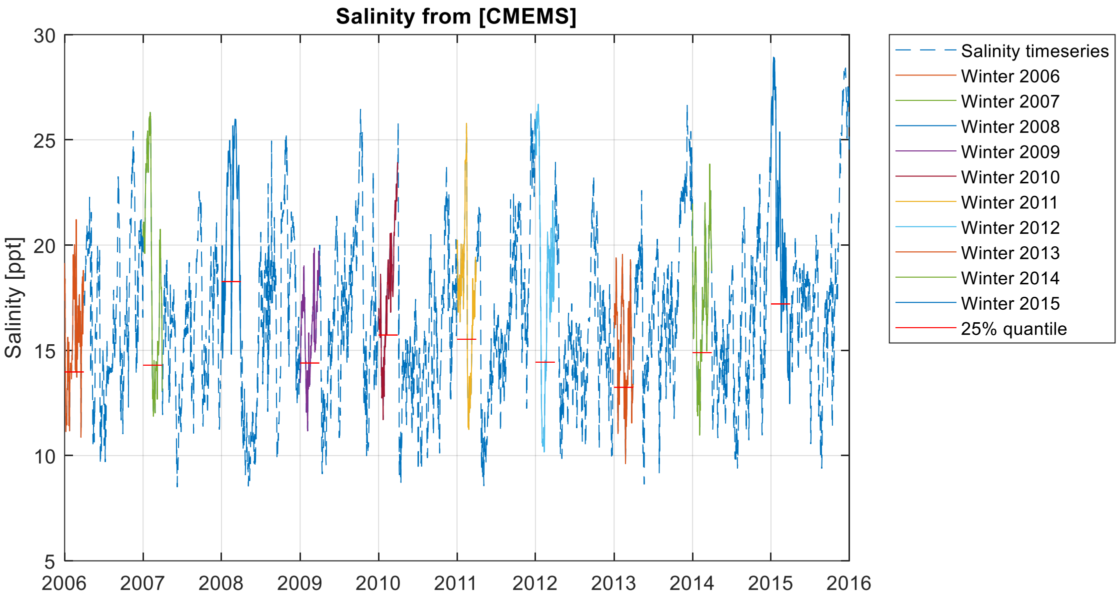

Figure 4-5: Salinity of the KG site from the modelled dataset of [CMEMS]. The individual winters from January to March are marked by unique colours. The 25% lower quantile of the modelled salinity is marked with a horizontal red line for each winter. As a conservative measure, the salinity level of 14 ppt is selected for use in the thermal ice growth model.

By the use of Eq. D.1 in [IEC6131], the freezing temperature of the saline water of the KG site is determined to T_f = -0.76°C. The upper SST limit for when the ice can thermally grow, $T_\mathrm{f,lim}$, is chosen by adding +0.5°C to T_f resulting in a value of -0.26°C. This is done as a conservative choice to account for measuring accuracy. This means that any potential ice growth for timestamps where $T_w > T_\mathrm{f,lim}$ is disregarded for all winters.

4.5 Hindcast dataset

The wind- and current data is used to determine the wind-ice drift directional misalignment, the ice drift velocity, and the duration of mobile sea ice as indicated in Table 4-1. These datasets are available in the hindcast datasets provided by the Client found in [HCWWDATA] and [HCCUDATA]. Individual hindcast datasets are available for each of the three reference locations of KG depicted in Figure 4-6, which is a partial reproduction of Figure 3-1 from [MA]. The hindcast data is examined in more detail in Section 5.5.

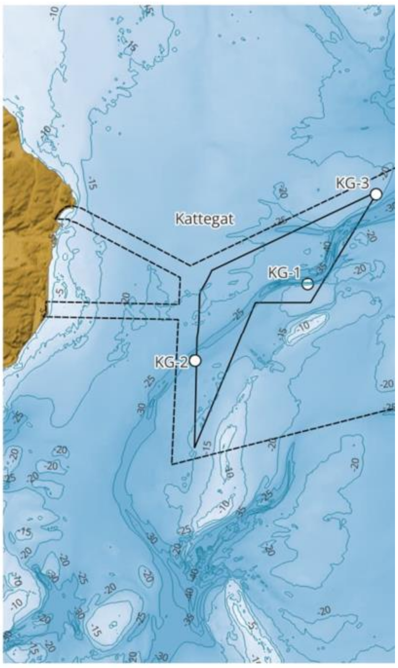

Figure 4-6: Overview of the reference locations for the metocean hindcast timeseries for KG. Partial reproduction of Figure 3-1 from [MA].

4.6 Data availability for evaluated winters

Some of the datasets used as inputs in the present report have demonstrated both longer periods of unavailability as well as invalid data. The availability of the various data sources used is depicted in Figure 4-7.

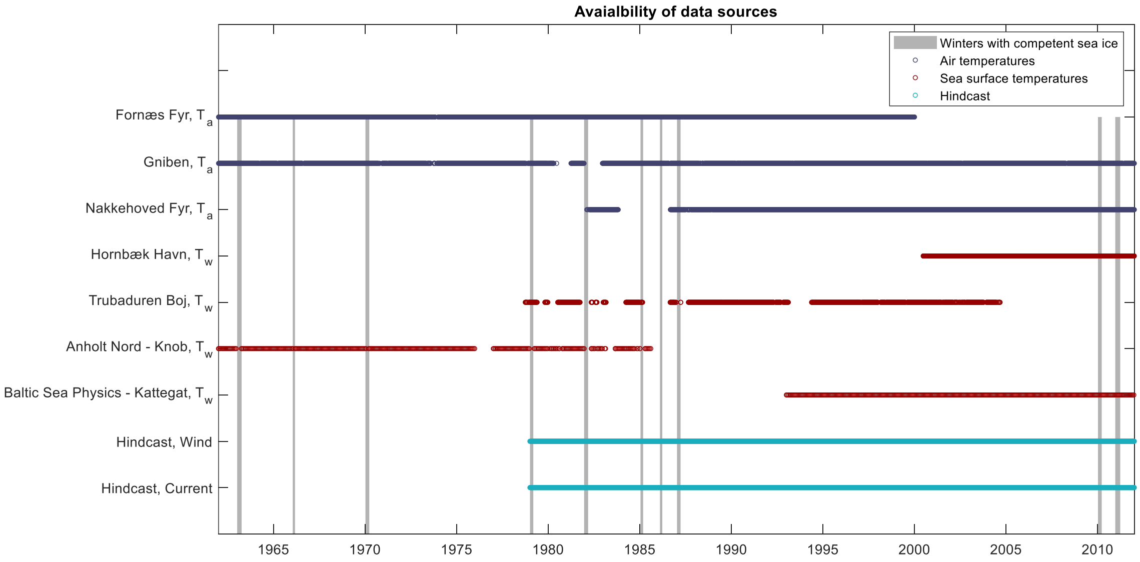

Figure 4-7: Overview of the availability of the various data sources used in the present evaluation. Air temperature availability from meteorological observation stations is marked with a blue colour scheme and T_a is appended to the station name. The avaibility of SST from oceanographic observation stations, including the BSPR model is marked with a red colour scheme and T_w is appended to the station name. The availability of the hindcast timeseries is shown as well. Winter periods used for the present evaluation are indicated by the vertical grey areas.

The data sources depicted in Figure 4-7 include both air temperature- and SST datasets. The prioritization of the datasets is indicated in the figure as the top station for either air-or SST data is the preferred station, the second station from the top is the second prioritization, etc. From Figure 4-7 it is noted that the winters of 1985/1986 and 1986/1987 are not covered by available SST measurements. The validity of the various datasets is examined in more detail in Section 5.2 and Section 5.3 before these are used as inputs to the thermal ice growth model.

5. Pre-processing of input data and review of data quality

Before the data presented in Section 4 is used to describe the sea ice condition at the KG site, pre-processing of the individual data types is performed. If possible and relevant, this includes a verification of the datasets. Each of the subsections presented below will be used in the sea ice calculations in this report.

5.1 Sea ice observations

Fundamentally, the sea ice observations from [ISBES] represent somewhat subjective historical records of the sea ice conditions at a given observation location for a specific winter. As for most records relying on human observations, some variance in the interpretation of the conditions is to be expected between the different observers. Thus, multiple sea ice observation stations are included in the study to reduce the risk of using erroneous recordings of sea ice conditions. This use of historical records from multiple observation stations requires a detailed preprocessing of the data before it can be applied as input to the analysis performed in this report. The outcome of the data pre-processing can be interpreted as site-specific processed ice observations based on the historical recordings across multiple sea ice observation stations. The various methodologies applied to populate categories of the site-specific ice observations are discussed individually below.

5.1.1 Selection of first and last ice observation date

As an input to the thermal ice growth model, the first- and last date with observed ice is needed as an input. The conservative approach of using the maximum envelope between the selected observation stations is applied. Further conservatism is included by adding 1 additional day to the last day with observed ice. By use of the first and last day envelope, the total number of observation days within this period is derived. Note that the observation period covers a full winter from the first- to the last date with observed ice, i.e., days without ice can occur in the observation period, see Section 5.1.2.

For specific winters, ice atlases are used to correct the first- and last ice observation date to reduce the level of conservatism of the calculated sheet ice thickness. This is done for the winters of 1984/1985, 1985/1986, and 1986/1987 as shown in Table 5-1. The reason for using the ice atlases for these years is to limit conservatism in the thermal ice growth model since sparse, or none, information on SSTs for these years is available. It is noted that the first date of observed sea ice, from the ice atlases, is conservatively selected as the date of the last recording of ice-free waters before sea ice is present at the site. The last date of observed sea ice, from the ice atlases, is conservatively selected as the date of the first recording of ice-free waters following the last recording of sea ice at the site. The sea ice atlases for the affected winters in the present evaluation are found in Appendix D.

Winter with ice	First ice observation day		Last ice observation day		Days in the ice observation period
[year range]	Date	Station	Date	Station	[days]
1962 to 1963	07/Jan/1963	Anholt Fyr	06/Apr/1963	Nakkehoved Fyr	89
1965 to 1966	19/Jan/1966	Fornæs Fyr	06/Mar/1966	Sletterhage	46
1969 to 1970	08/Jan/1970	Hundested	26/Mar/1970	Nakkehoved Fyr	77
1978 to 1979	03/Jan/1979	Fornæs Fyr	10/Mar/1979	Hundested	66
1981 to 1982	17/Dec/1981	Hundested	07/Mar/1982	Hundested	80
1984 to 1985	14/Jan/1985	SMHI ice atlas	08/Mar/1985	SMHI ice atlas	53
1985 to 1986	06/Feb/1986	SMHI ice atlas	20/Mar/1986	SMHI ice atlas	43
1986 to 1987	12/Jan/1987	SMHI ice atlas	23/Mar/1987	SMHI ice atlas	71
2009 to 2010	06/Jan/2010	Hundested	22/Mar/2010	Anholt Fyr	75
2010 to 2011	17/Dec/2010	Hundested	26/Mar/2011	Hundested	99

Table 5-1: Summation of all evaluated ice winters from 1960 to 2023 including first- and last ice observation date, and the total number of days in the observation period. The SMHI ice atlas can be found in Appendix D.

5.1.2 Number of days with observed ice

Prior to the winter of 1983, ice observations were recorded by use of the Danish Sea ice code. After 1983, the ice observation methodology was changed to follow the more detailed Baltic Sea ice code. As a result, winters before and after 1983 must be handled slightly differently in the pre-processing.

Before 1983, the number of days with ice is found as the sum of days of all categories for every winter. For the winter years after 1983, when the Baltic Sea ice code was implemented, the number of days with ice can be determined from any of the '*A*', '*S*', '*T*' or '*K*' categories since the number of days in each category shall match. When the number of ice days has been determined for all observation stations, the maximum envelope is chosen to represent the number of ice days at the KG site.

Winter with ice	Maximum envelope station	Days with observed ice	Days in the ice observation period
[year range]	[-]	[days]	[days]
1962 to 1963	Sletterhage	79	89
1965 to 1966	Sletterhage	28	46
1969 to 1970	Anholt Fyr	36	77
1978 to 1979	Sletterhage	45	66
1981 to 1982	Nakkehoved Fyr	45	80
1984 to 1985	Nakkehoved Fyr	53	53
1985 to 1986	Sletterhage	43	43
1986 to 1987	Hundested	71	71
2009 to 2010	Hundested	37	75
2010 to 2011	Hundested	92	99

Table 5-2: Summation of days with ice for the ice winters. The days in the observation period from Section 5.1.1 are shown as well to highlight that the days with observed ice are always less, or equal, to the days in the observation period.

5.1.3 Number of days with competent ice

The number of days with competent ice is used primarily to determine which winters to consider in the calculation of sea ice condition parameters for the KG site. To establish the days with competent ice, the ice types defining the competence of the ice must be settled. Since the observation recording methodology changed in 1983, the ice type categories treated as competent ice also changed. The categories defined as competent sea ice before 1983 are outlined in Table 5-3. The number of days with competent ice for a given winter for a single observation station is the sum of the days for the competent ice categories. The methodology for finding the number of days with competent ice before 1983, for a given winter for the KG site, is outlined below:

1. Determine the number of days with competent ice for each selected observation station by calculating the sum of the days for the competent ice categories.
2. Calculate the mean number of competent ice days across all observation stations.
3. Find the observation station with the number of competent ice closest to the mean value determined in Step 2.
4. When the observation station is found in Step 3, the number of days with competent ice is chosen from that observation station.

By following the method outlined above, all chosen observation stations are taken into account, and the resulting number of days with competent ice represents the ice observations from an actual observation station. The reason for not applying a maximum envelope approach is that some winters would end up having more days with competent ice than the number of days in the ice observation period outlined in Section 5.1.1, which would simply be incorrect. Therefore, the “average” approach is applied as outlined above.

Ice category	1	2	3	4	5	6	7	8	9
Ice types	Nyis	Svag landfast is	Spredt drivis	Sammenstuvet grødis	Svær landfast is	Tæt drivis	Sammenhæng-ende isfelter	Sammenstuvet is, pakis eller felter med svær is	Åben rende
Competent ice					x	x	x	x	x

Table 5-3: Categories before 1983 (Only available in Danish) where the chosen competent ice categories are highlighted.

After 1983, the observation recording methodology changed to the Baltic Sea ice code. The ‘*A*’, ‘*S*’ and ’*T*’ categories of the Baltic Sea ice code correspond to the ‘*Amount and arrangement of sea ice*’, the ‘*Stage of ice development*’, and ‘*The topography or form of ice*’ respectively. Each category contains the subcategories *0, 1, 2 … 9, X*, identifying a specific subcategory within each category.

The first step in finding the days with potential competent ice for a given winter after 1983 is to define the number of days of potential competent sea ice within each individual ‘*A*’, ‘*S*’, and ‘*T*’ category. The subcategories selected for potential competent sea ice are summarised in Table 5-4.

Subcategory from the Baltic Sea ice code	0	1	2	3	4	5	6	7	8	9	X
A (Amount and arrangement of sea ice)	Ice free	Open water	Very open drift ice	Open drift ice	Close drift ice	Very close drift ice	Compact drift ice including consolidated drift ice	Fast ice with drift ice outside	Fast ice	Lead in very close or compact drift ice	Unable to report
Competent ice			x	x	x	x	x	x	x	x	x
S (Stage of ice development)	New ice or dark nilas < 5 cm	Light nilas 5-10 cm thick	10-15 cm thick ice	15-30 cm thick ice	30-50 cm thick ice	50-70 cm thick ice	70-120 cm thick ice	Ice < 15 cm, w. thicker	Ice 15-30 cm w. thicker	Ice > 30 cm w. thinner	No information or unable to report
Competent ice				x	x	x	x		x	x	x
T (The topography or form of ice)	Pancake ice, bash ice < 20 m	Small ice floes – 20-100 m	Medium ice floes – 100-150 m	Big ice floes – 500-2000 m	Vast or giant ice floes > 2000 m	Rafted Ice	Compacted slush or shuga, or compacted brash ice	Hummocked or ridged ice	Thaw holes or many puddles on the ice	Rotten ice	No information or unable to report
Competent ice		x	x	x	x				x	x	x

Table 5-4: Overview of the *'A', 'S',* and *'T'* subcategories chosen to represent potential competent sea ice conditions.

The number of days with potential competent ice for a given winter is determined as:

1. Determine the number of days with potential competent ice for each '*A*', '*S*' and '*T*' category, for each selected observation station, by calculating the sum of the days for the competent ice subcategories.
2. Calculate the mean number of competent ice days between the observation stations for each '*A*', '*S*' and '*T*' category.
3. Determine the observation stations with the recorded number of competent ice days closest to the mean value found in Step 2 for each '*A*', '*S*' and '*T*' category.
4. When the observation stations are found in Step 3 for each '*A*', '*S*' and '*T*' category, the number of days with competent ice is chosen from that observation station for each '*A*', '*S*' and '*T*' category.
5. Use the minimum envelope of the '*A*', '*S*', and '*T*' closest to mean categories to determine the number of days with competent ice for the given winter.

An example of the method outlined above is shown in Figure 5-1.

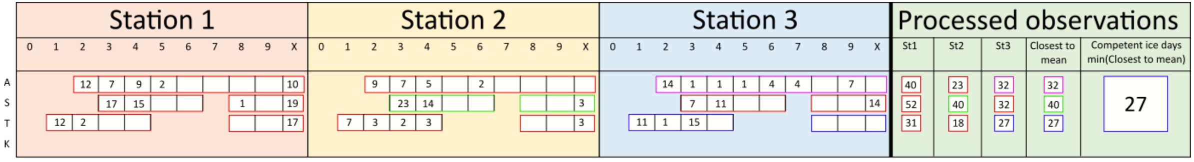

	Station 1											Station 2											Station 3											Processed observations				
	0	1	2	3	4	5	6	7	8	9	X	0	1	2	3	4	5	6	7	8	9	X	0	1	2	3	4	5	6	7	8	9	X	St1	St2	St3	Closest to mean	Competent ice days min(Closest to mean)
A			12	7	9	2					10			9	7	5		2							14	1	1	1	4	4		7		40	23	32	32	27
S				17	15				1		19				23	14						3				7	11						14	52	40	32	40	
T		12	2								17		7	3	2	3						3		11	1	15								31	18	27	27	
K																																						

Figure 5-1: Example of the "average" approach applied to preprocess the observations from multiple sea ice observation stations after 1983 and find the number of days with competent ice.

In the example of Figure 5-1, three stations with ice observations following the Baltic Sea ice code are given for a winter period. The subcategories within each of the ‘*A*’, ‘*S*’ and ‘*T*’ categories selected as the definition of competent ice are indicated by the white boxes in which some contain a recorded number of ice days. To the right of Figure 5-1, the processed observations are found. Initially, the number of competent ice days observations for each station is determined from the sum of days in the competent subcategories across the ‘*A*’, ‘*S*’ and ‘*T*’ categories following Step 1. From these, the mean values are determined as stated in Step 2. For this example case, the mean values are determined as 31.7, 41,3, and 25.3 for the ‘*A*’, ‘*S*’ and ‘*T*’ categories respectively. Following Step 3, the observation station with the number of competent ice observation days closest to this mean is determined for each of the ‘*A*’, ‘*S*’ and ‘*T*’ categories. These are indicated in purple, green, and blue in Figure 5-1, originating from the observation stations ‘*Station 3’, ‘Station 2’,* and *‘Station 3’* respectively. The number of days of competent ice within each ‘*A*’, ‘*S*’ and ‘*T*’ category is determined in accordance with Step 4, and finally, the minimum envelope approach is applied to determine the number of days with competent sea ice for the given winter, in this example 27 from the ‘*T*’ category of ‘*Station 3’* indicated in blue.

The reason for applying the minimum envelope approach is that all criteria of the ‘*A*’, ‘*S*’ and ‘*T*’ categories must be fulfilled before competent ice is present. Please note that this leads to conservative upper bounds since correlations between the A-, S-, and T-occurrences could have led to smaller numbers (e.g. a potentially severe A-category occurrence may have occurred at the same time as an insignificant S-category occurrence).

As for the winters before 1983, the method outlined above takes all chosen observation stations into account, but the resulting number of days with competent ice is from an actual observation station.

The number of days with potential competent ice is outlined in Table 5-5 for the winters with a resulting number of days of potential sea ice larger than 0 (zero). The winters shown in Table 5-5 will form the basis for the calculation of the sea ice condition parameters for the KG site.

Winter with ice	Days with competent ice, *'A'*, *'S'* and *'T'* categories			Days with competent ice	Observation station for competent ice
	A	S	T		
[year range]	[days]			[days]	[-]
1962 to 1963	-	-	-	43	Anholt Fyr
1965 to 1966	-	-	-	10	Fornæs Fyr
1969 to 1970	-	-	-	7	Nakkehoved Fyr
1978 to 1979	-	-	-	15	Fornæs Fyr
1981 to 1982	-	-	-	5	Anholt Fyr
1984 to 1985	40	32	31	31	Sletterhage
1985 to 1986	28	27	32	27	Fornæs Fyr
1986 to 1987	46	54	51	46	Hundested
2009 to 2010	5	4	9	4	Anholt Fyr
2010 to 2011	5	4	8	4	Nakkehoved Fyr

Table 5-5: Days with competent ice for the winters where the days with competent ice were not equal to 0 (zero).

5.1.4 Populating the *'S'* category

The '*S'* category in the Baltic Sea ice code corresponds to the '*Stage of ice development*'. In this category, the number of days with different ice thickness intervals and types are recorded. These recordings are used to populate the durations for a defined number of ice thickness bins to be used in the Fatigue Limit State (FLS) DLCs D4 and D7 according to Table 4-1. The methodology for estimating a representative *'S'*-category distribution for the KG site follows a somewhat similar method as outlined in Section 5.1.3 with small differences:

1. Calculate the mean number of days for each subcategory of the *'S'*-category across all observation stations.
2. Determine the observation stations with the number of days closest to the mean value found in Step 1 for each subcategory of the *'S'*-category.
3. When the observation stations for each subcategory have been determined in Step 2, the number of days for the individual subcategories are selected to populate the subcategories of the site-specific processed ice observations.

The approach is exemplified in Figure 5-2, in which the observations recorded in subcategory *'4'* of the *'S'* category from three different observation stations are processed.

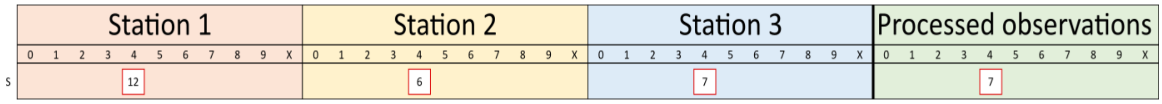

Figure 5-2: Example of the "average" approach applied to preprocess the observations from multiple sea ice observation stations and populate the *'S'*-category of the Baltic Sea ice code.

Based on the example recordings from the three sea ice observation stations exemplified in Figure 5-2, (12, 6, and 7 days) the mean value of 8.3 days is determined. The closest actual observation to the mean value of 8.3 days is the 7 days from observation station '*Station 3*', which is used to populate this subcategory in the site-specific processed ice observations. By following the method above, a populated *'S'*-category representative for the KG site is found and used to distribute ice thicknesses in thickness bins in Section 6.4.

As previously discussed, the Danish Sea ice code was used for the ice recordings before 1983. Thus, detailed information from the *'S'*-category of the Baltic Sea ice code is not available for winters before 1983. To estimate the *'S'*-category of these earlier winters, the concept of *winter parring* is introduced. Parried winters are determined for all winters before 1983, by parring the most comparable winter after 1983 based on the *Kuldesum* parameter – a measure for the severity of the given winter (see Appendix A). By use of the ice thickness records from the comparable paired winter, the ice details for the *'S'*-category in accordance with the Baltic Sea ice code for winters before 1983 can be estimated. The result of the pairing is outlined in Table 5-6 where the winters included are based on the winters with competent ice according to Section 5.1.3.

Winters before 1983/1984		Paired winter after 1983/1984	
Year range	Kuldesum	Year range	Kuldesum
1962 to 1963	300.3	1984 to 1985	273.4
1965 to 1966	163.0	2009 to 2010	162.8
1969 to 1970	208.4	1985 to 1986	193.3
1978 to 1979	215.2	1985 to 1986	193.3
1981 to 1982	218.7	1985 to 1986	193.3

Table 5-6: Pairing of winters with competent ice before the winter 1983/1984 to winters with competent ice after the winter 1983/1984. The selection of winters with competent ice is outlined in Section 5.1.3.

Based on the outlined methodology in this section, the *'S'*-category is populated for all ice winters and shown in Table 5-7 for the subcategories needed in Section 6.4.2. Please note that the number of days with competent ice is less than the sum of the days in the *'S'*-categories shown in Table 5-7 for some of the winters before 1983. This is due to the winter paring exercise and will be further discussed in Section 6.4.2.

Winter with ice	Days with competent ice	Subcategory 3 h = 15-30 cm		Subcategory 4 h = 30-50 cm		Subcategory 8 h = 15-30 cm with thicker ice		Subcategory 9 h > 15-30 cm with thinner ice	
[year range]	[days]	[days]	Station	[days]	Station	[days]	Station	[days]	Station
1962 to 1963	43	15	Sletterhage	11	Hundested	1	Sletterhage	0	Fornæs Fyr
1965 to 1966	10	0	Fornæs Fyr	0	Fornæs Fyr	0	Fornæs Fyr	0	Fornæs Fyr
1969 to 1970	7	12	Hundested	8	Fornæs Fyr	0	Fornæs Fyr	0	Fornæs Fyr
1978 to 1979	15	12	Hundested	8	Fornæs Fyr	0	Fornæs Fyr	0	Fornæs Fyr
1981 to 1982	5	12	Hundested	8	Fornæs Fyr	0	Fornæs Fyr	0	Fornæs Fyr
1984 to 1985	31	15	Sletterhage	11	Hundested	1	Sletterhage	0	Fornæs Fyr
1985 to 1986	27	12	Hundested	8	Fornæs Fyr	0	Fornæs Fyr	0	Fornæs Fyr
1986 to 1987	46	30	Fornæs Fyr	3	Sletterhage	2	Fornæs Fyr	0	Fornæs Fyr
2009 to 2010	4	0	Fornæs Fyr	0	Fornæs Fyr	0	Fornæs Fyr	0	Fornæs Fyr
2010 to 2011	4	0	Fornæs Fyr	0	Fornæs Fyr	0	Fornæs Fyr	0	Fornæs Fyr

Table 5-7: Days in the *'S'*-category for the ice winters. The observation stations where the number of days originates from is also shown. The number of days in the subcategories before 1983 is based on the winter pairing method shown in Table 5-6.

5.2 Air temperature timeseries

The timeseries of air temperatures are key in the evaluation of the sheet ice thickness by use of the thermal ice growth model. The sources of the air temperature timeseries are outlined in Section 4.2. Multiple meteorological observation stations can be utilized in the evaluation. When more meteorological observation stations are applied, these are used in a prioritized order based on their proximity to the site. As the historical temperature datasets may contain periods of inaccurate or missing data, the validity of each temperature dataset is evaluated before it is used as input to the thermal ice growth model. In case invalid or missing data is detected within the winter period being evaluated, the next highest prioritized temperature dataset is selected. This process continues until a temperature dataset with valid data covering the evaluated winter period is found.

Erroneous air temperature measurements have previously been identified in some datasets for ‘*Anholt’* from [DMIMET], why the validity of the applied air temperature data is examined by comparison to measurements from nearby stations for all relevant winter periods. The comparisons of the measured temperatures for the individual winter periods are given in Figure 5-3 and Figure 5-4.

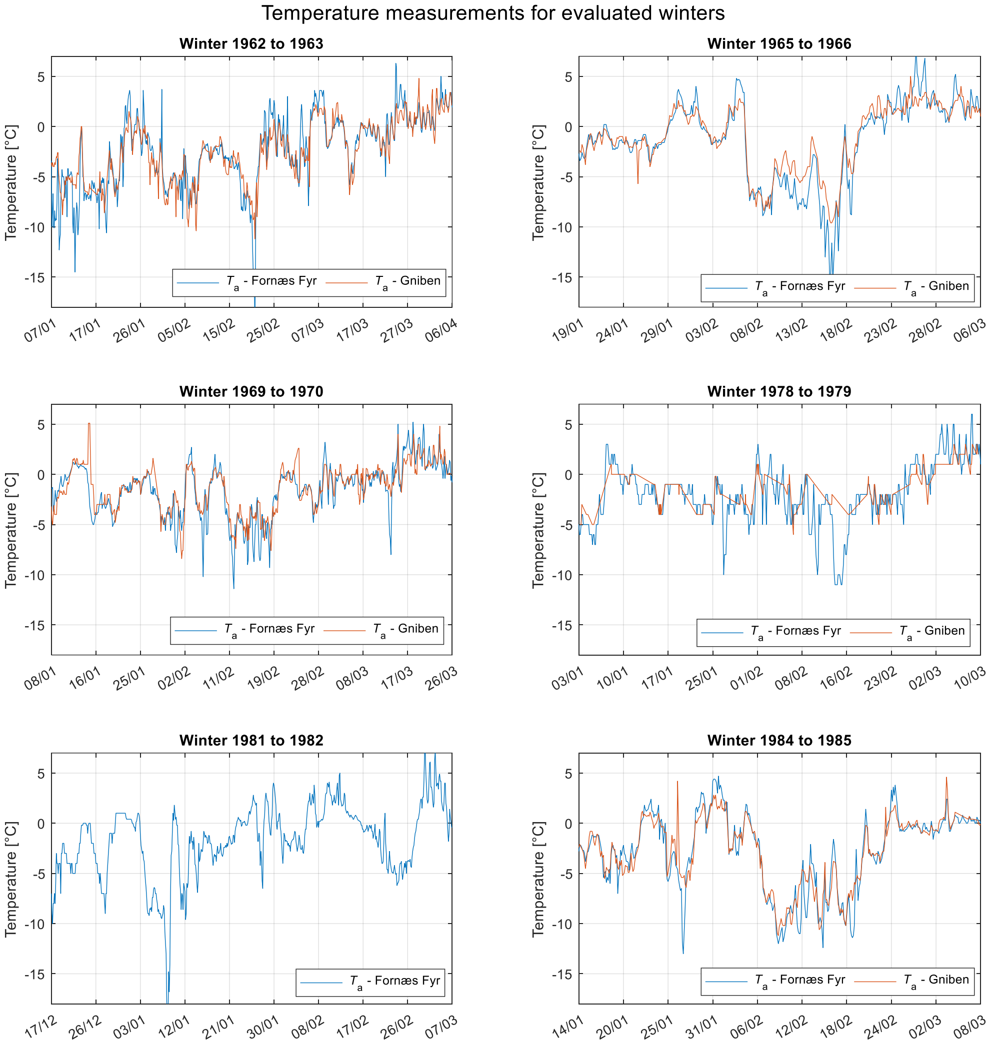

Figure 5-3: Comparison of air temperature measurements from two selected meteorological observation stations for the selected winters between 1962 and 1985. Note however, that neither the ‘*Gniben’* or ‘*Nakkehoved’* observation station have available data for the winter of 1981/1982, why only measurements from the ‘*Fornæs Fyr’* station are shown for this period. The blue line represents the primary air temperature dataset used as input to the thermal ice growth model whereas the red line represents the measurements from the secondary observation station used for the sanity check.

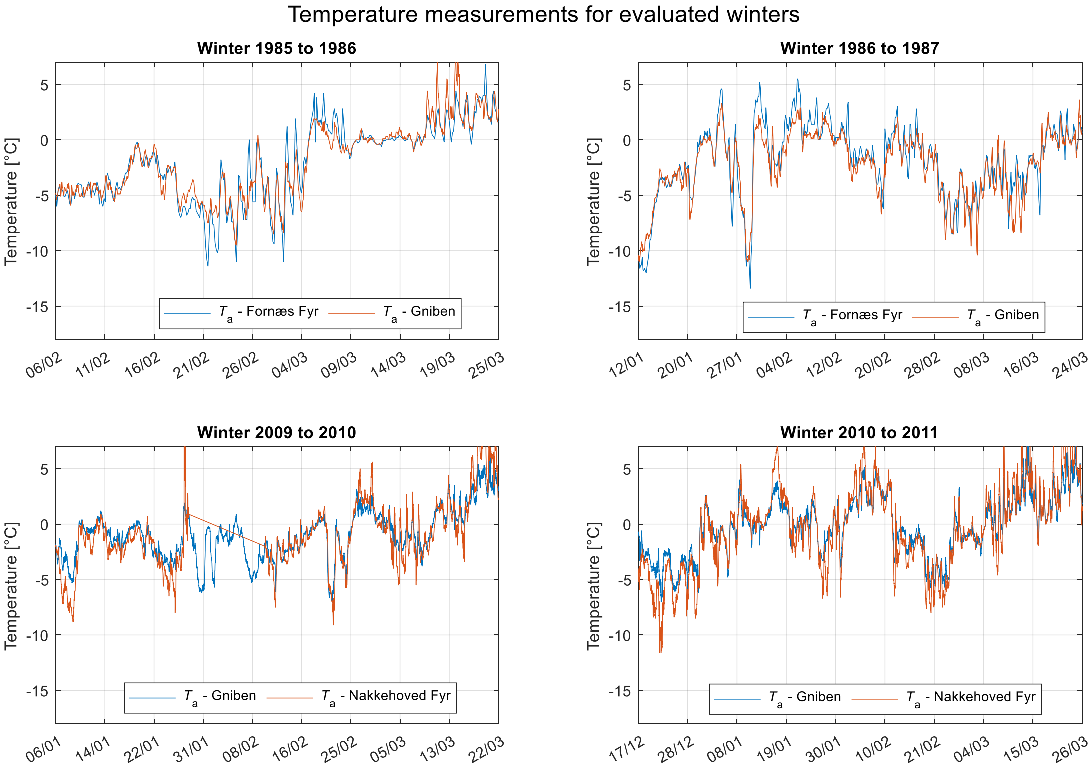

Figure 5-4: Comparison of air temperature measurements from two selected meteorological observation stations for the selected winters between 1985 and 2011. The blue line represents the primary air temperature dataset used as input to the thermal ice growth model whereas the red line represents the measurements from the secondary observation station used for the sanity check.

In the air temperature measurements of Figure 5-3 and Figure 5-4 various outliers and periods of missing data are noted. In addition, it is noted that the temperature measurements of the '*Gniben'* observation station for the winter of 1978/1979 have been recorded with a different frequency than what is seen for the remaining winters. Despite some obvious outliers and the expected differences between the measurements from two stations located a distance apart, an overall acceptable agreement in the measured air temperature is found. As a result, it is concluded that the air temperature measurements from the chosen meteorological observation stations are suited as inputs for the thermal ice growth model.

5.3 Sea surface temperature timeseries

As mentioned in Section 4.3, the sea surface temperatures (SST) are used to limit the thermal ice growth. These are applied when available and are based on a prioritized list as discussed in Section 4.6. If no SSTs are available for a given period, it is disregarded in the calculation of the ice growth. Next, the validity of the SST data is examined in detail.

The SST for the KG site is extracted from the Baltic Sea Physics Reanalysis (BSPR) product of [CMEMS]. These SST model data are used to justify the use of the SST measurements from stations located at a distance from the evaluated site. In addition, the modelled SST dataset is used to assess the validity of the measured SST datasets before these are used as inputs to the thermal ice growth model. The validity of the SST measurements from '*Hornbæk Havn'* is examined for the period from the 1st of December to the 1st of March for all winters from 2008 to 2013. The correlation between the measured and the modelled SST data is given in the left plot of Figure 5-5. Note, that the selected year range overlaps with the winters in which the SST measurements from this dataset are applied in the analysis in this report. The SST measurements from *'Trubaduren Boj'* are applied for thermal ice growth for earlier winters, prior to the availability of the modelled SST data of BSPR. Thus, the sanity check cannot be performed for the winters in which this dataset is applied in this report, as was the case for the '*Hornbæk Havn'* dataset. Instead, the SST correlation is performed for the period from the 1st of December to the 1st of March for all winters from 2000 to 2004 where no winters with competent ice is observed. The results are presented in the right plot of Figure 5-5.

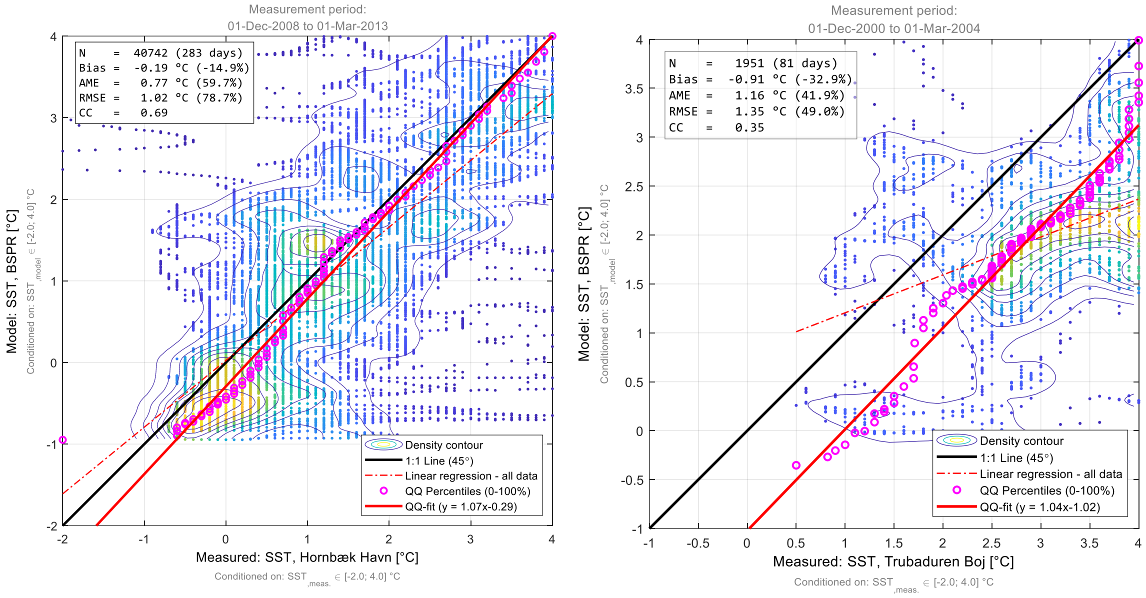

Figure 5-5: Correlation between measured and modelled SST for the temperature range -2 °C to 4 °C. **Left**: the modelled data from [CMEMS] and measured data from [DMIOCE]. **Right**: The modelled data from [CMEMS] and the measured data from [SMHIOCE].

The SST data from the BSPR model and the measured SST from '*Hornbæk Havn',* found to the left of Figure 5-5, are generally seen to agree in the low-temperature range from -2 °C to 4 °C. However, the modelled SST data from Copernicus seems to be lower than the SST measurements for the lowest temperatures below 1 °C. However, based on the overall agreement in the data it is assessed that the SST measurements from *'Hornbæk Havn*' are representative of the OWF site despite the relative distance.

The comparison between the SST data from the BSPR model and the measurements from the '*Trubaduren Boj*' oceanographic observation bouy is seen in the right plot of Figure 5-5. Compared to the correlation plot for '*Hornbæk Havn*', a higher discrepancy in the datasets is noted. From Figure 5-5, it is seen how the modelled SSTs are generally lower than the measured SST for the entire temperature range depicted. This could indicate that the SSTs measured at the *'Trubaduren Boj'* may be slightly higher than what is observed near the Kattegat OWF site. To account for this, the measurements from the

‘*Trubaduren Boj’* are adjusted accordingly[3] as -1°C is subtracted from the SST measurements before these are used as inputs to the thermal ice growth model.

As evident in the data availability overview of Figure 4-7, no overlap is found for the SST measurements from the lightship of *‘Anholt Nord – Knob’* and the site-specific SSTs from the BSPR dataset. Thus, a correlation check of the SSTs from *‘Anholt Nord – Knob’* is not performed and the measured SSTs are used as is. The lack of a sanity check for these measurements is however acceptable, due to the limited number of SST measurements available from the lightship in the evaluated winters as is seen in Figure 5-6.

5.4 Temperature timeseries for ice winters

The air- and SST measurements used as inputs to the thermal ice growth model are summarised in Figure 5-6 and Figure 5-7.

Figure 5-6: Air temperature, T_a, and sea surface temperature (SST), T_w, measurements from preferred meteorological- and oceanographic observation stations for the selected winters between 1962 and 1985. The freezing temperature of the seawater, $T_{f,lim}$, found from Section 4.4 is also shown. Note, how the measurements of the ‘*Anholt Nord – Knob’* lightship are missing in the periods in which sea ice is present, as a result of the common practice of retracting the lightships to the harbours applied at the time according to Section VII of [SPARRE].

---

[3] The resulting h_{50} has been evaluated for two additional scenarios using first: the uncorrected SST measurements, and second: excluding the SST measurements from the Trubaduren Boj. This resulted in a h_{50} of 0.37 m and 0.38 m for the two scenarios, respectively.

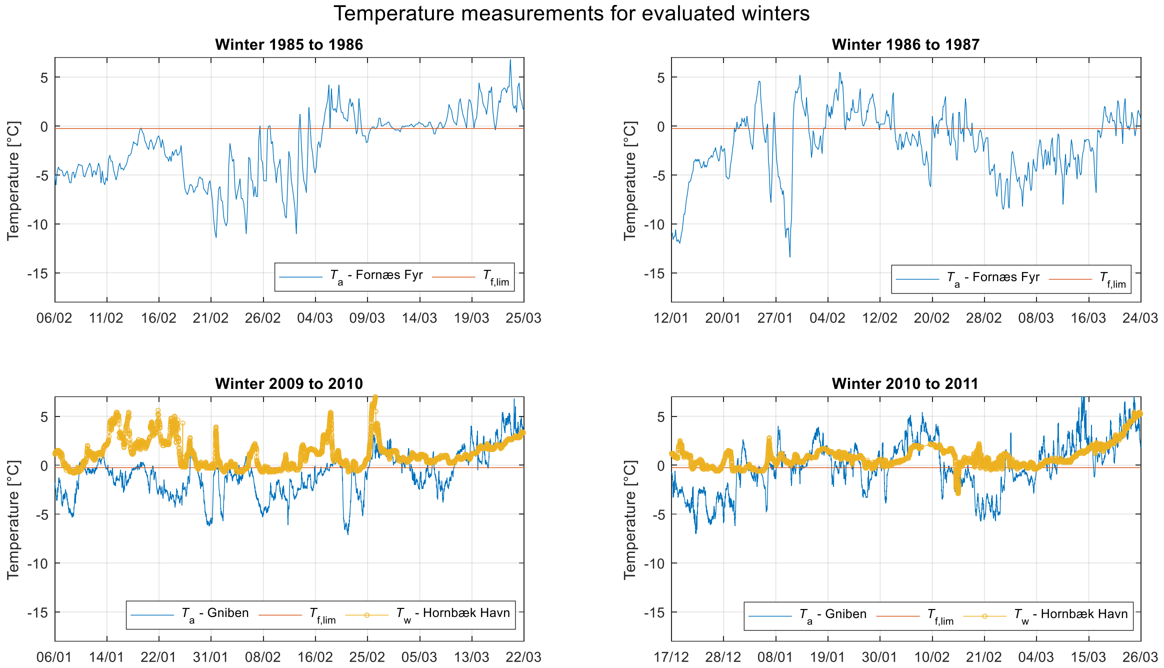

Figure 5-7: Air temperature, T_{a}, and sea surface temperature (SST), T_{w}, measurements from preferred meteorological- and oceanographic observation stations for the selected winters between 1986 and 2011. The freezing temperature of the seawater, T_{f}, found from Section 4.4 is also shown. No available source of qualitative SST data was found for the two winters of 1985/1986 and 1986/1987 as hinted in Figure 4-7.

These air- and SST measurements, used as inputs to the thermal ice growth model, are repeated below each evaluated winter in the detailed overview plots found in Figure C-1 and Figure C-2 in Appendix C.

5.5 Selection of hindcast dataset

In Section 4.5, hindcast datasets for three individual reference locations are identified for the KG site. The risk of subjecting the support structures at the site to ice-induced vibrations is increasing for low ice drift velocities. Thus, the hindcast dataset to use for the present evaluation is selected from an evaluation of the number of occurrences of ice drift velocities below 0.2 m/s. The ice drift velocity is estimated by use of both the paired wind- and current hindcast datasets for the three individual reference locations within the site. The approach of Eq. 3.3.3. of Section 3.3 of [VICE] is applied to determine the ice drift velocity of an ice floe from the wind- and current velocities. A reference ice floe of 1 km^2 is used[4] for assessing the ice drift velocity for all three reference locations.

The histograms of the calculated ice velocities for the three reference locations are given in Figure 5-8.

---

[4] The choice of ice floe size is of minor importance since it is only used in the selection of the hindcast dataset and not anywhere else in this report. The used ice floe of 1 km^2 is not necessarily a representative ice floe size for the KG site.

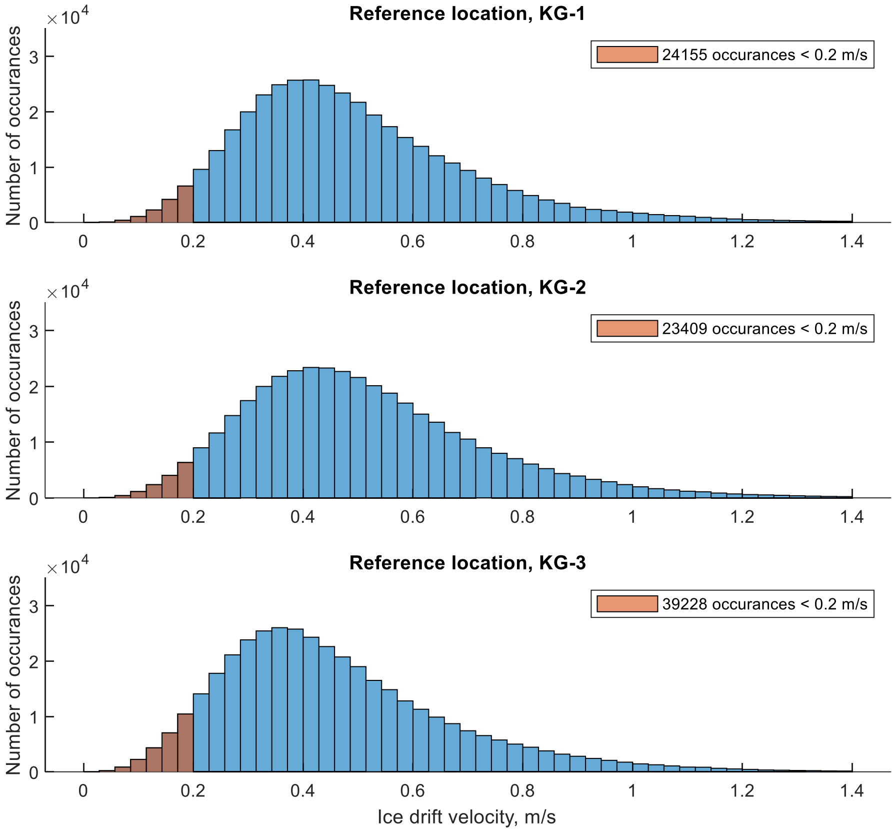

Figure 5-8: Histogram of the estimated ice drift velocities calculated from the wind- and current hindcast data for the three reference locations *'KG-1', 'KG-2',* and *'KG-3'* within the KG site. All ice drift velocity bins below 0.2 m/s are indicated in orange, and the summed number of occurrences within these are stated in the figure label.

From Figure 5-8, it is seen how the number of occurrences of the estimated ice drift velocities below 0.2 m/s is highest for the reference location of '*KG-3*'. As a result, the wind- and current hindcast datasets for reference location '*KG-3*' are used for the evaluations of the present report.

5.5.1 Selection of surface current

According to Equation D.9 of [IEC6131], the current velocity 1 m below the lower ice surface shall be applied in the evaluation of the forces from currents on the sheet ice. In the 3D model hindcast data of [HCCUDATA], a total of 20 current bins are distributed evenly throughout the water column. The current profile at '*KG-1*' is given in Figure 6-16 of [MA] and reproduced in Figure 5-9. Note, that it is assumed that the current profile at the selected reference location of '*KG-3*' is very comparable.

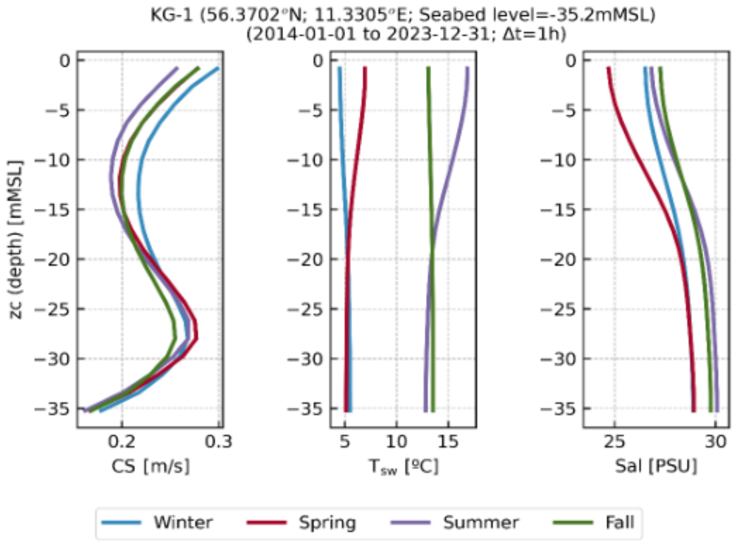

Figure 5-9: Seasonal current speed profile (left) for the reference location of *'KG-1'* for a 10-year period. Reproduced from Figure 6-16 of [MA].

In the hindcast model, the currents in the layers near the sea surface are affected by the wind. In the presence of ice coverage, the currents near the sea surface are not affected by the wind. Thus, for situations of ice coverage, the current is selected from an elevation for which the effect of wind is less pronounced and hence driven by tidal current. It is assumed that the effect from the wind is small at approximately -12 mMSL. In the presence of ice coverage, a slowdown of the current speeds in the near-surface layers is expected – similar to the current behaviour near the seafloor. This potential slowdown is neglected in the present report, and the surface current in the presence of ice coverage is assumed equal to the current for the layer of approximately -12 mMSL. Please note that it is conservative to choose a small current speed as outlined in Section 5.5.

6. Sheet ice thickness

A step in the process of establishing several ice parameters as required in Table 3-1, is to establish the historical sheet ice thickness. The historical sheet ice thickness is used to find the following ice parameters:

- Sheet ice thickness for ULS DLCs for a 50-year return period, h_{50}.
- Bin size including upper bin bound for binning of ice thickness for FLS DLCs.

The sheet ice growth is simulated for each ice winter using a thermal ice growth model which is explained in Section 6.1. The result of this analysis is an extreme thickness for each ice winter primarily used to determine h_{50}. In addition, it is used to determine an appropriate upper bin bound and bin size for the binning of ice thickness distributions to support the FLS DLCs. The FLS distributions though, are solely based on the sea ice observations as outlined in Section 5.1.

6.1 Thermal ice growth model

The thermal ice growth model is presented in Appendix B, where the air temperature, T_a is needed as an input. T_a is a function of time, that must be used as an input during the periods when the ice is expected to thermally grow. The start of the period can be determined in two different ways:

1. First timestamp in the winter when the air temperature is smaller than the freezing temperature of saline water ($T_\mathrm{a} < T_\mathrm{f,lim}$).
2. Timestamp of first ice observation.

Option 1 could lead to the model predicting ice growth despite the SST being larger than T_f. Furthermore, saline water, as that at the evaluated site, will not start to freeze before the temperature of the water column is smaller than T_f. Option 2 is chosen instead since this is a more accurate representation of the actual starting point of ice growth. The date range for the winters where ice may be present at the site is selected as detailed in Section 5.1.1. These dates are then used as the start- and end points for the thermal ice growth model using the methodology detailed in Appendix B.

The number of days with observed ice is not necessarily equal to the number of days between the first and last ice observation dates as outlined in Section 5.1.2. If these number of days are not the same, it means that ice has not been present for the whole period between the first and last ice observation dates. An example of this is shown in Figure 6-1 for the winter of 1981/1982 where the number of days with observed ice is 45 and the number of days from the first ice observation day (17th of December 1981) to, and including, the last ice observation day (7th of March 1982) is 80. Here, the grey areas show the selected days where the ice will not grow. The selection of these days is made through a ranking of the days with the lowest T_a for the given day. In the example shown in Figure 6-1, the 45 days with the lowest T_a are chosen for ice growth. By applying this method, it is ensured that the ice will grow in the days with the lowest air temperatures, which will ensure an upper bound for the thermally grown ice thickness is calculated. The values shown in the legend in Figure 6-1 for the winter of 1981/1982 are the maximum sheet ice thickness, $h_{\max}$, and the maximum consolidated layer thickness, $h_{\mathrm{c,max}}$. The method used to calculate the consolidated layer thickness is discussed in Section 7.1.

As outlined in Appendix B, the SST is not directly an input to the thermal ice growth model. In the original model by [STEFAN], the water temperature is used as the primary input, but since this is only occasionally available, the air temperature is used instead. The SST is still used as a limiting factor for ice growth, as the ice can only thermally grow if the SST is equal to, or below, the freezing temperature of the seawater determined in Section 4.4. This is evident in the example in Figure 6-1 where $T_{\mathrm{a}} < T_{\mathrm{f,lim}}$ in the first ~5 days but $T_{\mathrm{w}} > T_{\mathrm{f,lim}}$ in that period. As a result, the ice does not grow in these first ~5 days.

A summary of the inputs listed in Table 6-1 shall also be used as outlined in Appendix B.

Parameter	Variable	Unit	Value	Reference
Thermal conductivity of ice	κ	[W/(m·K)]	2.11	Table A.1 in [LEPP]
Freezing temperature of saline water	$T_{\mathrm{f,lim}}$	°C	-0.26	Section 4.4
Air temperature	T_{a}	°C	-	Sections 5.2 and 5.4
Sea surface temperature	T_{w}	°C	-	Sections 5.3 and 5.4
Density of ice	ρ_{ice}	[kg/m3]	917	Table A.1 in [LEPP]
Latent heat of melting for ice	L_{f}	[kJ/kg]	333.5	Table A.1 in [LEPP]

Table 6-1: Input parameters to the thermal ice growth model.

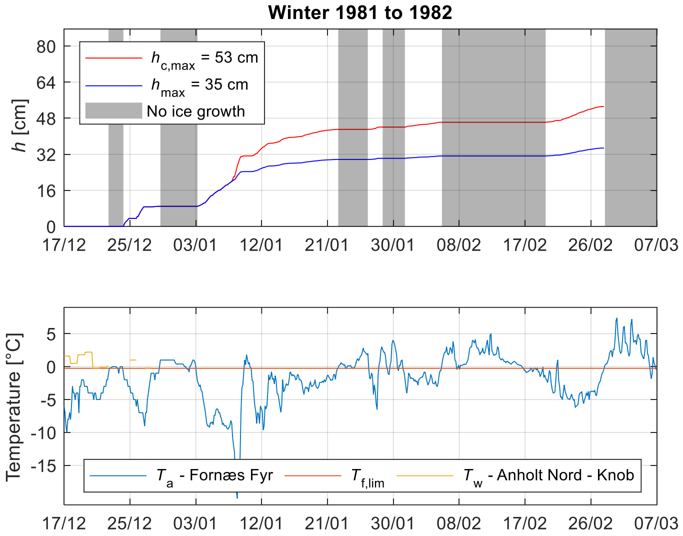

Figure 6-1: Example of thermal ice growth for the winter of 1981/1982. The grey areas are the selected days in which the ice will not grow due to the limiting number of days where ice can thermally grow.

6.2 Sheet ice thickness model results

Using the input data from Table 6-1, the sheet ice thickness as a function of time is shown in Figure C-1 and Figure C-2 for the ice winters. As for the example shown in Figure 6-1, the chosen days where the ice will not grow are marked with grey. The thickness of the consolidated layer in an ice ridge is shown in the same plots and will be discussed in Section 7.1. For each winter, $h_{\max}$ is shown in the legend in Figure C-1 and Figure C-2. The modelled $h_{\max}$ is reached on the last day where ice growth is modelled. Below each plot of the ice thickness for each winter with ice, the values of T_{a}, from [DMIMET] used for the calculation, are shown together with $T_{\mathrm{f,lim}}$. The meteorological observation station from which the air temperature measurements originate is noted in the figure legend for all evaluated winters. For winters in which SST are applied as part of the thermal ice growth model, these are included as a yellow line, denoted T_w, in the lower plot. As for the air temperature, the oceanographic observation station from which the measurements originate is indicated in the figure legend.

The significance of applying SST measurements as part of the thermal ice growth model cannot be underestimated, as this can lower the level of conservatism with which the sheet ice thicknesses are determined. To exemplify this, the most recent winter of 2010/2011, would, if evaluated without the use of the SST measurements from *'Hornbæk Havn'* or similar, result in a $h_{\max}$-value of 30 cm instead of the reported 15 cm. This suggests that the $h_{\max}$-values for any winters evaluated without the use of SST measurements may be significantly overestimated. The availability of qualitative historical SST measurements is however scarce, why the collection and evaluation of SST measurements have been a key focus point for the present study.

A summary of the sheet ice thickness result is shown in Table 6-2.

Winter with ice	**Maximum sheet ice thickness, $h_{\max}$**
Year range	[cm]
1962 to 1963	48
1965 to 1966	30
1969 to 1970	32
1978 to 1979	32
1981 to 1982	35
1984 to 1985	36
1985 to 1986	33
1986 to 1987	38
2009 to 2010	18
2010 to 2011	15

Table 6-2: Maximum sheet ice thickness from the ice growth model.

6.3 50-year sheet ice thickness

For determining the 50-year sheet ice thickness, h_{50}, the maximum sheet ice thickness, $h_{\max}$, for each winter with ice is used. A plot of $h_{\max}$ as a function of the winter start year ranging from 1960 to 2023 is shown in Figure 6-2 where the winters without any sea ice are included with zero sheet ice thickness.

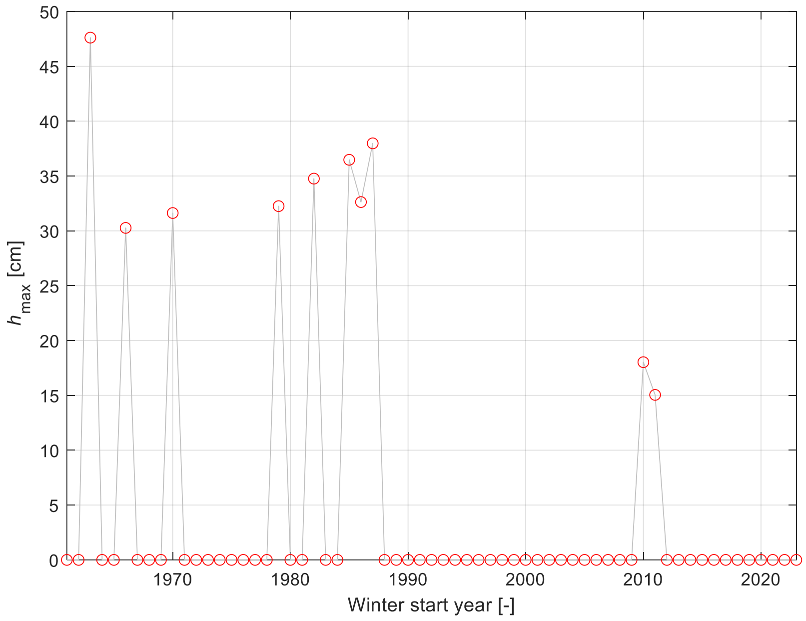

Figure 6-2: Maximum sheet ice thickness for each winter from 1960 to 2023 as a function of time (start year of the winter). The winters without any observations of sea ice are included as $h_{\text{max}} = 0$.

To create the Extreme Value Analysis (EVA), a Weibull distribution fit to the values of h_{max} applying a peak-over-threshold method in Figure 6-2 is created. Here, a threshold of 1 cm is applied ensuring that only the non-zero values are considered as extreme values. The MATLAB built-in function `fitdist`[5] has been used for this. Two examples of this are shown in Figure 6-3 where two different durations are included in the fit. The duration for the left plot is from 1961 – 2023 and the right plot is from 1979 to 2023. The 50-year exceedance value for the start year 1961 is shown to the left of Figure 6-3 and is calculated to be approximately 42 cm. For the start year 1979, the 50-year exceedance value is determined to be approximately 38 cm as seen to the right of Figure 6-3.

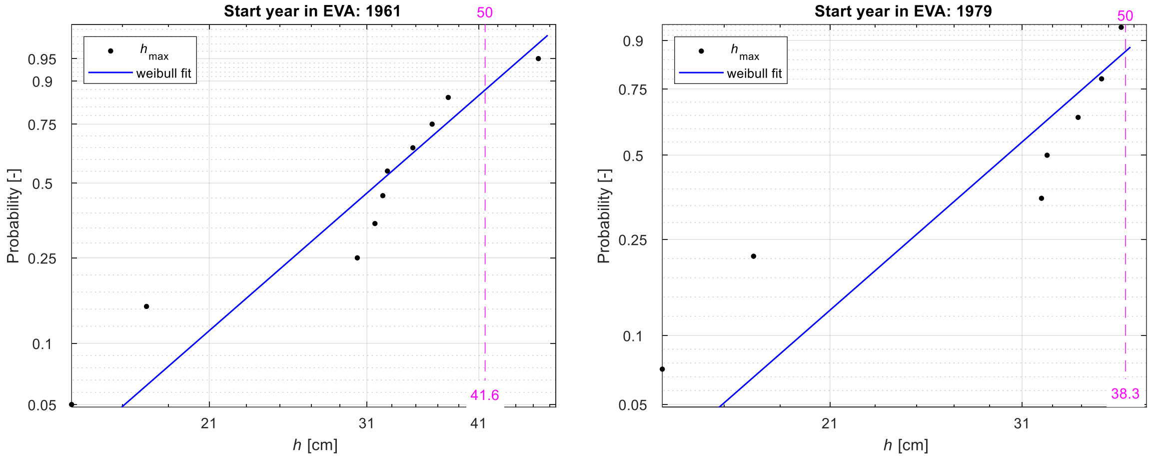

Figure 6-3: Probability of h_{max} including a cumulative Weibull distribution fit. Please note that ice-free winters are not included. **Left:** The 50-year exceedance value of approximately 42 cm is indicated for the start year of 1961. **Right:** The 50-year exceedance value of approximately 38 cm is indicated for the start year of 1979.

---

[5] https://se.mathworks.com/help/stats/fitdist.html

From the plots shown in Figure 6-3, it is seen how a change in the start year affects the 50-year exceedance value since fewer winters are included in the dataset for the EVA. To investigate this further, the same analysis is repeated for increasing start years since 1960. The result of h_{50} by changing the start year of the dataset is shown in Figure 6-4. Here, it can be seen that h_{50} is decreased for the start year of 1964 underlining the severity of the 1962/1963 winter. Further, the curve is seen to increase slightly (on a coarse scale) from the start year 1964 to 1979. This is a result of the decreasing number of years included in the EVA. No EVA is performed for start years after 1979 since too few ice winters are recorded to ensure a valid result from the fit.

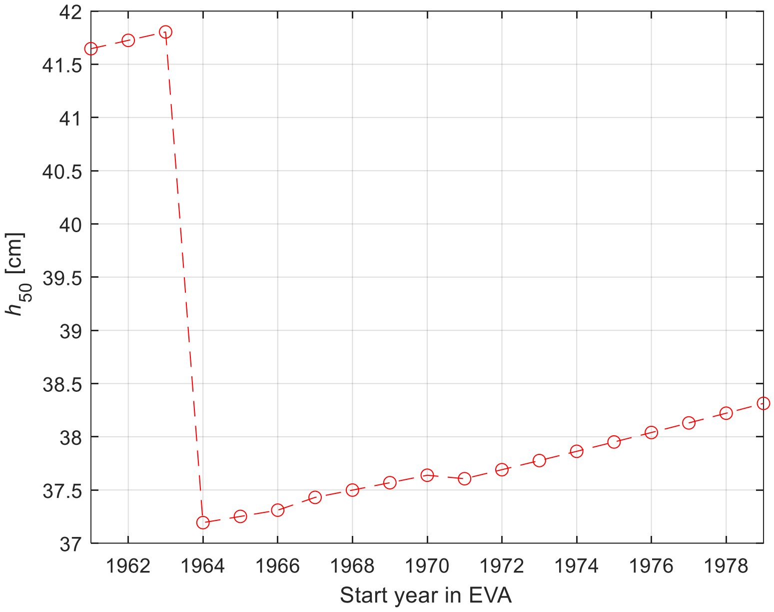

Figure 6-4: The 50-year sheet ice thickness, h_{50}, as a function of the start year in the Extreme Value Analysis (EVA). The reason for the curve's slight upward slope is due to there being progressively fewer years used to assess the h_{50}-value. No EVA results are produced for start years after 1979 due to having too few data points to perform an EVA with sufficient quality.

In conclusion, the 50-year sheet ice thickness must be determined. Before a value is chosen, it is worth reflecting on the conservative assumptions in the thermal ice growth model examined in detail in Appendix B. The significance of the availability of quality historical SST measurements was previously discussed. Without such measurements, the thermal ice growth model has been seen to produce overly conservative sheet ice thicknesses. In addition, the ice observations used to define the winter periods for evaluation are to a large extent performed from land-based observation stations, but the observations are applied to a site located in more open water. Further, any potential melting of the sea ice for warmer days in the evaluated winter period is discarded, why the determined sheet ice thickness can only increase during the evaluated winter period. Besides this, the sea ice observations used for the present evaluation indicate that the winters at the site have become increasingly milder and less frequent in recent decades, which is in line with the findings of Section 13 in which the effect of climate change is discussed – although not directly applied here. This suggests that the analysis made in the present section, which only uses what has already happened, could result in a conservative assessment of the 50-year return period sheet ice thickness.

With this in mind, the choice of the design value for the 50-year sheet ice thickness may be considered a conservative choice. However, the 50-year sheet ice thickness design value is chosen to represent the approximate start year of 1976 from Figure 6-4.

Thus, the design value for the 50-year sheet ice thickness is chosen to:

$\boldsymbol{h_{50}}$ $=$ **0.38 m.** **Valid for the entire site.**

It is worth mentioning that this result is based on the results of the modelling and observations of sea ice but does not require the utilization of any findings of the climate change effects discussed in Section 13.

6.4 Sheet ice thickness distribution and duration

According to Table 3-1, the sheet ice thickness distribution is a required input to the FLS DLCs D4 and D7. Table 3 of [IEC6131] specifies that the expected history of mobile/moving sea ice thicknesses should be used. The mobility of the ice is detailed in Section 6.4.1 where additional external factors influencing the considered durations are discussed.

The sheet ice thickness distribution and durations to be used for the FLS DLCs are outlined in Section 6.4.2 taking the findings in Section 6.4.1 into account.

6.4.1 External influence on FLS durations

For use in the FLS DLCs D4 and D7, Table 3 of [IEC6131] specifies that an expected history of moving sea ice thicknesses should be used. Whereas the history of sea ice thicknesses is discussed in Section 6.4.2, the present section deals with the topic of mobility and competence of the sea ice due to external factors.

From the arguments of [KARNA20] discussed in detail in Section 11, it is concluded that a wide range of ice action speeds should be treated as part of the evaluation of the ice load effects on the support structure. The primary load effects from ice occur once the sheet ice is mobile. The mobility of sheet ice, competent of subjecting the WTG support structures to ice-induced vibrations, is affected by multiple factors such as:

- Wind- and current speed necessary to make the ice mobile.
- Exposure to unbroken ice.
- Upstream ridged, rafted, or deformed ice.

The mobility of sheet ice is highly dependent on the wind- and current conditions, as indicated by Eq. 10-1, describing the resulting drag force subjected to an ice floe from the applied wind and current. It seems only logical, that smaller ice floes are easier moved than larger ice floes by the applied wind and current. This suggests that the necessary wind- and current speeds to make the ice mobile, are to some extent dependent on the ice conditions and floe size on site, which is seen to vary significantly in the presented historical ice recordings. As a conservative approach, Table 3-3 of [DNV0437], suggests considering all recorded ice days as days with mobile ice.

In addition to the mobility of the sheet ice, the configuration of the ice floe is of key importance when assessing if the sheet ice is capable of subjecting the WTG support structures to ice-induced vibrations. For ice-induced vibrations to occur, the support structure must be exposed to unbroken ice. If the wind- and current are driving the sea ice in a direction where it will be either broken by another structure or is shielded in another way, ice-induced vibrations will not occur. The KG site is located in open waters with limited to no shielding islands or shores nearby. It is however, noted that the neighbouring, fully commissioned wind farm of *‘Anholt Havmøllepark’* is located 10-15 km North of the KG site, why ice from the North may potentially not be unbroken. This report seeks to provide site condition inputs for all possible layout configurations and any number of WTGs at KG, why any layout-specific assumptions are disregarded in this discussion. Thus, the configuration of the sheet ice used for the evaluation is assumed to always be unbroken and thus capable of subjecting the support structures to ice-induced vibrations.

The mechanism shown later in this report in Figure 11-1, and the schematic results shown in Figure 11-2, give the possibility for long periods with the quasi-constant ice action speeds necessary for inducing ice-induced vibrations. However, as seen in Figure 11-1, this entails the build-up of an area upstream of the wind farm with ridged, rafted, or deformed ice. Therefore, after a long period with ice-induced vibrations, this upstream area needs to pass the wind farm before un-deformed competent ice can again cause ice-induced vibrations. Although this will not necessarily reduce the time of mobile ice, it will reduce the time when the mobile sea ice is capable of subjecting the support structures to ice-induced vibrations. Since it cannot be guaranteed how large a fraction of the time the support structures will experience ice that is not capable of inducing ice-induced vibrations, it is conservatively chosen that all ice passing through the wind farm will be treated as being capable of inducing ice-induced vibrations.

Despite being argued that the suggested approach is conservative, the present report makes the following design choice for the mobility and competence of the sheet ice:

Sea ice for FLS DLCs D4 and D7 will be mobile and competent 100% of the time.
Valid for the entire site.

6.4.2 Distribution and duration

The distribution and durations introduced in the present section are determined by the use of the pre-processed sea ice observation data from Section 5.1. The sheet ice thicknesses from the thermal ice growth model summarised in Section 6.2 are also included as a reference to the severity of the winter. In addition, the ice thicknesses of the thermal ice growth model are used to justify the ice thickness bins used in the present section. Since it was concluded that the ice is mobile 100% of the time and not broken up or rafted, the durations found in this section are total duration which shall be used for design directly without reducing them.

The preprocessing of the days in the *‘S’*-category was performed in Section 5.1.4 where the number of days in each subcategory for all winters was populated using the paired winter method and average station approach. It can be noted that subcategories 5 and 6 are not included since no sheet ice thicknesses from the thermal ice growth model shown in Section 6 were found larger than 50 cm. This means that it is unlikely that any potential recordings of days in these subcategories are thermally grown ice but rather ridged or rafted ice. In addition, subcategory 2 is not included either since it is not considered as competent ice according to Table 5-4.

In Table 5-7, some of the ice winters before 1983 have more days in the '*S*'-subcategories than the number of days with competent ice. This is a result of the winter paring method so the winters with too many days are artificial. To overcome this problem, the number of days in each subcategory is reduced such that the sum of the days across all subcategories is equal to the number of days with competent ice.

A summary of the days in the subcategories of the *'S'*-category originating from Table 5-7 is shown in Table 6-3. Here, the adjusted days are marked with red.

Winter with ice	Days with competent ice	Subcategory 3 *h* = 15-30 cm	Subcategory 4 *h* = 30-50 cm	Subcategory 8 *h* = 15-30 cm with thicker ice	Subcategory 9 *h* > 15-30 cm with thinner ice
Year range	[days]	[days]	[days]	[days]	[days]
1962 to 1963	43	15	11	1	0
1965 to 1966	10	0	0	0	0
1969 to 1970	7	4.2	2.8	0	0
1978 to 1979	15	9	6	0	0
1981 to 1982	5	3	2	0	0
1984 to 1985	31	15	11	1	0
1985 to 1986	27	12	8	0	0
1986 to 1987	46	30	3	2	0
2009 to 2010	4	0	0	0	0
2010 to 2011	4	0	0	0	0
Sum:	192	88.2	43.8	4	0

Table 6-3: Overview of the number of days in the '*S*'-subcategories, 3, 4, 8, and 9 including the number of days with competent ice. The number of days presented is found in Section 5.1.4, where the reduced days are marked with red.

By observing the days of thickness interval per winter in the 3rd to the 6th columns of Table 6-3, the sum of these days is not the same as the days in the 2nd column for all winters. This is due to fewer days observed with ice thicker than 15 cm compared to the number of days with competent ice. To adjust the sum of the number of days for all thickness intervals, the following is conducted:

1. Limiting the number of days, for each winter with ice, by the number in the second column of Table 6-3. For example, for the winter of 1986/1987, this is 46 days.
2. For these numbers of days, pick out the largest ice thicknesses, and proceed to smaller ice thicknesses until the limiting number of days stated in item 1 above are exhausted. In this treatment, subcategory 8 is treated as being part of subcategory 3; i.e. the areas with ice thicker than 30 cm cannot be competent sheet ice if all of the surrounding ice has a thickness of [15-30[cm. Subcategory 9 is also treated as being part of subcategory 3 with the argument that predominantly thicker ice than 30 cm with surrounding thinner ice cannot be thermally grown sheet ice thicker than 30 cm – instead, it could be ridged or rafted ice.

3. For the winters where the number of days in the 2nd column is larger than the sum of the days in the 3rd to the 6th column, the necessary days to achieve the number in the second column are therefore assigned to the [0-15[cm ice thickness bin. The number of days for the [15-30[cm bin is taken as the sum of the subcategories 3, 8, and 9.
4. For the winters where there have been no observations of days with ice thicknesses in any of the sub-categories in Table 6-3, the necessary days in Column 2 are added to the [0-15[cm thickness bin.

The result of the above procedure is shown in Table 6-4, where the maximum ice thickness from the thermal ice growth model is shown in the 6th column as a reference.

Winter with ice	Days with competent ice	Days of ice thickness interval limited by days with competent ice, D_{int}			Maximum ice thickness, $h_{\max}$, From Table 6-2
Year range	[days]	[0-15[cm [days]	[15-30[cm [days]	[30-50] cm [days]	[cm]
1962 to 1963	43	16	16	11	48
1965 to 1966	10	10	0	0	30
1969 to 1970	7	0	4.2	2.8	32
1978 to 1979	15	0	9	6	32
1981 to 1982	5	0	3	2	35
1984 to 1985	31	4	16	11	36
1985 to 1986	27	7	12	8	33
1986 to 1987	46	11	32	3	38
2009 to 2010	4	4	0	0	18
2010 to 2011	4	4	0	0	15

Table 6-4: Number of days for each ice thickness interval limited by the envelope in the 2nd column. For comparison, the maximum ice thickness is included as well.

The next step in the analysis is to turn these intervals, for the winters in question, into durations for each ice thickness bin. As stated at the end of Section D.3 of [IEC6131], in a simplified model of ice thickness durations, the ice thickness can be taken to grow as the square root of time in the absence of more detailed knowledge. This implies that larger durations should be ascribed to the upper parts of each ice thickness interval than to its lower parts. At the same time, the maximum ice thicknesses calculated and reported in Table 6-4 should be considered. Using the assumption of ice thickness growing as the square root of time, the interval [0-15[cm has been distributed across the ice thicknesses {5, 10} cm, the interval [15-30[cm has been distributed across the ice thicknesses {15, 20, 25, 30} cm and the interval [30-50] cm has been added to the 30 cm bin. The reason for not including thickness bins larger than 30 cm is due to the declining trend in $h_{\max}$ as outlined in Table 6-4, why it would be too conservative to include thicknesses larger than 30 cm for FLS. The days in each of the bins for ice thicknesses {5, 10} cm are calculated as:

$$D_{\text{bin}} = D_{\text{int},0-15} \frac{h_{\text{bin}}^2}{(5^2 + 10^2)\ \text{cm}^2} \tag*{Eq. 6-1}$$

Where:

D_{bin}	Days in the h_{bin} bin.
$D_{\text{int},0-15}$	Days of ice thickness interval, for interval [0-15[cm.
h_{bin}	Ice thickness bin, $h_{\text{bin}} \in \{5, 10\}$ cm.

The days in each of the bins for ice thicknesses {15, 20, 25} cm are calculated as:

$$D_{\text{bin}} = D_{\text{int},15-30} \frac{h_{\text{bin}}^2}{(15^2 + 20^2 + 25^2 + 30^2)\ \text{cm}^2} \tag*{Eq. 6-2}$$

Where:

D_{bin}	Days in the h_{bin} bin.
$D_{\text{int},15-30}$	Days of ice thickness interval, for interval [15-30[cm.
h_{bin}	Ice thickness bin, $h_{\text{bin}} \in \{15, 20, 25\}$ cm.

The 30 cm ice thickness bin is a combination of days from the [15-30[cm bin and the [30-50] cm bin. This is expressed as:

$$D_{\text{bin},30} = D_{\text{int},15-30} \frac{30^2}{15^2 + 20^2 + 25^2 + 30^2} + D_{\text{int},30-50} \tag*{Eq. 6-3}$$

Where:

D_{bin}	Days in the h_{bin} bin.
$D_{\text{int},15-30}$	Days of ice thickness interval, for interval [15-30[cm.
$D_{\text{int},30-50}$	Days of ice thickness interval, for interval [30-50] cm.

The results of the calculations using Eq. 6-1, Eq. 6-2, and Eq. 6-3 are shown in Table 6-5.

Winter with ice	**Days of occurrence of h_{bin}, D_{bin}**					
Year range	$h_{\text{bin}} =$ 5 cm	$h_{\text{bin}} =$ 10 cm	$h_{\text{bin}} =$ 15 cm	$h_{\text{bin}} =$ 20 cm	$h_{\text{bin}} =$ 25 cm	$h_{\text{bin}} =$ 30 cm
1962 to 1963	3.2	12.8	1.7	3	4.7	17.7
1965 to 1966	2	8	0	0	0	0
1969 to 1970	0	0	0.4	0.8	1.2	4.6
1978 to 1979	0	0	0.9	1.7	2.6	9.8
1981 to 1982	0	0	0.3	0.6	0.9	3.3
1984 to 1985	0.8	3.2	1.7	3	4.7	17.7
1985 to 1986	1.4	5.6	1.3	2.2	3.5	13
1986 to 1987	2.2	8.8	3.3	6	9.3	16.4
2009 to 2010	0.8	3.2	0	0	0	0
2010 to 2011	0.8	3.2	0	0	0	0
Sum	11.2	44.8	9.6	17.3	26.9	82.5

Table 6-5: Days of occurrence in each ice thickness bin calculated using Eq. 6-1, Eq. 6-2, and Eq. 6-3. The sum of days for each ice thickness bin is shown as well.

The findings in Table 6-5 are the number of days for all of the years considered in this report (1960-2023). For the design lifetime of the wind farm, the duration for each of the thickness bins in Table 6-5 is found as:

$$D_{\text{bin,lifetime}} = \frac{L_{\text{design}}}{63\text{ years}} \sum_{i_{\text{w}}} D_{\text{bin},i_{\text{w}}} \qquad \text{Eq. 6-4}$$

Where:

$D_{\text{bin,lifetime}}$	Days of occurrence for each ice thickness bin in the lifetime of the wind farm.
L_{design}	Design lifetime of the wind farm in years.
i_{w}	Index of winters in the selected range (1960/1961 – 2022/2023).
$D_{\text{bin,iw}}$	Days of occurrence for each ice thickness bin per winter.

The duration of 63 years in Eq. 6-4 is the number of winters used, i.e. the winters starting in years 1960 to 2023. Since the design lifetime of the WTGs is not known, the number of days of occurrence for each sheet ice thickness bin is calculated per year of WTG lifetime. Thereby, the yearly duration of mobile competent sheet ice is shown in Table 6-6.

Days of occurrence valid for	**Days of occurrence of h_{bin}**					
Years	$h_{\text{bin}} =$ 5 cm	$h_{\text{bin}} =$ 10 cm	$h_{\text{bin}} =$ 15 cm	$h_{\text{bin}} =$ 20 cm	$h_{\text{bin}} =$ 25 cm	$h_{\text{bin}} =$ 30 cm
63	11.2	44.8	9.6	17.3	26.9	82.5
1	0.178	0.711	0.152	0.275	0.427	1.310

Table 6-6: Total durations of sheet ice thicknesses for 63 years and for 1 year. The days of occurrence for the design lifetime of the wind farm can be calculated by multiplying the values in the bottom row by the wind farm lifetime in units of years.

7. Ice ridge parameters

In accordance with the DLCs of Table 3-1, the ice ridge geometry is a required input for the DLCs D6 from [IEC6131] and SeIc.3 from [DNV0437], in which pressure from an ice ridge must be applied to the substructure. This section summarises the ice ridge parameters to be used for the actions caused by the ice ridge. While little guidance on the modelling of ice ridges and their forces can be found in [IEC6131], sufficient information is found in [ISO19906]. Following Section A.8.2.4.5.1 of [ISO19906], the ice ridge is modelled as a typical first-year ice ridge as shown in Figure 7-1 with the accompanying parameters listed in Table 7-1.

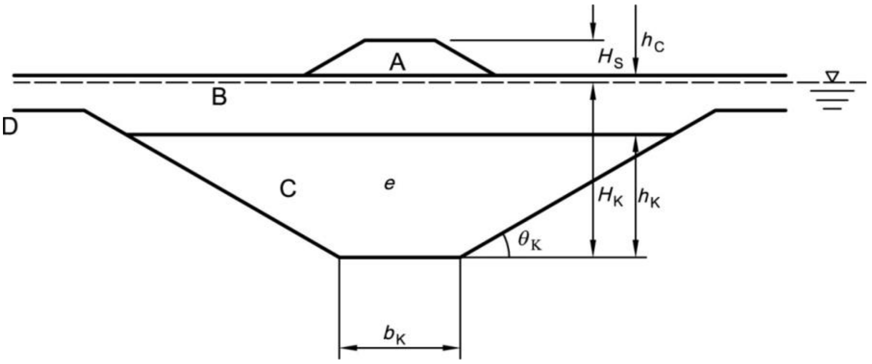

Figure 7-1: Idealised geometry of a first-year ice ridge. Reproduction of Figure A.8-16 of [ISO19906].

Item on Figure 7-1	Description	Value	Reference
A	Ridge sail.	-	-
B	Ridge consolidated layer.	-	-
C	Ridge keel.	-	-
D	Level ice (sheet ice).	-	-
H_s	Sail height.	1.73 m	According to Eq. 12 in [KANK] where the surrounding sheet ice is chosen as h_{50}: $H_s = 2.8\text{ m} \cdot \sqrt{h_{50}/\text{m}}$.
H_k	Keel depth.	7.79 m	Found as $4.5H_s$ in accordance with Section A.8.2.4.5.1 of [ISO19906].
h_c	Consolidated layer thickness.	0.61 m	See Section 7.2.
h_k	Distance between the base of the consolidated layer bottom and the base of the keel.	7.18 m	$H_k - h_c$.
b_k	Width of the base of the keel.	Not used	-
e	Porosity of ice rubble.	0.3	Table 7 in [KANK].
θ_k	Keel angle.	Not used	-

Table 7-1: Ice ridge definitions and dimensions.

To determine the actions caused by a first-year ice ridge, the methodology from Section A.8.2.4.5.1 in [ISO19906] is expected to be adopted in the calculation of the forces acting on the support structure by an ice ridge. The environmental parameters needed as an input to this method, as well as the thermal conductivity factor found in Appendix B, are listed in Table 7-2.

Parameter	Description	Value	Notes
β	Thermal conductivity factor.	0.9	See Section 7.1.
ϕ	Angle of internal friction in ice rubble in the keel.	30°	Section 7.3.
c	Apparent cohesion in ice rubble in keel.	5.5 kPa	Section 7.3.
ρ_w	Density of water.	1023 kg/m3	Based on Table 10-13 of [MA].
ρ_ice	Density of ice.	917 kg/m3	Table 6-1.
g	Acceleration of gravity.	9.817 m/s2	-
$C_\mathrm{R,A,NC}$	Ice (crushing) strength coefficient for non-compliant structures and large relative velocity between the support structure and ice.	0.65 MPa	Section 8.

Table 7-2: Environmental parameters to be used for structural ice ridge actions for DLCs D6 and Selc.3.

7.1 Consolidated layer thickness

The consolidated layer is shown schematically as area B in Figure 7-1. It contains a part of the ice rubble where the cavities between the ice blocks have frozen.

To calculate the action from the consolidated layer, the thickness of the layer, h_c, is needed as input. To simulate the thickness of the consolidated layer, the method as explained in Appendix B is reused, except that Eq. B-4 is modified by including a thermal conductivity factor, β, and the porosity of the ice rubble, e. It was found in Section 5.1.2 in [HØY2005] that using [STEFAN] to simulate the growth of the consolidated layer fits well with measurement if β is included in the calculation. The thermal conductivity factor, β, is included to account for the effect of thick ice, snow, oceanic flux, solar radiation, and the isolating effect of the sail of the ice ridge. The rubble porosity, e, is included to account for the assumption that the latent heat of melting is reduced by the rubble porosity as described in Section 4.7 of [HØY1999]. This yields the following equation for thermal ice growth as described in Section 4.7 of [HØY1999]:

$$h_{c,2} = \sqrt{h_{c,1}^2 + \beta \frac{2\kappa}{e\rho_\mathrm{ice} L_\mathrm{f}} S_\mathrm{f}} \qquad \text{Eq. 7-1}$$

Where:

$h_{c,1}$	Consolidated ice thickness at time t_1.
$h_{c,2}$	Consolidated ice thickness at time t_2.
β	Thermal conductivity factor.
κ	Thermal conductivity of ice.
ρ_ice	Density of ice.
e	Porosity of ice rubble.
L_f	Latent heat of melting for ice.
S_f	Cumulative freezing degree days between t_1 and t_2.

In Table 6 in [HØY2005], β was evaluated to be 0.9 for an ice ridge in Marjaniemi, whereas it was smaller for all the other ice ridges listed in ibid. As a conservative measure, $\beta = 0.9$ is chosen for the simulation of the consolidated layer thickness of the KG site.

It was found on pages 206 and 190 in [KANK] and Table 2 in [LEPP1992] that the thickness of the ice blocks inside the ice ridge had a thickness of approximately 20 cm. This means that larger ice ridges do not form before the thickness of sheet ice is larger than approximately 20 cm. For sheet ice thickness smaller than 20 cm, the ice tends to raft instead of forming ridges according to page 190 in [KANK]. Therefore, in simulating the consolidated layer thickness, it is estimated that a single layer of sheet ice is already present at the beginning of the freezing of the consolidated layer, i.e. the initial thickness of the consolidated layer is 20 cm.

A simulation of h_c is performed using the same methodology as described in Section 6.2, but with Eq. B-4 replaced by Eq. 7-1. The results are shown together with the sheet ice thickness from Section 6.2 in Figure C-1 and Figure C-2 for the winters with potentially competent ice where the maximum sheet ice thickness exceeds 20 cm. The results are summarised in Table 7-3, where a comparison with the sheet ice thicknesses is shown as well.

Winter with ice	Maximum consolidated layer thickness, h_c	Maximum sheet ice thickness, h	h_c/h
[year range]	[cm]	[cm]	[-]
1962 to 1963	78	48	1.63
1965 to 1966	44	30	1.47
1969 to 1970	47	32	1.47
1978 to 1979	48	32	1.50
1981 to 1982	53	35	1.51
1984 to 1985	57	36	1.58
1985 to 1986	49	33	1.48
1986 to 1987	59	38	1.55
2009 to 2010	-	18	-
2010 to 2011	-	15	-

Table 7-3: Maximum consolidated layer thickness, h_c, for each winter with ice calculated from the thermal ice growth model. A comparison with the maximum sheet ice thickness, h, from Section 6.2 is shown as well.

7.2 50-year consolidated layer ice thickness

As for the sheet ice thickness, a 50-year extreme consolidated layer thickness, $h_{\mathrm{c},50}$, must be established. The same extreme value analysis methodology as was used for the sheet ice thickness in Section 6.3 is applied to determine $h_{\mathrm{c},50}$, why the method is not repeated here. A plot of $h_{\mathrm{c},50}$ as a function of different start years in the dataset is shown in Figure 7-2. A similar tendency to the one found for h_{50} is observed in Figure 7-2.

In Section 6.3, the value of h_{50} was determined to be 38 cm representing the approximate start year of 1976. The 50-year consolidated ice thickness is determined to $h_{\mathrm{c},50} \approx 61$ cm by selecting the same start year in Figure 7-2. This corresponds to the ratio:

$$R_{\mathrm{c},50} = \frac{h_{c,50}}{h_{50}} = \frac{61}{38} = 1.61 \qquad \text{Eq. 7-2}$$

Where:

$R_{\mathrm{c},50}$	Ratio of 50-year consolidated layer thickness to 50-year sheet ice thickness.

$h_{c,50}$ 50-year consolidated layer thickness.
h_{50} 50-year sheet ice thickness.

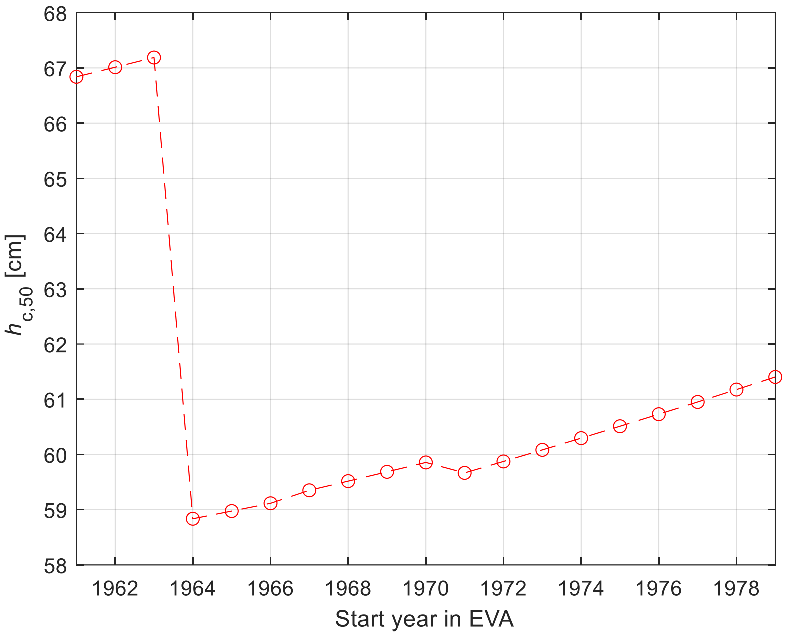

Figure 7-2: $h_{c,50}$ as a function of the start year in the dataset used for the extreme value analysis.

In Section A.8.2.4.5.1 in [ISO19906], it is mentioned that a typical ratio h_c/h is 1.6. This is almost identical to the value found in Eq. 7-2 and in the upper range of the ratio shown in Table 7-3. Thus, the design choice for the 50-year consolidated layer is:

$\boldsymbol{h_{c,50}} =$ **0.61 m.** **Valid for the entire site.**

7.3 Friction angle and cohesion of ice ridge keel

The angle of internal friction, ϕ, and the cohesion, c, are directly related. In Section A.8.2.8.8 in [ISO19906], the angle of internal friction is recommended to be between 25° and 45°. The relation to cohesion is found from the experiments referenced in Section 3 in [HEINO]. The relationship between c and ϕ is shown for five different experiments and reproduced in Figure 7-3. The experiments were conducted as punch test cases at the northern part of the Gulf of Bothnia, west of the island Hailuoto, Finland where the cumulative freezing degree days, S_f, (see Eq. B-5) is much larger than for the KG site at the return periods used in the present report. Since cohesion increases with increasing S_f, it is expected that the cohesion for the KG site is in the lower range compared to the tests from [HEINO]. By selecting a friction angle of 30°, the value of c is estimated to be 5.5 kPa as indicated with the red circle in Figure 7-3.

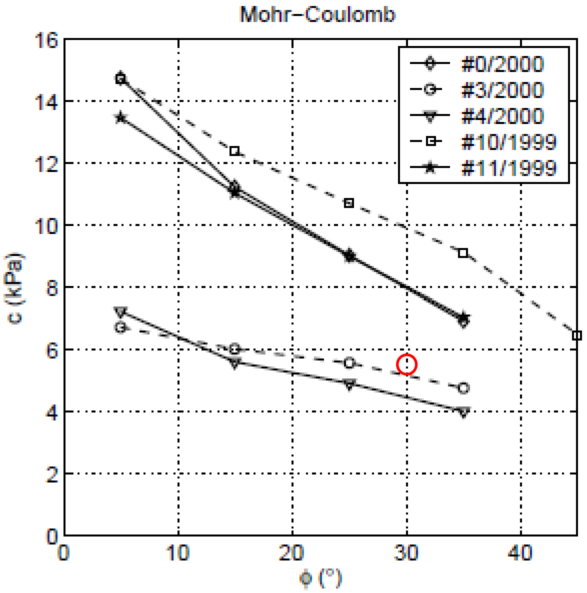

Figure 7-3: Relation between friction angle, ϕ, and cohesion, c, for the Mohr-Coulomb material model from 5 different experiments of a punch test. The red circle indicates the chosen design parameters. Reproduced from Figure 7.14 of [HEINO].

8. Crushing failure mode ice strength coefficient

For calculation of the global action for crushing of sheet ice, as well as from the consolidated layer part of the ice ridge, Equation A.8-21 of [ISO19906] may be used for the global ice pressure:

$$P_{\mathrm{G}} = C_{\mathrm{R}}\left(\left(\frac{h}{h_1}\right)^n\left(\frac{w}{h}\right)^m + f_{\mathrm{AR}}\right) \qquad \text{Eq. 8-1}$$

Where:

P_{G}	Global ice pressure.
C_{R}	Ice crushing strength coefficient.
h	Ice thickness (both sheet ice and consolidated layer).
h_1	Reference thickness = 1 m.
n	$= \begin{cases} -0.50 + h/(5h_1) & \text{for } h < 1.0 \text{ m.} \\ -0.30 & \text{for } h \geq 1.0 \text{ m.} \end{cases}$
w	Projected width of the support structure.
m	Empirical exponent = -0.16.
f_{AR}	Empirical term.

Here, the consolidated layer of the ice ridge is treated by the same equation as for sheet ice, in line with the recommendation of Section A.8.2.4.5.1 of [ISO19906]. Additionally, it is also assumed that the ratio between the structural width and the ice thickness is greater than 5 ($w/h > 5$) why the term f_{AR} can be disregarded according to the statement below Equation A.8-22 in [ISO19906]. This assumption is most likely fulfilled for the outer diameter of the support structures at the KG site considering the size of the newest generation of offshore WTGs. Next, the horizontal force from the sheet ice, or consolidated layer, is found according to Equation A.8-20 in [ISO19906] as:

$$F_{\mathrm{G}} = P_{\mathrm{G}} \cdot h \cdot w \qquad \text{Eq. 8-2}$$

Where:

F_{G}	Global ice force.
P_{G}	Global ice pressure.
h	Ice thickness (either of sheet ice or of the consolidated layer).
w	Projected width of the structure.

Eq. 8-1 and Eq. 8-2 apply to rigid support structures. In Section A.8.2.4.3.3 in [ISO19906], it is stated that the value of C_{R} is dependent on the compliance of the support structure that the ice is interacting with. For compliant support structures, a magnification of C_{R} can be expected. This goes in combination with the relative velocity between the ice and the support structure since the crushing strength of the ice will increase for small relative velocities. This effect shall be taken into account in the methods used in the Integrated Load Analysis (ILA).

8.1 1-year ice strength coefficient

In the DLC overview of Table 3-1 the 1-year ice crushing strength coefficient is marked as a required input for the DLCs D3 and D8 corresponding to the DLCs SeIc.1 and SeIc.4 respectively. The strength of the ice depends on the exposure to ice events. This is shown in Table A.8-4 of [ISO19906] where a list of C_R values for various return periods are shown. This table also correlates the total distance of ice travelling through the wind farm with the return period and C_R. In the points above Table A.8-4 of ibid., it is stated that the actions from an Extreme Level Ice Event (ELIE) should be based on the maximum actions from the following combinations:

1. 1-year return period value of C_R paired with a 100-year return period ice thickness.
2. 100-year return period value of C_R paired with a 1-year return period ice thickness.

The ice thickness for a 1-year return period is 0 cm for the KG site since winters with ice occur far less commonly than every year: this rules out Item 2 above. The same approach as outlined in [ISO19906] is reused here, except that the return period of 100 years is exchanged with 50 years for Item 1. This is also in line with Table 9-3 of [DNV0437]. It is shown in Table A.8-4 of [ISO19906] that C_R depends on the exposure to ice events. This table also correlates the total distance of ice travelling through the wind farm with the return period and C_R. The total distance of ice travelling through the evaluated KG wind farm in one year, D_year, is calculated as:

$$D_\mathrm{year} = U_\mathrm{i,mean} \cdot T_\mathrm{year} \cdot 3600 \frac{\mathrm{s}}{\mathrm{hour}} \cdot 24 \frac{\mathrm{hours}}{\mathrm{day}} \approx 45.0 \frac{\mathrm{km}}{\mathrm{year}} \qquad \text{Eq. 8-3}$$

Where:

$U_\mathrm{i,mean}$	Mean ice drift velocity of mobile ice = 0.40 m/s.
T_year	Total number of days with mobile ice per year = 1.31 days/year. The 30 cm bin from Table 6-6.

The mean ice drift velocity, $U_\mathrm{i,mean}$ for the selected reference location *'KG-3'* is determined from the histogram of Figure 5-8, in which the ice drift velocity is estimated based on a reference ice floe of 1 km^2 driven by wind- and current. From Figure 5-8, an approximate mean ice drift velocity of 0.4 m/s is determined. In addition, the normal current profiles of Figure 6-16 of [MA], reproduced in Figure 5-9, suggest that surface currents for winter periods of up to 0.3 m/s are representative of the KG site, which is in line with the findings of Figure 5-8 where both wind and current are driving the ice floe. Please remember that a large ice drift velocity is conservative when establishing C_R.

The total number of days with mobile ice, T_year is determined using the durations of sheet ice thicknesses of 30 cm or above. The reason for including only the durations for 30 cm ice thickness or higher is that the C_R-value wanted is to be used for ULS DLCs, which is to be combined with the 50-year ice thickness, whereas thinner ice would lead to smaller load effects in spite of having potentially slightly larger C_R-values.

The values of C_R for a 1-year return period for a total distance of 6 km/year is determined to be 0.99 MPa using Table A.8-4 in [ISO19906]. The total distance of ice thicker than 30 cm travelling through the KG site is calculated to be approximately 45.0 km/year in Eq. 8-3 which is closer to the 6 km/year stated in Table A.8-4 in [ISO19906] than the following entry for 135 km/year. The use of this method for the site is substantiated by the conclusion of [FUGLEM], a reference which itself is referenced just below Table A.8-4 of [ISO19906] in connection with the use of this table.

A final source used for the justification of the determined C_R value is [JUSS], from which Figure 6 shows a comparison plot of a time series produced from a simulation model with a measured time series from the Nordströmsgrund Lighthouse. The sea ice conditions near the Nordströmsgrund Lighthouse are more severe than those at the evaluated site and the plot corresponds to a sheet ice thickness larger than the 50-year value at the KG site. Moreover, as stated in Table 2 of [JUSS], the figure is made using a value of C_R = 1.0 MPa.

On the basis of this discussion, the present report selects the following value of the 1-year strength coefficient, $C_{\mathrm{R},1,\mathrm{NC}}$, for the evaluated site:

$C_{\mathbf{R},1,\mathbf{NC}}$ = 0.99 MPa. **Valid for the entire site.**

Here the subscript **NC** indicates that this value can only be used for non-compliant support structures, or for large relative ice-structure velocities (> 0.1 m/s) between the ice and the support structure. For smaller relative velocities, or for compliant support structures, the effects of a larger ice strength coefficient shall be taken into account in the Integrated Load Analysis (ILA). A suggestion for the value of C_R, where this is accounted for, is listed in Table A.8-3 in [ISO19906]. Here a value of C_R= 1.8 MPa is suggested for the Baltic Sea[6]. It is noted that this value is conservative for the site as this is for a site with up to ca. 1000 freezing-degree days per winter – far more severe than the conditions reported in the area of the evaluated KG site.

8.2 Average ice strength coefficient

As per the DLC overview of Table 3-1, the average ice crushing strength coefficient is needed for the DLCs of D4, D6, D7, and SeIc.3. In the DLCs listed in Table 3 of [IEC6131], it is noted that the WTG is parked while exposed to the loads from an ice ridge in DLC D6. Since the WTG is expected to be in the power production condition far more often than the parked condition, the probability of an event with power production combined with the loads from an ice ridge is higher than the probability of an ice ridge exposure combined with parked WTG condition. Therefore, it is recommended by C2Wind to supplement the DLC D6 from Table 3 of [IEC6131] with the EDLC SeIc.3 from Table 9-3 of [DNV0437] which combines power production with an ice ridge event. For EDLC SeIc.3 it is stated that ice ridge geometry corresponding to a 50-year return period should be combined with average strength parameters, i.e. an average of C_R.

While some guidance is given in Section A.8.2.4.3.3 of [ISO19906] on how to reduce the C_R-value to correspond to smaller return periods, no detailed guidance on how to find average values is explicitly given therein. Instead, the measured global pressure at the Nordströmgrund Lighthouse outlined in Figure 9 of [POAC11] forms the basis for an average value of C_R. A reproduction of the measured global pressure, P_G, from Figure 9 of [POAC11] is shown to the left in Figure 8-1. Using Eq. 8-1 with a panel width w = 7.5 m, C_R for each point is shown to the right. An average value of C_R is found by taking the mean of all points where h < 50 cm. The reason for not including measured global pressure

---

[6] In [POAC9], a suggestion for the calculation of C_R based on the structural compliance is presented. It is assessed that the value of C_R = 1.8 MPa may be highly conservative for the analyses for this site.

when the sheet ice thickness is above 50 cm is that it would be non-conservative to do so, since C_R tends to drop for larger values of h.

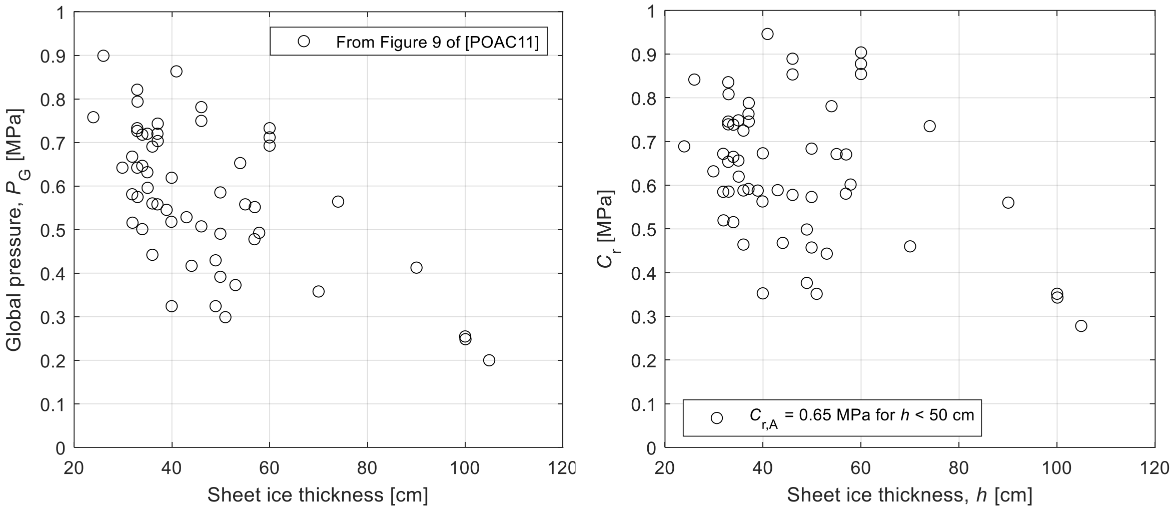

Figure 8-1: **Left:** Global pressure, P_G, measured at the Nordströmgrund Lighthouse. Reproduction of Figure 9 of [POAC11]. **Right**: Calculated C_R-values using the measured P_G in Eq. 8-1 with w = 7.5 m. The average value, $C_\mathrm{R,A}$, is found as 0.65 MPa for h < 50 cm.

Furthermore, Figure 10 of [POAC11], reproduced in Figure 8-2, shows how both local- and global extreme ice pressures depend on the return period. Here, two structural widths are shown, corresponding to the width of pressure panels, and the entire structural width, in the full-scale experiments on the Nordströmsgrund Lighthouse, described in [POAC11]. The waterline width of the support structures for the evaluated KG site is expected to be comparable to that of the green curve shown in Figure 8-2.

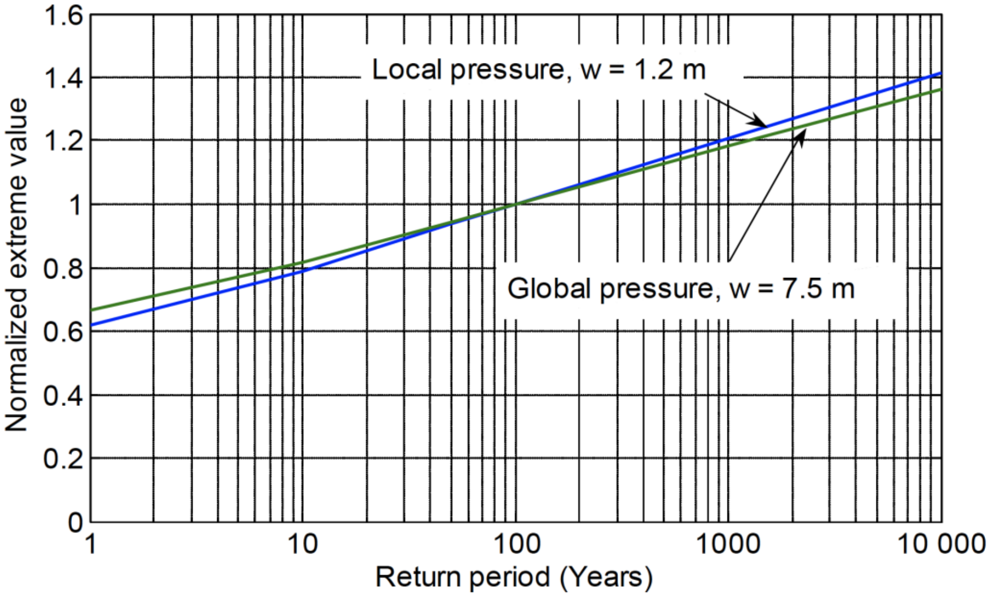

Figure 8-2: The figure shows extreme values of global- and local ice pressures, based on extreme value analyses on measurements on the Nordströmsgrund Lighthouse. Reproduction of Figure 10 of [POAC11].

On the basis of the discussion above, the following average strength coefficient, $C_{\mathrm{R,A,NC}}$, is chosen for the evaluated KG site:

$C_{\mathrm{R,A,NC}}$ = 0.65 MPa. **Valid for the entire site.**

As for the 1-year ice strength coefficient, the subscript **NC** is included to indicate that this value is only applicable for non-compliant support structures or for relative ice-structure velocities above 0.1 m/s.

9. Flexural failure mode parameters

In the situation where the support structures of the KG site are equipped with ice cones, the ice is more likely to fail in a flexural (i.e. bending) failure mode compared to a crushing failure mode. To determine the vertical and horizontal forces on the support structure from a flexural failure mode, the methodology in Section A.8.2.4.4 in [ISO19906] may be used. In addition to the parameters defined in Table 6-1, Table 7-1, and Table 7-2, the parameters shown in Table 9-1 must be used as well.

The parameters used for the simulation of the flexural failure mode of the sheet ice are not specified separately for ULS and FLS DLCs. This means that the same flexural failure parameters shall be used for all DLCs of Table 3 in [IEC6131].

Parameter	Variable	Unit	Value	Reference
Flexural strength of the ice sheet.	σ_{f}	MPa	0.5	See Section 9.1
Young's modulus of the ice sheet.	E_{f}	MPa	5000	See Section 9.2
Poisson's ratio for ice sheet.	ν	-	0.42	See Section 9.2
Coefficient of kinetic friction, ice-concrete.	μ_{ic}	-	0.15	See Section 9.3
Coefficient of kinetic friction, ice-ice.	μ_{ii}	-	0.10	See Section 9.3

Table 9-1: Input parameters to calculate vertical- and horizontal forces acting on the support structure from a flexural bending failure mode of sheet ice or consolidated layer of an ice ridge. The parameters are valid for the entire site.

9.1 Flexural strength of the ice sheet

An expression for determining the mean flexural strength of the ice sheet is shown in Equation A.8-96 of [ISO19906]. Here, the flexural strength depends on the brine volume fraction in the ice, which is unknown for the sheet ice and consolidated layers at the KG site. Instead, the results obtained by [CHRSKO] and reported in [POAC3] for the Great Belt in Denmark are used[7]. The analysis done in [CHRSKO] was intended to be used for the design of the Great Belt West Bridge. The 50-year flexural strength in Table 1 in [POAC3] is reported as 0.5 MPa, which is also noted as a typical upper value in Section A.8.2.8.3 in [ISO19906].

9.2 Young's modulus and Poisson's ratio

An expression for the effective Young's modulus, E_{f}, as a function of brine volume fraction is given in Equation A.8-100 in [ISO19906]. Here, it is also mentioned that E_{f} depends on temperature and loading rate. As noted in Section 9.1, no information on brine volume is available for the evaluated KG site, whereas E_{f}-values of 3 GPa for saline water and 5 GPa for freshwater can be considered according to Section A.8.2.8.9 in [ISO19906]. As a conservative measure, 5 GPa is chosen to be representative for the KG site.

The recommended value for Poisson's ratio in Section A.8.2.8.9 in [ISO19906] is 0.42. This includes some deformation of non-elastic- or creep behaviour which is recommended to be used for design.

---

[7] The author of this report was not able to find the data in [CHRSKO] which is referenced in Table 1 in [POAC3]. Nevertheless, the values from [POAC3] is still used as a reference in this report.

9.3 Coefficients of kinetic friction

To evaluate the frictional forces from the ice sliding on the ice-cone, the kinetic frictional coefficient is needed. This depends on the sliding velocity and on the surface roughness of the ice-cone. Suggestions are given in Table A.8-7 in [ISO19906] for various types of construction materials for the ice-cone and for different sliding velocities. Section D.4.4.3 of [IEC6131] states that a value of 0.15 may be used for ice-concrete or ice-corroded steel. For comparison, the value for rough concrete and a sliding velocity of 0.1 m/s in Table A.8-7 in [ISO19906] is 0.1. On this basis, a value of 0.15 is chosen as the friction coefficient between ice and concrete or corroded steel.

In the methodology in Section A.8.2.4.4 in [ISO19906], the ice-ice frictional coefficient is needed as well. In Section A.8.2.8.7, it is recommended to use 0.1 for the ice-ice friction, why this value is selected for the KG site.

10. Wind direction-ice drift coming direction misalignment

The evaluation of the misalignment between the ice drift coming direction[8] of sheet ice, and the hub height wind direction is of key importance in calculating FLS load effects on the support structure, particularly the substructure and the upper parts of the foundation. In cases where the ice drift direction and wind direction are misaligned, a WTG in operation will, due to the small damping in the WTG's side-side direction, experience larger dynamical load effects due to the interaction with the ice than when the directions are aligned. Thus, by providing analysis results of the misalignment between the ice drift coming direction and the wind direction, the present section answers an important question in assessing the severity of dynamical ice FLS loads.

10.1 Applied data

In Section 5.5, the reference location within the KG site, and associated hindcast datasets to use for the assessment of the wind direction-ice drift coming direction misalignment were selected. The ice drift coming direction is calculated based on the method outlined in Section 10.2 below. For this evaluation, the wind speed at 10 mDVR90 and at hub height as well as the wind direction at 10 mDVR90 are needed. Here, it is assumed that the wind direction is the same at 10 mDVR90 and at hub height. In addition, the current direction and speed, both of the latter two in the presence of ice, is needed. The present section gives an overview of the input data used.

The analyses in the present section use the hindcast dataset provided by the Client through, [HCCUDATA] and [HCWWDATA]. The hub height wind speed timeseries have been adjusted to match the omnidirectional Weibull *A* and *k* parameters from Section 9.1.1 of [WA] summarised in Table 10-1. Since there can only be ice during the winter season, the data used in this section is limited to only cover December, January, February, and March for each winter in the dataset. The earliest date for an ice observation in a winter season is determined as the 17th of December, see Table 5-1. The latest date of an ice observation is determined to 6th of April. Observed ice in April is however only seen for a single winter, as all other winters demonstrate a last ice observation date in March. Thus, the analysis is limited to include the aforementioned winter months.

The current timeseries used for the analysis is selected from the hindcast data of [HCCUDATA] in Section 5.5 as the layer with approximate mid-level at -12 mMSL.

The wind speed needed in Equation D.9 of [IEC6131], is the wind speed at 10 m above the ice surface. The wind speed is given at 10 mDVR90 in [HCWWDATA] which is used directly for this purpose, thereby neglecting the small part of sheet ice above 0 mDVR90.

---

[8] The reason for the somewhat cumbersome and long, name "Ice drift coming direction" is meant to clarify that the present report deals with the direction that ice comes *from* – just like wind direction *coming* direction (and oppositely to current direction, which is traditionally defined as a going-to direction). Thus, a wind-ice drift coming direction misalignment of zero means that the wind and ice approach from the same direction.

10.2 Ice drift direction

The ice drift direction depends on the interaction between wind, currents, and ice conditions. The influences from these depend on many ice-dependent factors, e.g. ice thickness, ice floe size, the initial speed of the ice floe, etc. Except for the ice thickness, which is the focus of Section 6, the other parameters affecting the ice drift direction are unknown. The ice drift direction time series is calculated according to the method stated in Section D.4.4.5 of [IEC6131]. Here, Equation D.9 of ibid. is applied in calculating the vector of drag force per unit area acting on the ice due to wind and current, $\vec{F}_{\mathrm{drag}}$, where the wind velocity vector, $\vec{U}_{\mathrm{W}}$, and the current velocity vector, $\vec{U}_{\mathrm{C}}$, enter in Eq. 10-1[9]. The values used in the calculation are shown in Table 10-1.

$$\vec{F}_{\mathrm{drag}} = \vec{F}_{\mathrm{w}} + \vec{F}_{\mathrm{c}} = \frac{1}{2} C_{\mathrm{W}} \rho_a \left|\vec{U}_{\mathrm{W}}\right| \vec{U}_{\mathrm{W}} + \frac{1}{2} C_{\mathrm{C}} \rho_{\mathrm{w}} \left|\vec{U}_{\mathrm{C}}\right| \vec{U}_{\mathrm{C}} + \overrightarrow{PL} \tag{Eq. 10-1}$$

Where:

$\vec{F}_{\mathrm{drag}}$	Vector of the drag force, per unit horizontal area, acting horizontally on the ice.
$\vec{F}_{\mathrm{w}}$	Vector of the drag force from wind, per unit horizontal area, acting horizontally on the ice.
$\vec{F}_{\mathrm{c}}$	Vector of the drag force from currents, per unit horizontal area, acting horizontally on the ice.
C_{w}	Wind drag coefficient.
ρ_a	Density of air.
$\vec{U}_{\mathrm{W}}$	Wind velocity vector 10 m above the ice upper surface.
C_{c}	Current drag coefficient.
ρ_w	Density of water.
$\vec{U}_{\mathrm{c}}$	Current velocity vector (see Section 5.5.1).
$\overrightarrow{PL}$	Pack ice load vector.

Parameter	Variable	Unit	Value	Reference
Wind drag coefficient.	C_{w}	[-]	0.004	Recommended for the Baltic Sea in Section D.4.4.5 in [IEC6131].
Density of air.	ρ_a	[kg/m^3]	1.23	Section 9.1.4 of [WA].
Wind velocity.	$\vec{U}_{\mathrm{W}}$	[m/s]	-	Free stream wind velocity at 10 mDVR90 from [HCWWDATA].
Current drag coefficient.	C_{c}	[-]	0.006	Recommended for the Baltic Sea in Section D.4.4.5 in [IEC6131].
Density of water.	ρ_w	[kg/m^3]	1023	See Table 7-2.
Current velocity.	$\vec{U}_{\mathrm{c}}$	[m/s]	-	Current velocity from the layer at approximately -12 mMSL from [HCCUDATA].
Pack ice load vector.	$\overrightarrow{PL}$	[-]	-	Neglected.
Wind, Weibull scale parameter @ 150 mDVR90.	A	[m/s]	10.83	Mean values from Section 9.1.1 of [WA].
Wind Weibull shape parameter @ 150 mDVR90.	k	[-]	2.27	

Table 10-1: Input parameters to the drag force on ice in Eq. 10-1.

---

[9] For ease of reading, the present report denotes the horizontal forces per unit area by the symbol $\vec{F}$; i.e. implicitly assuming a unit area, instead of denoting it as a shear stress by the symbol $\vec{\tau}$.

In Eq. 10-1, the term $\overrightarrow{PL}$ (due to forces from pack ice) is neglected since this will on average have the same direction as the drag force. Next, the misalignment angle between the ice drift coming direction and the wind direction is calculated and shown in Figure 10-1. In Table 10-2, the occurrence frequency table of wind-ice drift coming direction misalignment is shown. The wind velocity at hub height has been adjusted by use of the Weibull parameters for the KG site summarised in Table 10-1. Please note, that the adjustment of the wind speed at hub height by use of the Weibull parameters has been performed for the complete time series. Since only the winter season is used to create the misalignment table in Table 10-2, the wind speed distribution in the rightmost column does not correspond exactly to the Weibull parameters from Table 10-1.

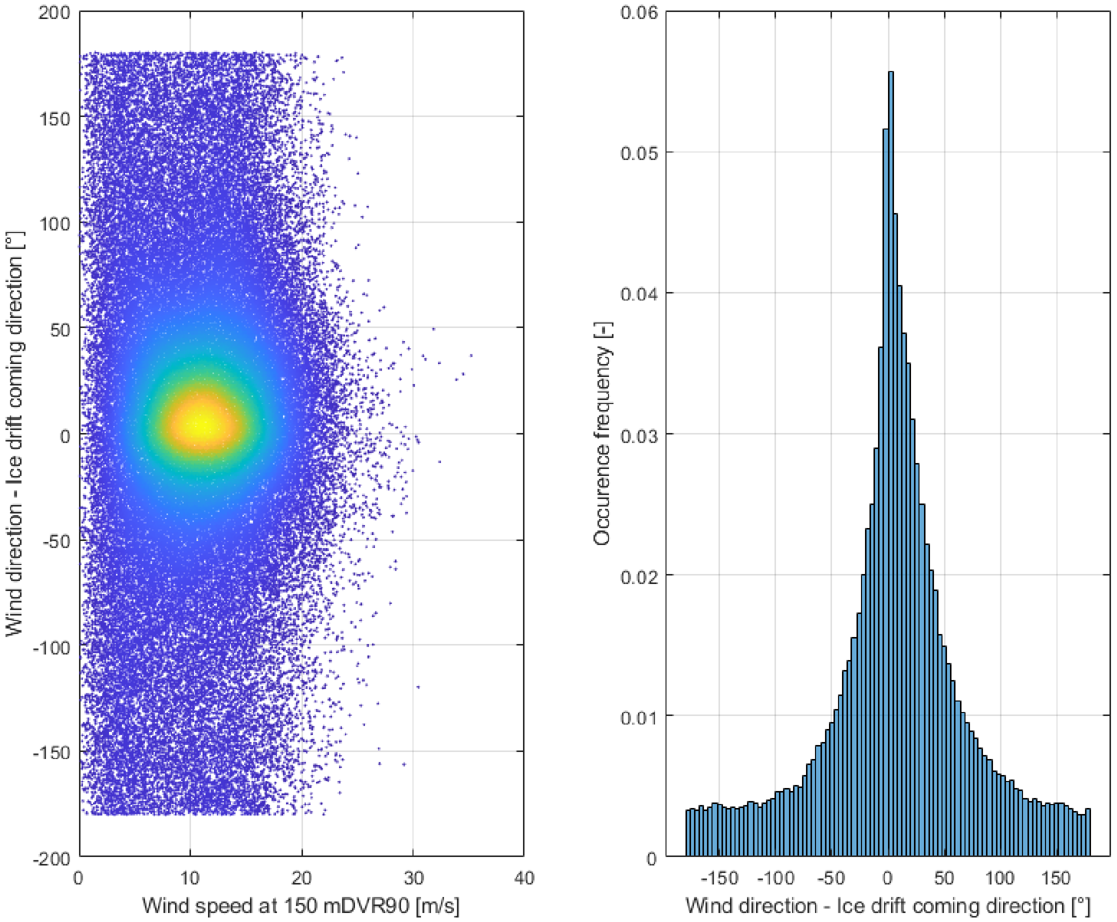

Figure 10-1: Density scatter plot of wind-ice drift coming direction misalignment as a function of wind speed at 150 mDVR90 (left) and histogram of wind-ice drift coming direction misalignment occurrences (right). The ice drift vector's direction is the same as the direction of the drag vector, $\vec{F}_{\mathrm{drag}}$, from Eq. 10-1.

For completeness, a plot of the occurrence frequency of the surface current speed selected in Section 5.5 is shown in Figure 10-2 below.

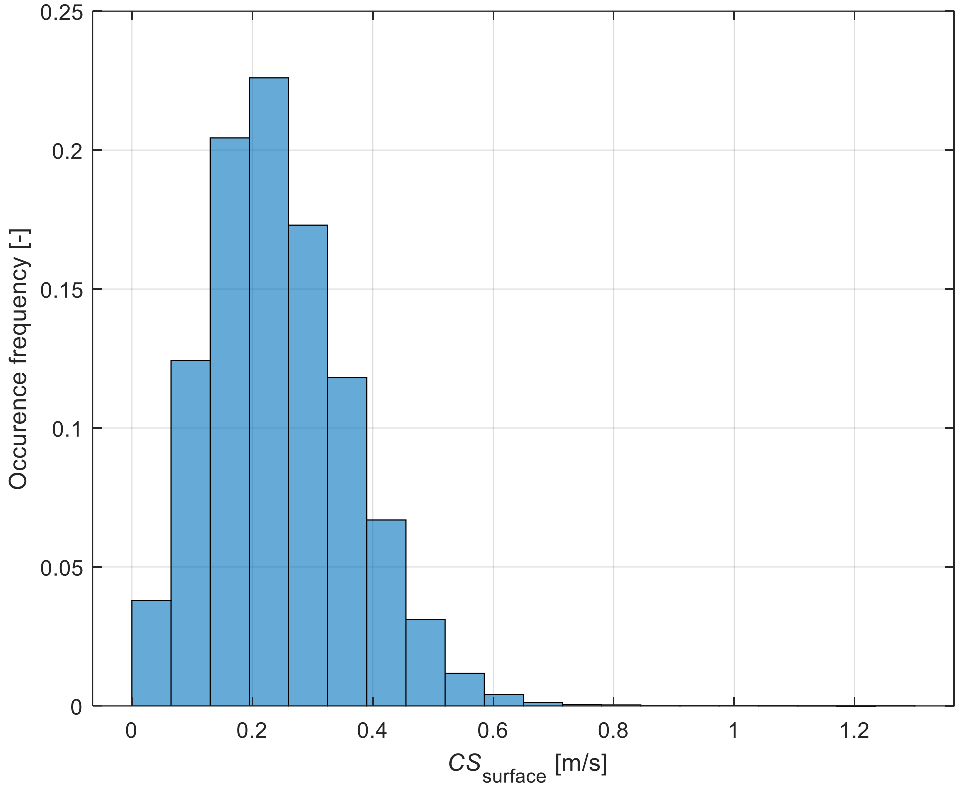

Figure 10-2: Occurrence frequency of the surface current speeds used for the evaluation of the wind-ice drift direction misalignment. The surface current timeseries was selected in Section 5.5.1.

Wind Speed @150 mDVR90,			Misalignment angle (WindDir – Ice drift coming dir). Bins span Centre +/- 15°, including lower limit only.												Sum over all misalignment angles
Bin min [m/s]	Bin mean [m/s]	Bin max [m/s]	0	30	60	90	120	150	180	210	240	270	300	330	
0	1.25	2.5	3.27E-03	3.03E-03	2.39E-03	2.54E-03	2.31E-03	1.97E-03	1.95E-03	2.06E-03	2.30E-03	2.31E-03	2.67E-03	2.99E-03	2.98E-02
2.5	3	3.5	4.22E-03	3.34E-03	2.78E-03	2.13E-03	1.69E-03	1.63E-03	1.68E-03	1.75E-03	1.80E-03	2.11E-03	2.60E-03	3.26E-03	2.90E-02
3.5	4	4.5	6.97E-03	5.68E-03	3.72E-03	2.72E-03	2.12E-03	1.94E-03	1.60E-03	1.94E-03	2.16E-03	2.48E-03	3.14E-03	4.60E-03	3.91E-02
4.5	5	5.5	1.01E-02	7.13E-03	4.41E-03	2.93E-03	2.12E-03	1.61E-03	1.59E-03	1.83E-03	2.08E-03	2.18E-03	3.23E-03	5.50E-03	4.47E-02
5.5	6	6.5	1.34E-02	8.95E-03	5.32E-03	2.91E-03	2.06E-03	1.52E-03	1.43E-03	1.62E-03	1.79E-03	2.55E-03	3.83E-03	6.40E-03	5.18E-02
6.5	7	7.5	1.83E-02	1.16E-02	5.66E-03	2.95E-03	1.89E-03	1.69E-03	1.24E-03	1.42E-03	1.70E-03	2.10E-03	3.80E-03	7.49E-03	5.99E-02
7.5	8	8.5	2.16E-02	1.39E-02	5.55E-03	2.67E-03	1.87E-03	1.52E-03	1.21E-03	1.52E-03	1.55E-03	2.16E-03	3.93E-03	8.53E-03	6.60E-02
8.5	9	9.5	2.54E-02	1.45E-02	5.87E-03	3.09E-03	1.92E-03	1.44E-03	1.25E-03	1.38E-03	1.56E-03	2.56E-03	4.51E-03	9.01E-03	7.25E-02
9.5	10	10.5	2.80E-02	1.57E-02	5.77E-03	3.16E-03	2.04E-03	1.76E-03	1.51E-03	1.55E-03	1.67E-03	1.98E-03	4.50E-03	8.85E-03	7.64E-02
10.5	11	11.5	2.86E-02	1.61E-02	6.47E-03	3.24E-03	2.09E-03	1.86E-03	1.63E-03	1.63E-03	1.81E-03	2.16E-03	3.76E-03	9.45E-03	7.88E-02
11.5	12	12.5	2.78E-02	1.65E-02	6.55E-03	3.70E-03	2.43E-03	1.84E-03	1.70E-03	1.33E-03	1.49E-03	2.01E-03	3.51E-03	9.41E-03	7.83E-02
12.5	13	13.5	2.54E-02	1.50E-02	6.06E-03	3.77E-03	2.64E-03	1.73E-03	1.61E-03	1.74E-03	1.31E-03	2.14E-03	3.54E-03	8.43E-03	7.33E-02
13.5	14	14.5	2.32E-02	1.30E-02	6.07E-03	3.73E-03	2.20E-03	1.84E-03	1.37E-03	1.65E-03	1.47E-03	1.94E-03	3.37E-03	8.23E-03	6.81E-02
14.5	15	15.5	1.95E-02	1.18E-02	5.47E-03	3.04E-03	1.80E-03	1.65E-03	1.48E-03	1.17E-03	1.35E-03	1.78E-03	3.20E-03	6.94E-03	5.91E-02
15.5	16	16.5	1.55E-02	9.79E-03	4.93E-03	2.54E-03	1.59E-03	1.12E-03	1.24E-03	1.06E-03	9.56E-04	1.26E-03	2.74E-03	5.71E-03	4.84E-02
16.5	17	17.5	1.12E-02	8.47E-03	3.93E-03	1.95E-03	1.05E-03	9.64E-04	8.16E-04	9.56E-04	8.09E-04	9.72E-04	2.22E-03	5.18E-03	3.85E-02
17.5	18	18.5	7.99E-03	5.93E-03	3.02E-03	1.52E-03	9.10E-04	6.45E-04	4.04E-04	7.23E-04	7.07E-04	8.63E-04	1.56E-03	3.87E-03	2.82E-02
18.5	19	19.5	5.47E-03	4.64E-03	2.18E-03	1.26E-03	5.13E-04	4.12E-04	3.34E-04	5.52E-04	4.43E-04	5.68E-04	1.29E-03	2.53E-03	2.02E-02
19.5	20	20.5	4.04E-03	3.02E-03	1.53E-03	7.31E-04	3.65E-04	1.71E-04	1.55E-04	2.18E-04	3.73E-04	4.74E-04	9.25E-04	2.36E-03	1.44E-02
20.5	21	21.5	2.17E-03	2.18E-03	1.14E-03	4.66E-04	2.18E-04	1.79E-04	1.09E-04	1.63E-04	2.64E-04	3.19E-04	7.31E-04	1.65E-03	9.59E-03
21.5	22	22.5	1.34E-03	1.45E-03	6.30E-04	2.18E-04	2.18E-04	9.33E-05	3.11E-05	1.79E-04	8.55E-05	2.10E-04	4.43E-04	1.06E-03	5.96E-03
22.5	23	23.5	1.04E-03	9.25E-04	2.80E-04	1.17E-04	3.11E-05	3.89E-05	3.11E-05	8.55E-05	1.09E-04	8.55E-05	1.94E-04	6.76E-04	3.62E-03
23.5	24	24.5	4.82E-04	4.90E-04	1.48E-04	0.00E+00	2.33E-05	1.55E-05	1.55E-05	2.33E-05	3.11E-05	7.77E-05	1.09E-04	3.73E-04	1.79E-03
24.5	25	25.5	3.11E-04	2.18E-04	7.00E-05	2.33E-05	1.55E-05	7.77E-06	0.00E+00	0.00E+00	3.89E-05	3.89E-05	1.01E-04	1.94E-04	1.02E-03
25.5	26	26.5	2.41E-04	1.71E-04	3.11E-05	0.00E+00	7.77E-06	0.00E+00	0.00E+00	7.77E-06	2.33E-05	2.33E-05	6.22E-05	1.40E-04	7.07E-04
26.5	27	27.5	1.40E-04	9.33E-05	1.55E-05	0.00E+00	0.00E+00	0.00E+00	0.00E+00	1.55E-05	7.77E-06	7.77E-06	7.77E-06	1.48E-04	4.35E-04
27.5	28	28.5	7.77E-05	5.44E-05	0.00E+00	0.00E+00	0.00E+00	0.00E+00	0.00E+00	0.00E+00	0.00E+00	7.77E-06	3.11E-05	5.44E-05	2.25E-04
28.5	29	29.5	7.00E-05	3.11E-05	0.00E+00	0.00E+00	0.00E+00	0.00E+00	0.00E+00	7.77E-06	0.00E+00	0.00E+00	0.00E+00	7.77E-05	1.87E-04
29.5	30	30.5	3.11E-05	2.33E-05	0.00E+00	0.00E+00	0.00E+00	0.00E+00	0.00E+00	0.00E+00	7.77E-06	0.00E+00	0.00E+00	7.77E-06	7.00E-05
30.5	31	31.5	7.77E-06	1.55E-05	0.00E+00	0.00E+00	0.00E+00	0.00E+00	0.00E+00	0.00E+00	0.00E+00	0.00E+00	0.00E+00	0.00E+00	2.33E-05
31.5	32	32.5	7.77E-06	7.77E-06	7.77E-06	0.00E+00	0.00E+00	0.00E+00	0.00E+00	0.00E+00	0.00E+00	0.00E+00	0.00E+00	0.00E+00	2.33E-05
32.5	33	33.5	0.00E+00	0.00E+00	0.00E+00	0.00E+00	0.00E+00	0.00E+00	0.00E+00	0.00E+00	0.00E+00	0.00E+00	0.00E+00	0.00E+00	0.00E+00
33.5	34	34.5	0.00E+00	7.77E-06	0.00E+00	0.00E+00	0.00E+00	0.00E+00	0.00E+00	0.00E+00	0.00E+00	0.00E+00	0.00E+00	0.00E+00	7.77E-06
34.5	35	35.5	0.00E+00	1.55E-05	0.00E+00	0.00E+00	0.00E+00	0.00E+00	0.00E+00	0.00E+00	0.00E+00	0.00E+00	0.00E+00	0.00E+00	1.55E-05

Table 10-2: Omni directional probabilities for wind-ice drift coming direction misalignment, given as $\theta_{\text{Wind}} - \theta_{\text{Ice}}$, as well as their sums over all misalignment angles (rightmost column) for all relevant wind speed bins. The ice drift direction is identical to the direction of the vector of the drag force, $\vec{F}_{\text{drag}}$, from Eq. 10-1.

A final topic that needs to be addressed is the directional wind speed distribution, which through the Wind-ice drift coming direction misalignment distribution in Table 10-2 will yield the ice drift direction distribution. This directional distribution is given in Table 26 of [WA] and is reproduced in Table 10-3.

Directional bin centre [°N]	0	30	60	90	120	150	180	210	240	270	300	330
Occurrence frequency [%]	4.82	4.22	5.33	6.64	7.96	7.97	7.73	12.6	13.3	14.7	9.81	4.94

Table 10-3: Directional occurrence frequencies (in percent) for the wind rose; reproduced from Section 9.1.1 of [WA].

For the purposes of sea ice FLS DLC ILA, the comparatively brief duration of sea ice at the site concluded in Section 6.4, does not warrant the precision implied by the use of wind speed distributions that depend on wind direction. Instead, as a reasonable simplification, the same wind speed distribution may be used for all wind directions in connection with sea ice FLS DLCs:

The wind direction distribution stated in Table 10-3 can be used to directionally weight the sea ice FLS DLC durations, together with – for all individual wind directions – the hub height wind speed distribution given by the rightmost column of Table 10-2.

Valid for the entire site.

11. Limiting mechanisms and ice action speeds

For DLCs D3, D4, D6, D7, and D8, it is necessary to analyse whether the sea ice forces subjected to the substructure are limited by a limit force-, limit stress-, or limit energy-mechanism as specified in Section A.8.2.4.1 of [ISO19906]. The limit force mechanism occurs when the interaction loads between the ice and the impacted support structure are insufficient to cause failure of the ice. The limit stress mechanism covers ice-structure interactions in which the ice fails adjacent to the support structure for a number of different failure modes. The limit energy mechanism is used for large ice objects such as ice-islands or icebergs in which the ice force loads are determined from the kinetic energy describing the momentum of the large ice object.

For the evaluated KG site, the limiting energy mechanism for the evaluation of ice forces from large ice objects is not considered. The potentially critical phenomenon of ice-induced vibrations can e.g. be caused by intermittent crushing of a competent ice floe. As the failure mode is sudden ice crushing following a build-up of load over time, ice-induced vibrations are considered a combination of the limit force-, prior to ice failure, and the limit stress-, at ice failure, limiting mechanisms.

In addition to the consideration of the limiting mechanism for the ice, it is necessary to establish the possible range of speeds that the sea ice can have when it passes the support structure, i.e. the range of possible ice action speeds.

The concept of ice action speed is explained in Section 2 of [KARNA20] including Figure 1, which is reproduced in Figure 11-1 including a brief explanation in the caption. The schematic ice action displacements and -speeds are shown in Figure 11-2.

The importance of distinguishing between the speed of ice far from the support structure, named free-field ice speed in Section 2 of [KARNA20], and ice action speed, is that the current speed necessary to obtain driving forces large enough to make the sea ice mobile is also so large that it surpasses the ice action speed range where ice-induced vibrations can occur; see Section 2.3 of [KARNA20] for a discussion of this. Thus, if one simply uses the near-surface current speed histogram at the site, such as that of [HCCUDATA] to prescribe ice action speeds, one may correctly estimate the free-field ice speed (i.e. that of Floe 2 in Figure 11-1), but underestimate the occurrence frequency of ice action speeds in the range that can lead to ice-induced vibrations. Thus, it is necessary to investigate how the free-field ice speed relates to the possible ice action speeds. Such a study is made in Sections 2.1 to 2.2 of [KARNA20][10] for a situation, which has some qualitative similarities to that of the KG site.

---

[10] Although this study in Sections 2.1 to 2.2 of [KARNA20] used somewhat thicker ice for Floe 1 than that of the present report, its results are still conservatively transferable to the KG site. Among other reasons, it is conservatively transferable since the study in [KARNA20] used a very large ice floe size, leading to possibilities for a wide range of ice action speeds being realised (which may not be attainable with a smaller floe, that may have passed entirely before Floe 1 is slowed down to the ice action speeds capable of inducing ice-induced vibrations).

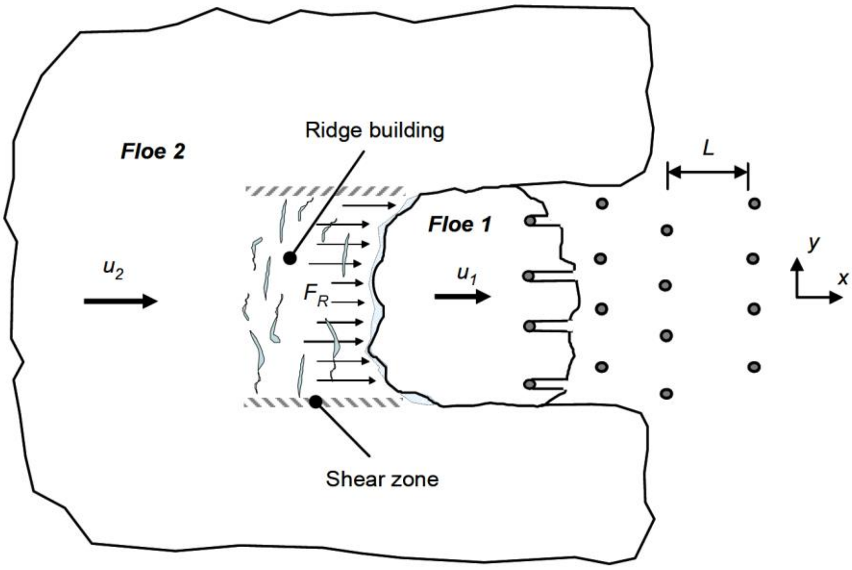

Figure 11-1: Illustration of the interaction between a large ice floe and a set of support structures (grey circles). The ice floe is initially composed of both Floe 1 and Floe 2, but the interaction with the support structures slows down Floe 1 to a speed u_1, which is smaller than that of Floe 2, u_2. Through ridge building and rafting, Floe 1 is pushed by Floe 2, allowing the speed u_1 to be reduced to smaller values capable of inducing ice-induced vibrations according to Section 2.3 of [KARNA20]. Reproduction of Figure 1 of [KARNA20].

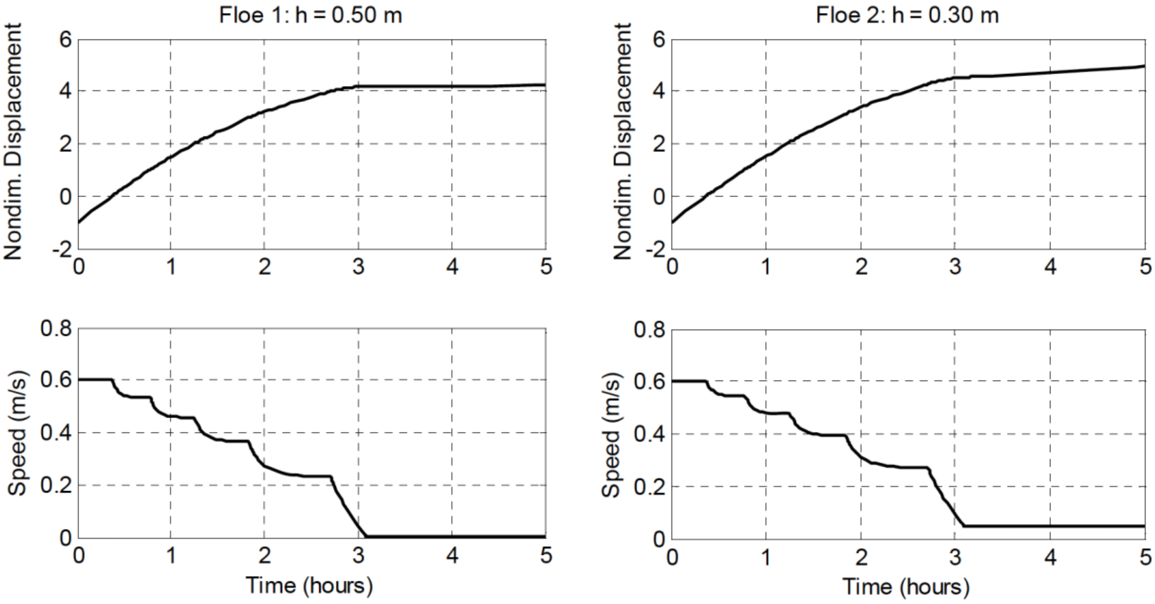

Figure 11-2: Schematic results for ice speeds of Floe 1 and Floe 2 shown in Figure 11-1, for the setup described in Sections 2.1 and 2.2 of [KARNA20]. Although the setup is somewhat different for the KG site, the qualitative situation is similar, where the ice action speed (of Floe 1) decreases stepwise, maintaining quasi-constant ice action speeds for tens of minutes, before possibly coming to a halt. Reproduction of Figure 2 of [KARNA20].

While it is sufficient to know the range of possible ice action speeds for ULS DLCs, it is also necessary to establish the occurrence frequencies for various ice action speeds to evaluate the FLS DLCs.

11.1 Ice action speeds for ULS DLCs

The sparse information on current conditions during severe winters with ice necessitates a large degree of conservatism when evaluating the ice action speeds. Thus, it is necessary to consider that large, or small, current speeds could potentially occur during the occurrence of the 50-year sheet ice thicknesses at the site, as well as during the occurrence of potential ice ridges. It can be seen conceptually from Figure 2 of [KARNA20] that periods of tens of minutes of semi-constant ice action speed can be attained as Floe 1 is slowed down. The ice action speeds of these periods can range from values of more than the 50-year current speed value down to close to 0 m/s. The 50-year surface current speed of 1.8 m/s is listed in Section 6.2.1 of [MA]. Following figure A.8.30 of [ISO19906], higher ice action speeds lead to continuous brittle crushing of the ice resulting in quasi-station ice loads. Thus, a smaller upper bound, than the 50-year surface current is selected for the evaluation of the ULS DLCs why:

Ice action speed range for dynamical ULS DLCs (D3 and D8): The values in Table 11-1.

Valid for the entire site.

Note, for the ULS evaluation of support structure designs containing an ice cone, ice action speeds up to the 50-year surface current should be evaluated, as the load effects from the ice are dependent on the ice speed for these designs. This should be performed in order to verify if the bending failure frequency of the ice could coincide with the natural frequency of the structure.

11.2 Ice action speeds for FLS DLCs

As shown in Figure 10-2, there is a tendency for small current speeds to occur more often than large current speeds. Furthermore, the mechanism shown in Figure 11-1, and the schematic results shown in Figure 11-2, demonstrate that the ice is progressively slowed down when impacting the wind farm, making smaller ice action speeds occur more often than large ones. The present report will assume that these effects cancel out the tendency for ice to be immobile at very small ice action speeds, why the ice action speeds used will be those corresponding to the surface current speed histogram in Figure 10-2 with a finer sampling. The reason for only using the current alone and not a combination of current and wind to determine the occurrence frequency of ice action speed, is that current alone gives higher occurrence frequencies for small ice action speeds which is conservative. This can be proven by comparison of the ice drift velocity histogram from Figure 5-8 These values are given in Table 11-1. As a consequence of the above points:

The relative occurrence frequencies of sea ice action speeds for FLS DLCs are given in Table 11-1.

Valid for the entire site.

Ice action speed	**Relative occurrence frequency**	**Ice action speed**	**Relative occurrence frequency**
[m/s]	[-]	[m/s]	[-]
0.01	0.001	0.21	0.036
0.02	0.003	0.23	0.072
0.03	0.004	0.25	0.070
0.04	0.006	0.27	0.062
0.05	0.008	0.29	0.056
0.06	0.010	0.31	0.050
0.07	0.012	0.33	0.047
0.08	0.015	0.35	0.041
0.09	0.017	0.37	0.035
0.10	0.018	0.39	0.030
0.11	0.020	0.41	0.116
0.12	0.024		
0.13	0.025		
0.14	0.026		
0.15	0.029		
0.16	0.031		
0.17	0.034		
0.18	0.033		
0.19	0.033		
0.20	0.034		

Table 11-1: Relative occurrence frequencies of the ice action speed. The values are found from a finer sampling of the current speed histogram shown in Figure 10-2. All ice action speeds larger than 0.41 m/s have been lumped into the value 0.41 m/s. These FLS ice action speed bins coincide with those specified for use in ULS Integrated Load Analysis at the end of Section 11.1.

In Section A.8.2.6.1.2 of [ISO19906] it is stated that frequency lock-in can occur for intermediate ice speeds of 0.04 to 0.1 m/s for the Baltic Sea. To account for the sensitivity of the dynamic interaction to the ice speed in this range, the occurrence frequencies are reported with a fine sampling of 0.01 m/s. In addition, fine sampling is also applied to the ice speed range from 0.1 to 0.2 m/s to capture any potential ice-structure dynamic behaviour not covered for ice speeds below 0.1 m/s. For ice speeds above 0.2 m/s, the ice failure will change to continuous brittle crushing for support structures without an ice cone. Thus, for these designs, all occurrences of ice speeds above 0.2 m/s may be combined in a single ice action speed for evaluation. However, for support structures equipped with an ice cone, the failure frequency for the ice is proportional to the ice speeds why these must be evaluated individually. As a result, ice action speeds above 0.2 m/s are included in Table 11-1 with a sampling of 0.02 m/s. Including the higher ice speeds in the structural evaluation of designs with an ice cone, can reveal coinciding ice failure- and natural eigenfrequencies otherwise overlooked.

11.3 FLS correlation between ice action speed and wind speed and -direction

Another topic that is necessary to address in order to perform FLS Integrated Load Analyses is the correlation between the wind speed at hub height and the ice action speed. Table 11-1 shows how often to apply the ice action speeds, and the directional wind speed occurrence frequencies can be found from the values in Table 10-2 and Table 10-3, but it is also necessary to specify how to match these together.

On the KG site, there is only a weak correlation between the ice drift direction and the hub height wind speed as shown in Figure 10-1. Furthermore, as discussed in [KARNA20], the ice action speed may be rather different from the far-field ice drift speed, which will tend to make the correlation even weaker. Thus, the present report will take the reasonable approach for sea ice FLS DLCs that the hub height wind speed and ice action speed should be treated as independent.

The hub height wind speed and sea ice action speeds for FLS DLCs shall be treated as uncorrelated. This means that:

a. **All hub height wind speed- and wind-ice drift coming directional misalignment values with (non-zero) occurrence frequencies in Table 10-2 shall be used, using the relative occurrence frequencies in that table.**
b. **All wind directions in Table 10-3 shall be used, using the relative occurrence frequencies in that table.**
c. **All ice action speed values in Table 11-1 shall be used, using the relative occurrence frequencies in that table.**
d. **All ice thicknesses in Table 6-6 shall be used, using the durations in that table.**

Valid for the entire site.

It is acknowledged that this procedure may lead to an unnecessarily large number of ILA simulations for FLS DLCs. Therefore, in the Design Basis- or ILA load effect documentation, the number of ILA simulations may be reduced considerably, by using knowledge of the WTG structure (e.g. its substructure- and foundation type) and the dynamical ice load model, by demonstrating that a smaller number of ILA simulations lead to load effects that are at least as onerous as those that would have been found by following the procedure above.

11.4 ULS correlation between ice action speed and wind speed and -direction

Similar to the treatment in Section 11.3, the present section specifies the combinations of hub height wind speeds, wind-ice drift coming direction misalignment angles, wind directions, and ice action speeds that must be used in Integrated Load Analysis for the purpose of the dynamical ULS DLCs D3 and D8. Analogously to the specifications in Section 11.3:

All hub height wind speeds relevant in these DLCs D3 and D8 shall be paired with all ice action speeds, using:

a. **All hub height wind speeds relevant for D3 and D8, i.e. for DLC D8 this is both the hub height wind speed interval used for DLC D3, as well as the 1-year hub height wind speed as specified in Table 3 of [IEC6131].**
b. **All combinations of (hub height wind speed, wind-ice drift coming directional misalignment) that fulfil the wind speed criteria in Item a above, and have non-zero occurrence frequency in Table 10-2.**
c. **All wind directions in Table 10-3.**
d. **All ice action speed values in Section 11.1.**

Valid for the entire site.

It is acknowledged that this procedure may lead to an unnecessarily large number of ILA simulations for DLCs D3 and D8. Therefore, in the Design Basis- or ILA load effect documentation, the number of ILA simulations may be reduced considerably, by using knowledge of the WTG structure (e.g. its substructure- and foundation type) and the dynamical ice load model, by demonstrating that a smaller number of ILA simulations lead to load effects that are at least as onerous as those that would have been found by following the procedure above.

12. Notes on DLCs D1, D2, and D5

The designer is required by Table 3 of [IEC6131] to consider the three DLCs D1, D2, and D5. Nevertheless, it will be shown in Section 12.1 that DLC D1 is negligible since other DLCs yield larger load effects. Similarly, it will be shown in Section 12.2 that DLC D2 can be neglected as well. Finally, in Section 12.3 it will be justified that DLC D5 is negligible for the primary structure design but must be used for the secondary structure design.

12.1 Notes on DLC D1

As specified in Section D.4.2 of [IEC6131], the characteristic horizontal force from sea ice in DLC D1 may be found as F = 300 kN/m · *D*, where *D* is the diameter of the substructure at the ice interaction elevation. By assuming a diameter of 8 m, the characteristic sea ice load effect from DLC D1 is 2.4 MN. This approximately equals the characteristic load effect from the sheet ice calculated using Eq. 8-1 and Eq. 8-2 and h_{50} as the sheet ice thickness and $C_{\mathrm{R}} = C_{\mathrm{R,1,NC}}$ from Section 8. In comparison to DLC D3, the wind conditions are similar, and the load effects in DLC D3 may have dynamic amplification as well, in addition to the increase of the value of C_{R} due to compliance effects. Thus, the quasi-static sea ice load effects from DLC D1 are negligible since they are exceeded by those from DLC D3.

12.2 Notes on DLC D2

As specified in Section D.4.3 of [IEC6131], the characteristic horizontal force from sea ice in DLC D2 may be found as F = 200 kN/m · *D*, where *D* is the maximum of:

1) The diameter of the substructure at the ice interaction elevation.
2) 4 m.

Since DLC D2 is a quasi-static sea ice DLC, just as DLC D1, by the same arguments as in Section 12.1, the load effects from DLC D2 are negligible since they are exceeded by those of DLC D3.

12.3 Notes on DLC D5

As specified in Section D.4.5 of [IEC6131], the characteristic sea ice vertical forces on the primary structure from DLC D5 are given by:

$$V = \min\left(V_{\tau}, V_{\mathrm{b}}\right) \quad \text{Eq. 12-1}$$

where V_{τ} and V_{b} are given by:

$$V_{\tau} = \pi D h_{50} \tau \qquad , \qquad V_{\mathrm{b}} = 0.6\sqrt{\sigma_{\mathrm{f}} \rho_w g \Delta z} \qquad \text{Eq. 12-2}$$

Where:

D	Diameter of support structure at the ice interaction elevation.
h_{50}	50-year sheet ice thickness (Section 6.3).
τ	Adhesive strength (see below).
σ_{f}	Flexural strength of ice (see Section 9.1).
ρ_w	Density of water (Table 7-2).
g	Gravitational acceleration (Table 7-2).
Δz	SWL range for ULS DLCs as per [MA].

The adhesive shear strength is set to 0.3 MPa as defined for steel–saline ice in Section D.4.5 in [IEC6131].

Once the diameter of the substructure, D, is known, V can be calculated using Eq. 12-1. Based on the experience from previous sea ice analyses, V is very small compared to the other ULS load effects and can therefore most likely be neglected for the primary structure. Nevertheless, the vertical forces on secondary structures from these mechanisms must be taken into account in the design of secondary structures.

13. Effects of climate change on sea ice conditions

In recent years, the public view of the topic of Climate Change has shifted: From being viewed as a scientific possibility, it is receiving great attention, from news media and politicians alike, and its existence is generally accepted as a fact.

Although the most widely communicated results are those of mean yearly global air temperature, tropospheric CO_2-concentration in Hawaii, yearly minimum arctic ice extent, and mean global sea-level rise, many more types of detailed information exist. The present section will focus on the area near the KG site. Information is collected through an elaborate literature study including the references given in Table 13-1.

Reference	Purpose
[IPCC_11], [IPCC_12], [IPCC_AR6], [IPCCBRO], [KLIMA6], [OMNY], [JYLHA], [NEUMANN], [LUOM1], [LUOM2], [HCOM111], [HCOM137]	Used to establish the effects of climate change on the sea ice occurrence during the lifetime of the KG site; included for information only, and not used as the basis for conclusions on design parameters.
[GULF1], [GULF2], [GULF3], [GULF4], [IPCC_AR6]	Used to substantiate the improbability of the situation that a weakening of the Atlantic Meridional Overturning Circulation (AMOC) could lead to a colder winter climate for the Baltic Sea (including the evaluated site) during the lifetime of the KG site.
[C2WCC24]	Method and data for quantitative analysis of the impact of climate change on mean- and extreme temperature events.

Table 13-1: Brief overview of the sources used in the present section including their respective purposes.

To assess the effects on the sea ice conditions at the KG site, it is necessary to clarify what has happened through the period where sea ice has been observed, particularly in recent years, which will be done in Section 13.1. Thereafter, it is necessary to clarify if the changes to a milder climate seen in recent years will revert to more severe sea ice conditions, will stabilise, or will continue to make the sea ice conditions milder: Such an overview is provided in Section 13.2. Additionally, Section 13.3 will provide an overview of whether a weakening of the Atlantic Meridional Overturning Circulation (AMOC), of which the Gulf Stream is an important part, could lead to a change of sea ice conditions at the site during the lifetime of the KG site. Finally, a site-specific quantitative analysis is performed using model data.

13.1 What has already happened

During the latter part of the 20th century, and until the present day, the Baltic Sea region has experienced an increase in mean yearly temperatures. This can be seen in Figure 13-1, which is reproduced from Figure SPM.1b of [IPCCBRO], based on the more detailed reports [IPCC_11] and [IPCC_12]. Here, an increase in yearly mean surface temperature of more than 1 °C is seen for the entire Baltic Sea region through the period 1901-2012.

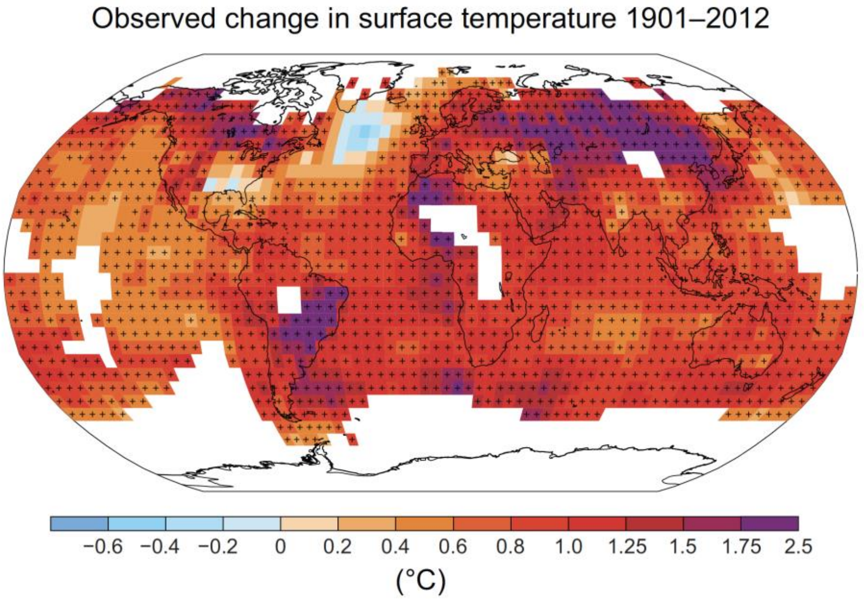

Figure 13-1: Map of the observed surface temperature change from 1901 to 2012, showing an increase of more than 1 °C for the entire Baltic Sea region. Reproduction of Figure SPM.1b of [IPCCBRO].

Although the yearly temperature means gives an indication of the conditions in winter, it is helpful to have winter-specific values. Such values for an area-average of Denmark, for the months of December-January-February (DJF) are provided by the black curve of Figure 13-2. The upper part of this figure shows that the winter-averaged temperatures have increased in recent years, particularly since the late 1980s. From the detailed investigations of ice observations used for the present report, this can be seen to have led to the following situation: Although the winters from 1960/1961 to 2022/2023 had 10 winters with competent sea ice conditions (the most severe of these in the start of the period, the winter 1962/1963), there has been no winters with such ice conditions in the 36 years from 1987/1988 to 2022/2023.

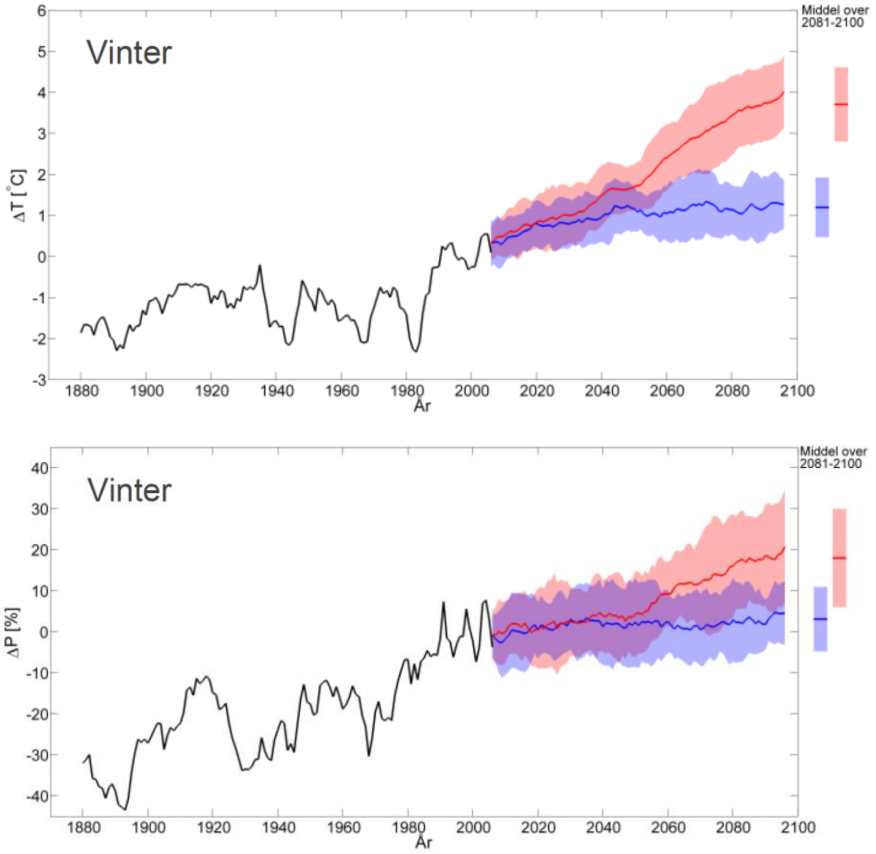

Figure 13-2: Temperature (upper plot) and precipitation (lower plot) changes in Denmark for the three winter months. The observations from 1874 to 2005 are shown with a black curve, model results with a blue curve for the RCP2.6-scenario, and model results with a red curve for the RCP8.5-scenario. The zero points on the vertical axis are the mean values of the reference period from 1986-2005. The shaded areas show ± one standard deviation. Reproductions of the upper left plots in Figures 3 and 6 of [KLIMA6].

A more recent overview of the change in cold extremes is given in Figure 13-3. Here, it can be observed that the cold extremes for Northern Europe (NEU) have decreased in severity with the largest certainty category (Very likely) and with the highest likelihood of potential human contribution (Likely). Further substantiating this is the overview of the change per 10 years in annual minimum daily minimum temperature (TNn) over the period 1960-2018, shown in Figure 13-4. These figures show that the relative mildness of recent winters is very unlikely to be random, but is instead very likely to be a systematic effect of climate change, and also likely to be due to the human contribution to it.

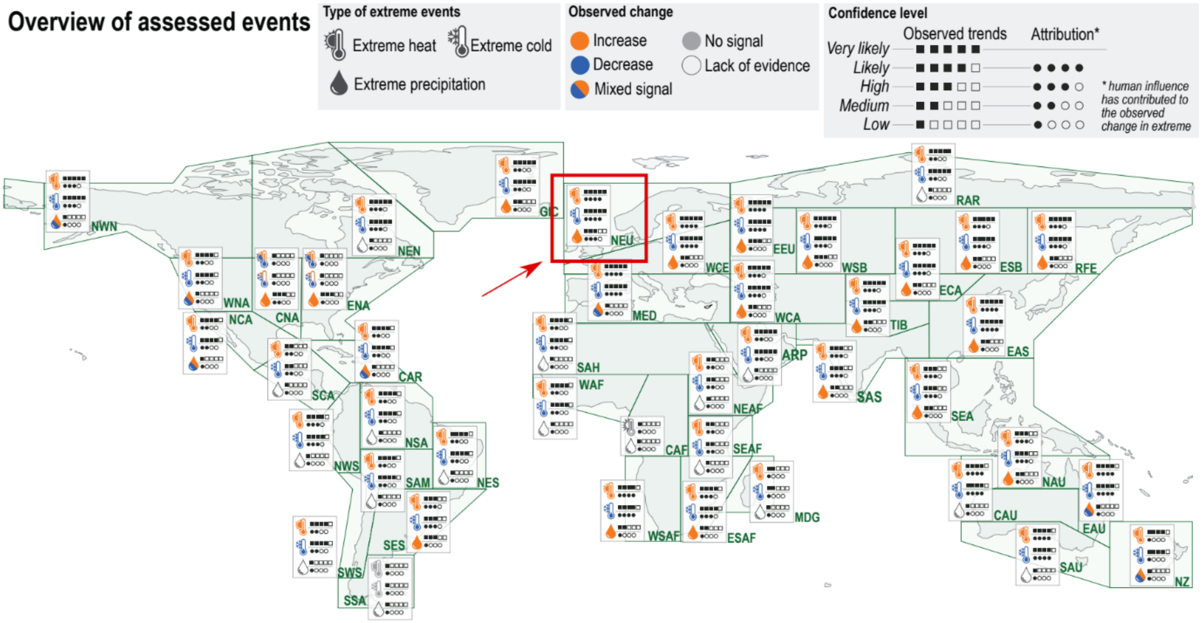

Figure 11.4 | Overview of observed changes for cold, hot, and wet extremes and their potential human contribution. Shown are the direction of change and the confidence in: 1) the observed changes in cold and hot as well as wet extremes across the world; and 2) whether human-induced climate change contributed to causing these changes (attribution). In each region changes in extremes are indicated by colour (orange – increase in the type of extreme; blue – decrease; both colours – changes of opposing direction within the region, with the signal depending on the exact event definition; grey – there are no changes observed; and no fill – the data/evidence is too sparse to make an assessment). The squares and dots next to the symbol indicate the level of confidence for observing the trend and the human contribution, respectively. The more black dots/squares, the higher the level of confidence. The information on this figure is based on regional assessment of the literature on observed trends, detection and attribution and event attribution in Section 11.9.

Figure 13-3: Reproduction of Figure 11.4 of [IPCC_AR6], as well as of its caption, but with the red box and arrow added to clearly show the conditions for Northern Europe (NEU), the decrease in its cold extremes, and its likelihood and potential human contribution.

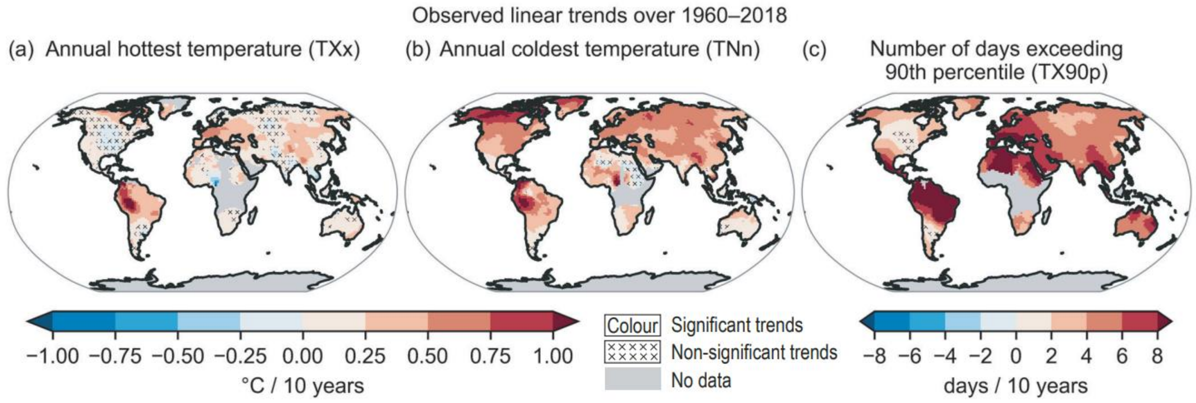

Figure 11.9 | Linear trends over 1960–2018 for three temperature extreme indices: (a) the annual maximum daily maximum temperature (TXx), **(b)** the annual minimum daily minimum temperature (TNn), and **(c)** the annual number of days when daily maximum temperature exceeds its 90th percentile from a base period of 1961–1990 (TX90p); based on the HadEX3 dataset (Dunn et al., 2020). Linear trends are calculated only for grid points with at least 66% of the annual values over the period and which extend to at least 2009. Areas without sufficient data are shown in grey. No overlay indicates regions where the trends are significant at the p = 0.1 level. Crosses indicate regions where trends are not significant. Further details on data sources and processing are available in the chapter data table (Table 11.SM.9).

Figure 13-4: The annual minimum daily minimum temperature (TNn) is shown in the centre plot. This plot shows that this parameter, for the region where the site is located, has increased by ca. 0.5 °C/10 years over the period 1960-2018. Reproduction of Figure 11.9 of [IPCC_AR6].

13.2 Model predictions, and what is likely to happen

As noted in Section 13.1, the recent 36 winters have had very mild sea ice conditions for the region where the KG site is located. The present section will explore whether this is connected with the climate change also discussed in Section 13.1, and what can be said about the future sea ice conditions at the site.

The sensitivity of the sea ice conditions in the Baltic Sea to the Climate Change effects in the region has been known for many years. For example, this is stated in both the abstract and summary of [OMNY], where the latter section states:

> *"The Baltic Sea is a system highly sensitive to climate change, particularly during the winter season. Warming may drastically decrease the number of winters classified as severe, forcing the climate towards oceanic conditions. On the other hand, cooling will increase the number of winters classified as severe and forcing the climate towards sub-arctic conditions."*

This statement, together with the model projections of winter temperatures in the upper plot of Figure 13-2 gives a clear indication that the sea ice conditions at the site will become increasingly mild during the anticipated lifetime, but before drawing a conclusion, the remaining part of the present section will examine this in more detail.

The frequency of future occurrence of severe ice winters is one of the topics of [JYLHA], who classified the severity of the ice conditions in Baltic Sea winters through sea ice extent using the categories shown in the upper part of Figure 13-5. Although, the focus in [JYLHA] was mainly on the Baltic Sea, a similar reduction in sea ice extent is expected in the inner Danish waters. Furthermore, [JYLHA] proceeds to show the occurrence frequencies of these ice winter severity categories in the bottom part of Figure 13-5 for the Climate Normal period of 1961-1990 and compared these with the results found from various climate models for the period 2071-2100. All but one of the models predict a complete absence of severe ice winters, whereas the one left shows a very small occurrence, and the occurrence of average ice winters is also almost absent in the projections. Furthermore, a new category, the Unprecedentedly mild category is seen to dominate. Although the anticipated end of service life of the KG wind farm, is expected to be significantly before the period 2071-2100 to which these results correspond, it is clear that the results show that a warming trend will make severe ice winters increasingly rare throughout the lifetime of the KG wind farm.

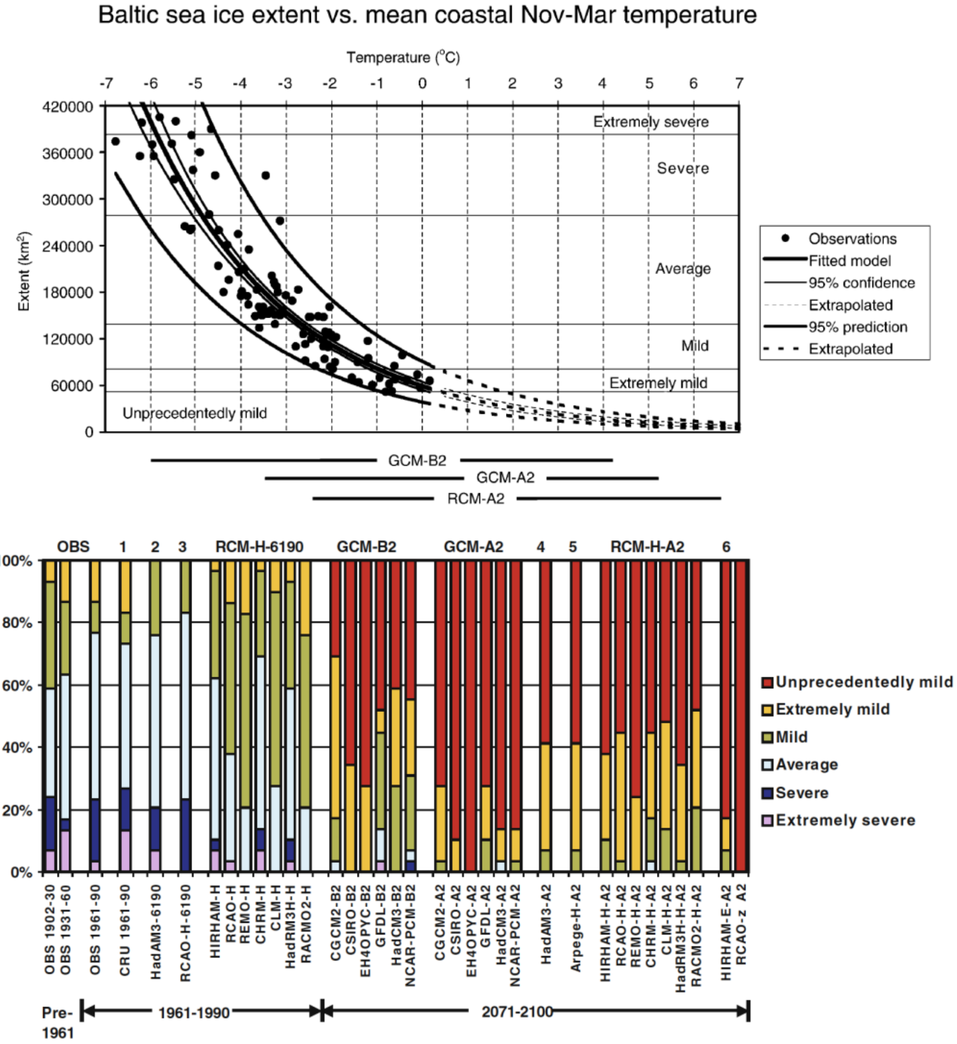

Figure 13-5: The upper plot shows the categories of Baltic Sea ice winter severity, using the sea ice extent for categorisation, used by [JYLHA]. The first axis shows the mean coastal November-March temperature ranges of the various models. Reproduction of Figure 7 of [JYLHA]. The bottom plot shows a comparison of the occurrence frequencies of the sea ice winter severity categories, using various models. The left part of the bottom plot shows results for the Climate Normal period 1961-1990, whereas the right part of the bottom plot shows results for the period 2071-2100. Reproduction of Figure 8 of [JYLHA].

Similar results are found in Section 4.2 of [NEUMANN], where simulation results from using two models are reproduced in Figure 13-6. Rather than taking the results of this figure literally for each year, they are perhaps better interpreted as being indicative of the trend of decreasing winter severity and the magnitudes of yearly variation.

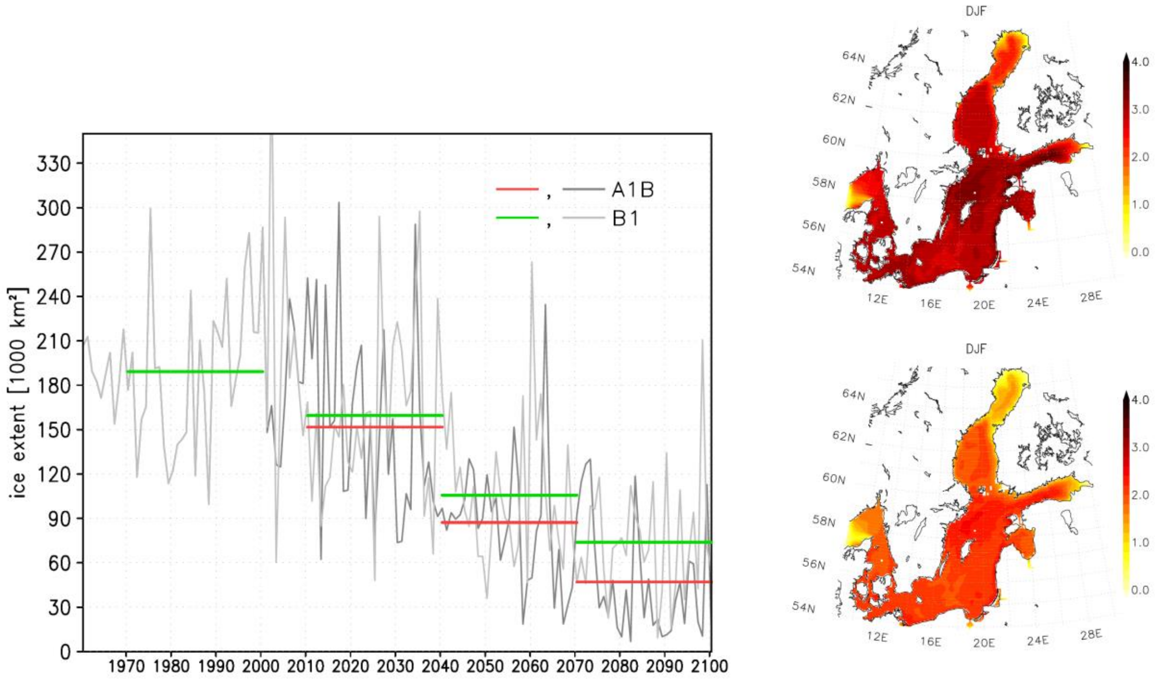

Figure 13-6: The left plot shows the projected yearly maximum Baltic Sea ice extent using two models, A1B and B1 (grey curves), and 30-year averages (green and red lines). Reproduction of Figure 5 of [NEUMANN]. The right maps are an excerpt from Figure 6 of [NEUMANN], showing modelled December-January-February mean sea surface temperature of the period 2070-2100 minus those of the period 1970-2000, for the same two models A1B (upper map) and B1 (lower map). All parts of the figure, are perhaps not meant to be taken literally for each year but are perhaps more indicative of the trend of winter severity and yearly variation.

The most modern and extensive study discussed here is the one documented in the journal paper [LUOM1] and the presentation [LUOM2]. Here, an extensive set of models is investigated and compared with the RCP-terminology of IPCC (e.g. that used in [IPCCBRO]). A selection of results is reproduced in Figure 13-7, where the main points relevant to the evaluated site are:

- Left plots:
    - Already at the anticipated construction of the KG wind farm, the 95th percentile sea ice winter occurrence probability approximately equals the upper limit of what is currently classified as an average ice winter. The tendency of winters getting milder continues throughout the expected lifetime of the KG site, rapidly decreasing the severity of ice winters throughout the lifetime.
    - There is not much difference between the (for the planet Earth, optimistic) RCP4.5 scenario (Figure 13-7 upper left) and the more severe RCP8.5 scenario (Figure 13-7 lower left) during the first years of the anticipated lifetime of the KG site, and only moderate difference during the late part of its expected service life. Thus, a conclusion is that, regardless of the global greenhouse gas emission policies, the probability distribution of various sea ice conditions during the expected lifetime of the KG site will be as mild, or far milder, than those of the last 36 winters. Therefore, it is highly unlikely that sea ice of thicknesses large enough to cause ice-induced vibrations will occur during the expected lifetime of the KG wind farm.

- Right plots:
  - While the left plots showed the maximum sea ice extent, which can be used as a proxy for winter sea ice severity, the plots on the right show ice thicknesses for three stations that are all located in places with varying, but more severe, sea ice conditions than those of the evaluated site. However, it is instructive to see that the decrease of both model-mean and model-maximum ice thicknesses decrease throughout the expected lifetime of the KG wind farm, in both RCP scenarios. It is thus reasonable to deduce that the expected sea ice thicknesses during the expected lifetime of the KG wind farm will be smaller than those of the last 36 winters.

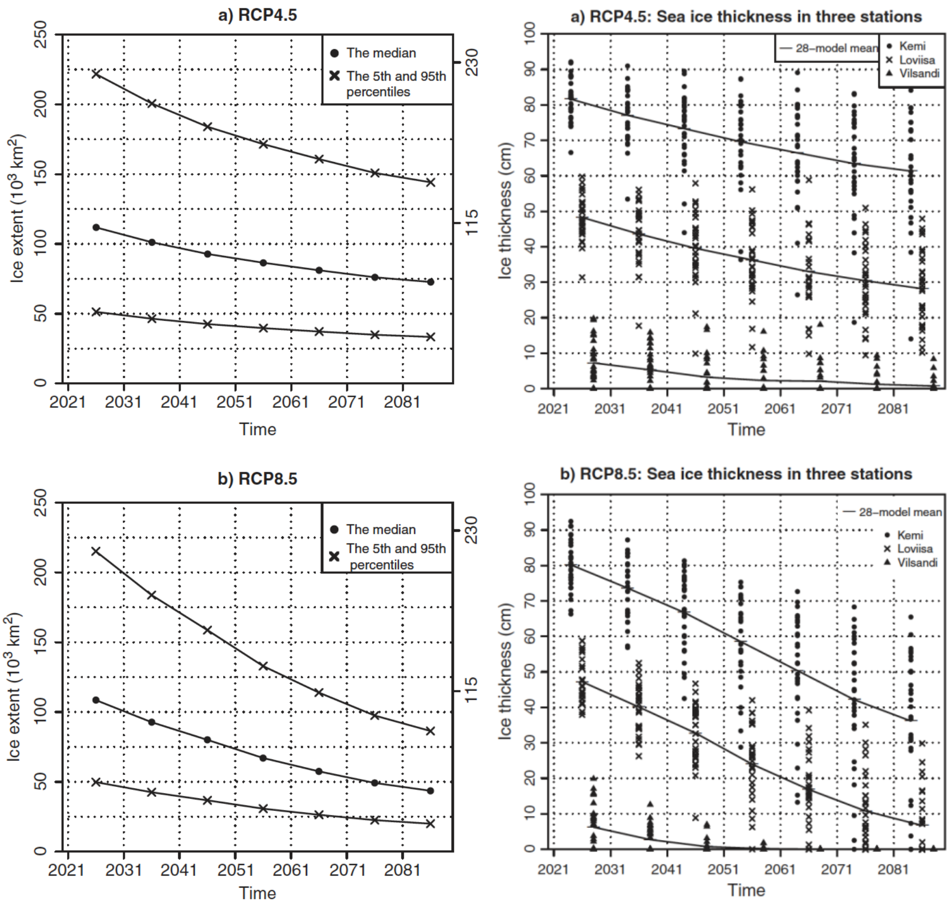

Figure 13-7: **Left**: Temporal evolution of the annual maximum ice extent. The estimates are given separately for the median values, representing a typical winter (line with dots), and for the 5th- and 95th percentiles, corresponding to scant and widespread ice cover (lines with crosses). All the results are ensemble means of sea ice projections, derived from temperature responses of 28 individual models listed in Table 1 of [LUOM1]. The values of 115,000 km2 and 230,000 km2 show the upper-class limits for mild and average ice winters, according to current standards. The limit for unprecedentedly mild winters is 49,000 km2. (a) The RCP4.5 scenario, (b) the RCP8.5 scenario. **Right**: Temporal evolution of the mean year-maximum ice thickness at the three locations shown in Figure 13-8. The ice projections for Kemi (dots), Loviisa (crosses) and Vilsandi (triangles) are based on the temperature responses of the individual global climate models. The short horizontal lines show the mean values of all the model-based projections for each decade. Please note that the position of the symbols within each decade is slightly shifted to make the figure more readable. (a) RCP4.5, (b) RCP8.5. The left plots are a reproduction of Figure 5 of [LUOM1], while the right plots are reproductions of Figure 9 of ibid.

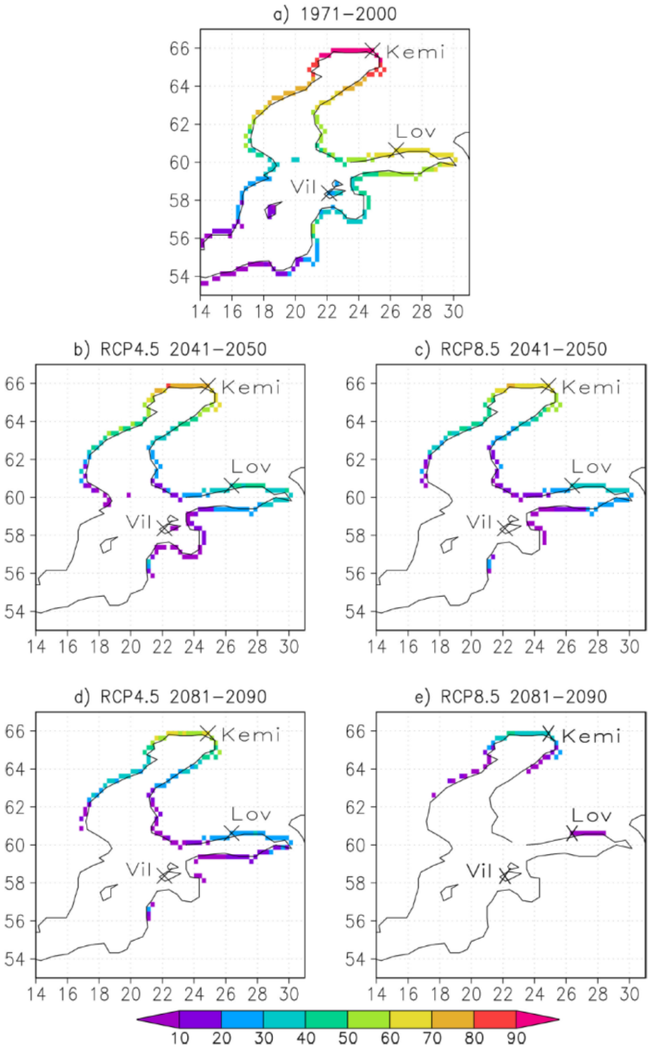

Figure 13-8: The annual maximum coastal sea ice thickness (cm) in typical past and future winters. The figure also shows the locations of the three observation stations referenced in the right part of Figure 13-7. Reproduction of Figure 8 of [LUOM1].

Similar conclusions can be drawn from [IPCC_AR6], explicitly in the excerpt from Section 12.4.5.1 of ibid. reproduced in Figure 13-9.

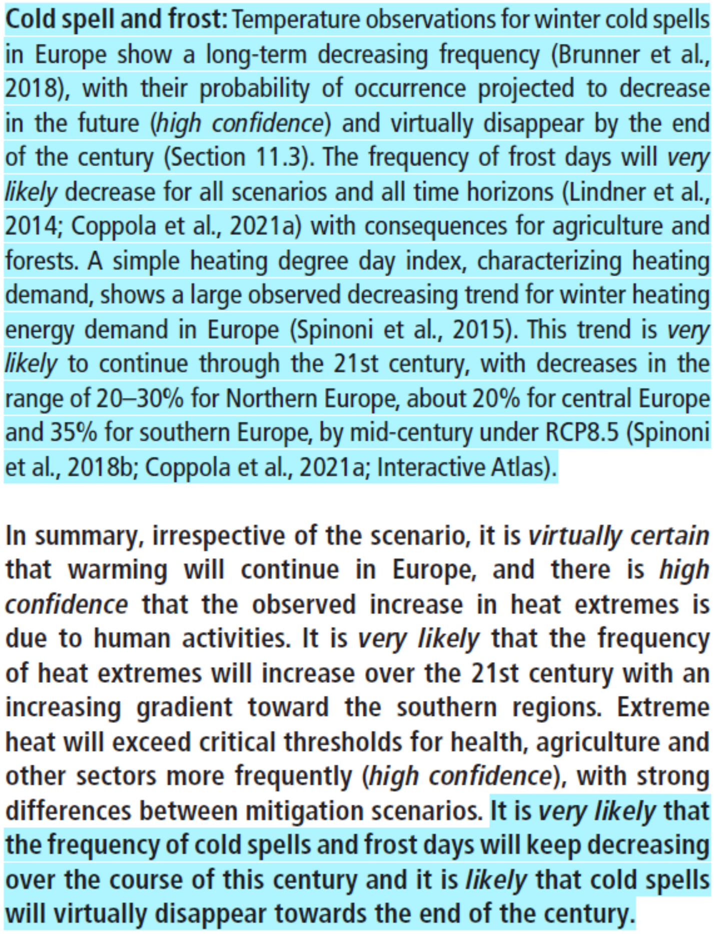

Cold spell and frost: Temperature observations for winter cold spells in Europe show a long-term decreasing frequency (Brunner et al., 2018), with their probability of occurrence projected to decrease in the future (*high confidence*) and virtually disappear by the end of the century (Section 11.3). The frequency of frost days will *very likely* decrease for all scenarios and all time horizons (Lindner et al., 2014; Coppola et al., 2021a) with consequences for agriculture and forests. A simple heating degree day index, characterizing heating demand, shows a large observed decreasing trend for winter heating energy demand in Europe (Spinoni et al., 2015). This trend is *very likely* to continue through the 21st century, with decreases in the range of 20–30% for Northern Europe, about 20% for central Europe and 35% for southern Europe, by mid-century under RCP8.5 (Spinoni et al., 2018b; Coppola et al., 2021a; Interactive Atlas).

In summary, irrespective of the scenario, it is *virtually certain* that warming will continue in Europe, and there is *high confidence* that the observed increase in heat extremes is due to human activities. It is *very likely* that the frequency of heat extremes will increase over the 21st century with an increasing gradient toward the southern regions. Extreme heat will exceed critical thresholds for health, agriculture and other sectors more frequently (*high confidence*), with strong differences between mitigation scenarios. It is *very likely* that the frequency of cold spells and frost days will keep decreasing over the course of this century and it is *likely* that cold spells will virtually disappear towards the end of the century.

Figure 13-9: Reproduction of an excerpt from Section 12.4.5.1 of [IPCC_AR6], with blue highlighting added to show the parts most relevant for the present report.

In closing, there are several other sources that state the decreasing sea ice extent in the coming decade concerning the Baltic Sea and inner Danish waters. One example is [HCOM111] and the newer, but less detailed, [HCOM137]. Another comprehensive example is Chapter 8 of [BACC] (recent changes to sea ice extent) and Chapter 13.4 of ibid. (future projections for sea ice). All these give similar statements to the ones presented in the present section. On a related note, and remarkably, the authors of the present report were unable to find any scientific references that demonstrate the opposite effect; thus, it seems there is great scientific consensus that the sea ice conditions during the anticipated lifetime of the KG wind farm will, to a very large degree of certainty, be significantly milder than those of recent years.

13.3 Effects of a collapse of the Gulf Stream

A widespread climate myth is that the Gulf Stream is the main cause of the warmer climate of Western Europe, compared to that of similar latitudes on the North American East Coast. A related myth is that the effects on climate of a potential collapse of the Atlantic Meridional Overturning Circulation (AMOC), of which the Gulf Stream is a large part, would by far overshadow the warming effects of Climate Change, effectively cooling Denmark and surrounding areas to a climate far colder than that of the Climate Normal of 1960-1990[11].

---

[11] For the Danish Climate Normal (Klimanormalen), see https://www.dmi.dk/vejrarkiv/normaler-danmark/.

It is relevant to address the risk that a change in the AMOC could lead to a colder climate during the lifetime of the OWF. This risk is addressed by examining:

a) First, the myth of the AMOC being the overwhelmingly dominating cause of the warmer climate of Denmark and the surrounding areas. This is shown convincingly in [GULF1], and a more easily accessible summary and a bit of history is provided here: http://ocp.ldeo.columbia.edu/res/div/ocp/gs/.

b) Second, it is helpful to establish the time scale of a weakening, or even a potential collapse, of the AMOC. This is the topic of the paper [GULF2], published in a subcategory of the esteemed journal Science, and in the more recent papers of [GULF3] and [GULF4]. Although [GULF2] is rather technical, a few key points are accessible with a moderate effort (or, for an even more accessible summary, see the link to RealClimate.org also provided in [GULF2]):
   Figure 1C of [GULF2] shows that the weakening, or near-total collapse, of the AMOC is expected to take several hundred years (note that the doubling of tropospheric CO_2-concentration and freshwater adjustment is made from $T = 200$ years in the figure). Although a main point of the paper is the overlooked risk of effects on the AMOC, and relative rapidity – on a climate scale – of this, the AMOC weakening over the lifetime of the OWF is at most to reduce the flow of the AMOC by 20%. In addition, it is argued that the weakening would likely not start at the same time as the construction of the OWF, since $T = 200$ years in the figure corresponds to a doubling of CO_2-concentration, which will not happen for several decades – see item c) below.

   i. In Chapter 9 of [IPCC_AR6], Executive Summary (Page 1214 of the pdf file) under the heading Ocean Circulation states:

> *The Atlantic Meridional Overturning Circulation (AMOC) will very likely decline over the 21st century for all SSP scenarios. There is medium confidence that the decline will not involve an abrupt collapse before 2100.*

   Some more context on this statement is provided at the end of Section 9.2.3.1 of [IPCC_AR6], where it is explained that the previous AR5 assessment of it being very unlikely that the AMOC would collapse before the year 2100 was changed to the statement above due to the 2021 paper by Lohmann and Ditlevsen cited in ibid.

   In the more recent papers of [GULF3] and [GULF4], the conclusion of [IPCC_AR6] is challenged, as the two independent studies both predict a mid-century collapse of the AMOC. In [GULF3] the average probability of the collapse of the AMOC before 2050 is given as 59%, with an estimated collapse time between 2037-2064 using current emission level predictions. Further, the authors of [GULF3] directly call for a reconsideration of the claim from [IPCC_AR6] stating that a collapse is unlikely before 2100 in the upcoming IPCC_AR7 report. By use of alternate analysis methods using Early Warning Signals (EWS), the authors of [GULF4] estimate a collapse of the AMOC around 2050, in agreement with [GULF3].

A final important piece of context is given in FAQ 9.3 of [IPCC_AR6] (Page 1320 of the pdf file), where it is explained that:

> *Based on models and theory, scientific studies indicate that, while the AMOC is expected to slow in a warming climate, the Gulf Stream will not change much and would not shut down totally, even if the AMOC did.*

c) Thirdly, it is key to note the potential magnitude of the changes to the winter temperatures of Denmark and surrounding areas from a collapse of the AMOC. This information is not directly available in the Science Advances paper of [GULF2], but is provided by the same authors in the RealClimate.org-link also provided in [GULF2], and is reproduced in Figure 13-10 below. Here, it can be seen that a doubling of the atmospheric CO$_2$-concentration compared to 1990-levels (i.e. from ca. 350 ppm to ca. 700 ppm) will cause a very significant cooling of the Northern North Atlantic winter temperatures 300 years after the doubling takes place – i.e. after a near-complete collapse of the AMOC[12]. In contrast, for the site, and the Baltic Sea in general, the cooling will be only ca. -0.5 °C. By comparison with the winter temperature increase shown in the upper part of Figure 13-2, it is clear that the effects of Climate Change are very likely to happen far more rapidly and overshadow the effects of the weakening or potential collapse of the AMOC within the lifetime of the evaluated KG wind farm.

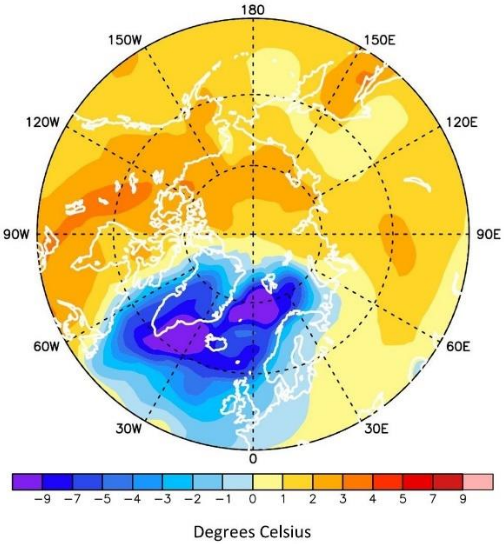

Figure 13-10: The figure shows the temperature change in the winter months, 300 years after CO$_2$ doubling (compared to 1990-levels) in [GULF2]. Due to the almost completely extinct AMOC flow, the northern Atlantic region has cooled significantly, but the evaluated site experiences temperature changes of only ca. -0.5 °C. Please note that a doubling of CO2 will be reached in 2055 in the most severe RCP8.5 scenario. Further, the weakening of the AMOC is so slow that, during the lifetime of the OWF, the effects of weakening the AMOC, in inner Danish waters, will be far overshadowed by the increase of greenhouse gases. Reproduction of a figure from the RealClimate.org-link provided in [GULF2].

---

[12] For comparison, for the Representative Concentration Pathway RCP8.5, this doubling is reached approximately in the year 2055, while in the milder – unfortunately difficultly achievable and still awful – RCP6.0-scenario, this doubling will be reached in the year 2090. For the RCP4.5, the atmospheric CO$_2$-concentration will level off just below 600 ppm around the year 2080. Although it is difficult to see how it can succeed, the RCP4.5-scenario yields the conditions that are agreed as the maximum air temperature increases in the Paris Agreement.

In summary, it has now been convincingly shown that the effects of a collapse of the AMOC, disastrous as it may be, have relatively mild effects on the inner Danish waters and the Baltic Sea winter temperatures. Further, in [IPCC_AR6] it is argued that a potential collapse of the AMOC is not likely to occur before 2100 - thus after the end of the service life of the KG wind farm. Note, however, that challenges to this statement have been found in multiple more recent studies.

13.4 Site-specific quantitative analysis

As a follow-up to the comprehensive literature review and discussion presented in the previous subsections, this subsection presents a site-specific quantitative analysis of the predictions by an ensemble of climate models.

The methodology employed in the analysis follows that presented in [C2WCC24], making use of a total of 25 Climate Models from the CMIP6 climate projections which have coverage over the area surrounding the KG site. While [C2WCC24] details a number of metrics and tests for narrowing down the model selection, it does so by focusing on wind speed as a primary variable. The present study has used the same methodology but adapted it to use air temperature at the surface level as the primary variable, adding low temperature extremes to the analysis, and adding the analysis of the number- and duration of threshold-crossing events.

Climate models with daily results for SSP2-4.5, SSP3-7.0 and SSP5-8.5 were downloaded from the Copernicus Data Store covering the historical period (1850-2014) and future period (2014-2100). The models were subject to a number of tests and analyses to determine whether they were to remain in the final ensemble. The tests mainly revolved around comparing key metrics to a trusted reference, in this case, the ERA5 reanalysis timeseries at its nearest node to the KG site. The model tests and filtering consisted of the following:

- **Interannual and inter-monthly variability**. The Coefficient of Variation (COV) of the annual- and monthly mean air temperatures were computed, both from the raw time series and using a 20-yr rolling average window, for the climate models and for the ERA5 dataset. Climate models that had a COV outside the range of ±15% of that found in the ERA5 dataset. See Figure 13-11 for an example.
- **20-year rolling average anomaly**. Defining monthly- and yearly anomalies as the deviation of the specific monthly- and yearly average value from the average value over the reference period, and then taking a rolling average with a 20-yr window, models with monthly- or yearly anomalies out of phase with those in ERA5 (ie. with a negative correlation coefficient) were filtered out.
  - While this criterion clearly picks out outlier models with regard to wind speeds, no models failed this particular criterion for air temperature. This is an expected result as surface level air temperature is one of the key variables in the climate models.
- **Similarity in probability distribution functions**. The probability distributions of monthly means and yearly mean anomalies were compared to the ERA5 reference using the Earth Mover's Distance metric. Like the criterion above, this had a much smaller impact when using temperature as a key variable rather than

wind speed, however, this did indeed filter out a small number of climate models. See Figure 13-12 for an example.

- Please note that for all tests above, the tests were carried out only on the portion of the climate model historical dataset (1850-2014) that is concurrent with the available ERA5 dataset (1940-2024). To avoid bias due to the higher uncertainty of ERA5 data too far in the past, the checks were repeated with the ERA5 period (1979-2024) and the results were found to be unaltered.

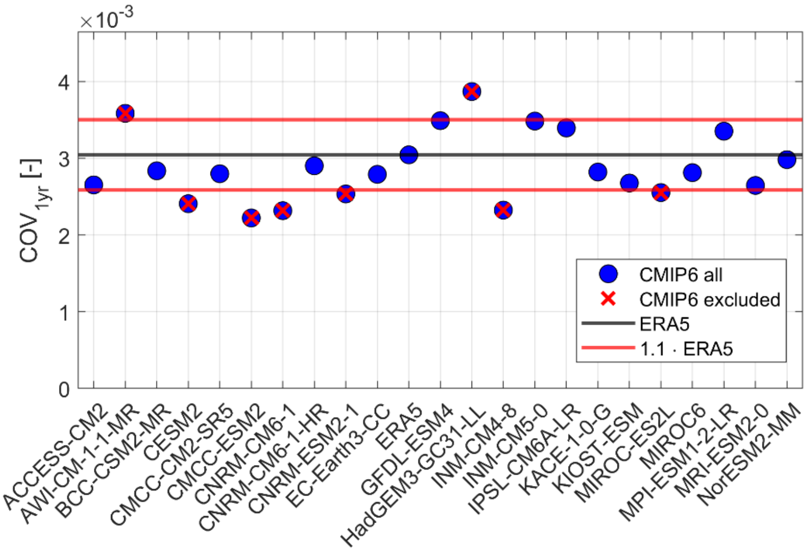

Figure 13-11: Example of IAV test. Climate models which exhibit a too large- or too small interannual variability compared to that in the ERA5 dataset are discarded.

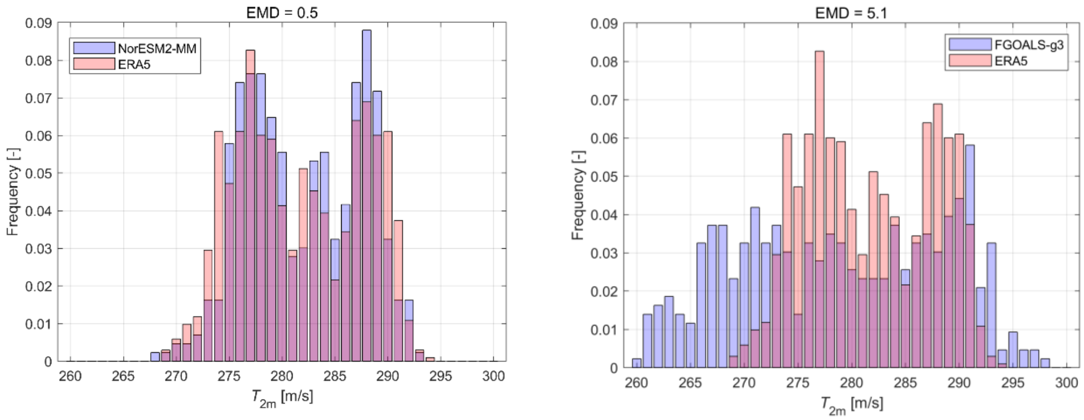

Figure 13-12: Example of climate models that passed (left) and failed (right) the EMD test of probability distribution similarity.

When the above filters are applied, the ensemble of climate models is significantly reduced, see Figure 13-13 for an example. Most notably, the filtering doesn’t necessarily remove the models with the highest- or lowest absolute values, which is clear from the non-greyed-out models in the figure. These models are not immediately classified as unreliable just because of their predictions in the past or far future, but rather they are retained because they predicted values consistent with those in ERA5 during the test period. Furthermore, as shown in Figure 13-14, the careful model selection does change the projected ensemble means for the future period, but it has an even larger impact on the variance of the individual predictions within the ensemble, seen as the spread between the 95% confidence intervals.

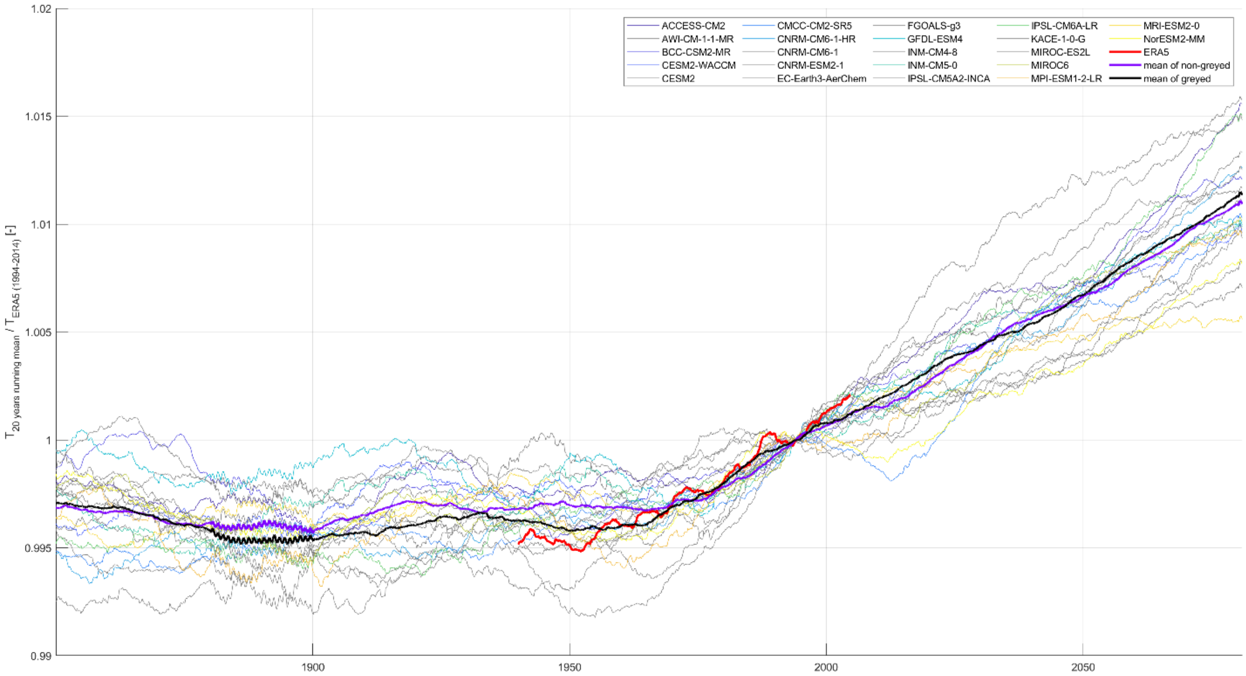

Figure 13-13: Example of climate model ensemble and surface level air temperature predictions before- and after filtering models that did not pass the consistency tests.

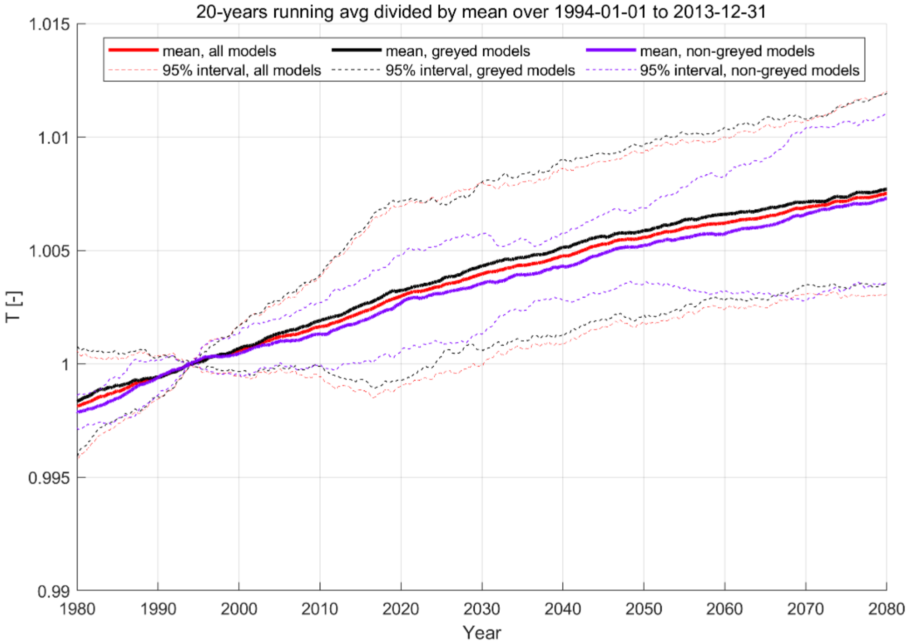

Figure 13-14: Example of model ensemble average and 95% confidence intervals for surface level air temperature in a 20-year running average relative to that of the period 1994-2014 (last 20 years of the climate model historical run). The red lines show the result that would be obtained when retaining all models, the black lines show the results only with the excluded models, and the purple lines show the results with the models retained after filtering.

After the climate model ensemble was thinned out following the methodology from [C2WCC24], the retained models are used to assess any predicted change in key quantities relevant for sea ice assessments, namely:

- **Change in mean air temperature at surface level**. This is simply assessed as the mean surface level air temperature in the climate model dataset evaluated over the assumed OWF operational period and over the reference period. See the blue dataset on the left side of Figure 13-15.
- **Change in the severity of extreme temperature events.** This is assessed as the value with a 2% probability of exceedance – or in the case of extremely low temperatures, a 98% probability of exceedance – corresponding to an event with a 50-year return period. The value is derived from an empirical cumulative distribution function fitted to the daily values in the selected climate models. See the red- and green datasets on the left side of Figure 13-15.
- **Change in frequency- and duration of low temperature events**. For this metric, a low temperature event was defined as having a surface air temperature lower than 2°C. See the right side of Figure 13-15.
- For comparison purposes, the quantities above are calculated as the value over the period 2025-2055 (an indicative 30-year lifetime for an OWF with COD in 2025) relative to the value over the period 2000-2020 (an indicative design basis reference period for an OWF with COD in 2025).

For all the analyses above, the climate model ensemble found that the surface air temperature conditions projected for the KG wind farm lifetime are less severe than over the reference period in the context of their impact on sea ice formation. That is, mean temperatures are higher, extreme low temperatures are higher, the frequency of occurrence of low temperature events is lower, and the duration of low temperature events is shorter. Moreover, all ensemble predictions within a 95% confidence interval follow this trend; and while the ensemble variance increases for the higher emission SSPs, the conclusions are consistent throughout all three SSPs considered in the analysis.

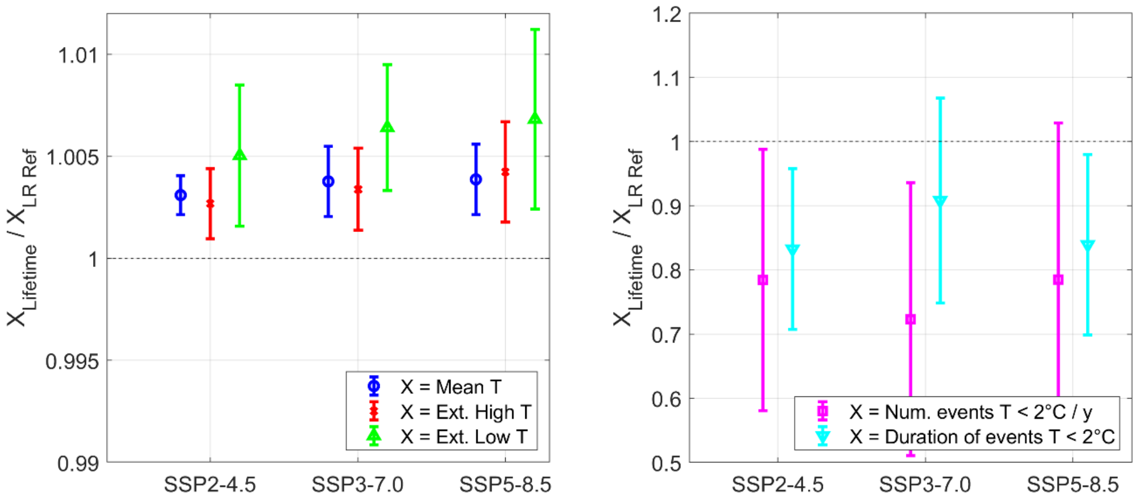

Figure 13-15: Comparison of key metrics during an indicative OWF lifetime 2025-2055 and a reference period for design 2000-2020. **Left**: mean temperature, extreme high temperature, extreme low temperature. **Right**: number of events with air temperature under 2°C and duration of such events.

The air temperature predictions from the ensemble of climate models summarised to the left of Figure 13-15, are aligned with the findings of the '*Klima atlas'* published by DMI, see [KLIMATL]. Here, the findings of the global IPCC 6 climate study are processed to represent local climate changes in Denmark. The predicted change in the low- and high extreme air temperatures from [KLIMATL], for the start-, mid-, and end of the century are summarised in Figure 13-16 as the upper and lower plot, respectively. The three RCPs of 2.6, 4.5 and 8.5 are colour-coded using individual colours.

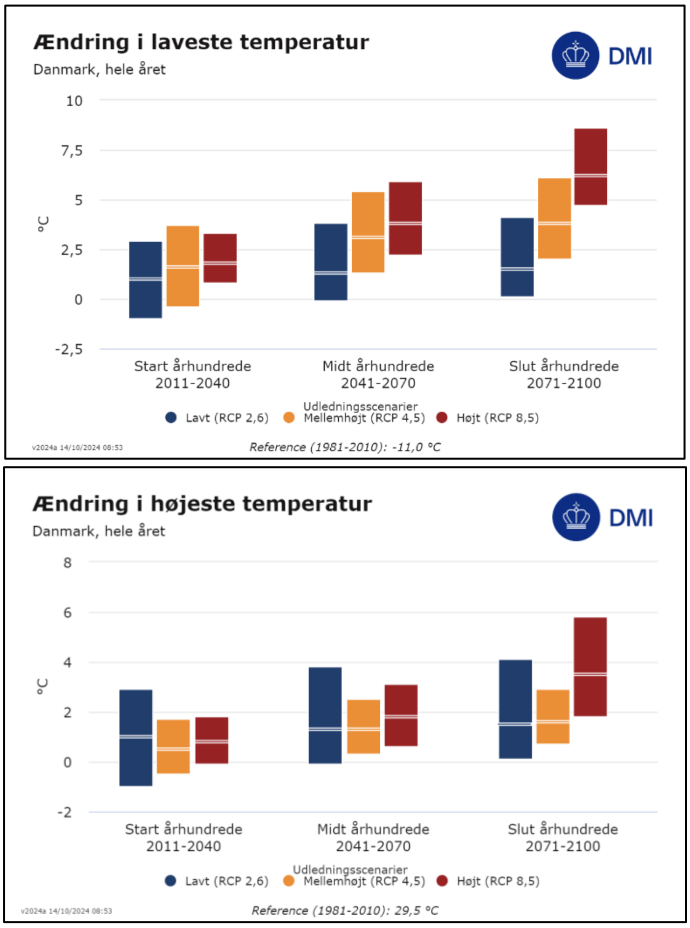

Figure 13-16: Change in the extreme air temperature as given in the findings of [KLIMATL], (Only available in Danish). **Upper:** The change in the extreme low air temperature for the start-, mid-, and end of the century for the three RCP scenarios of 2.6, 4.5, and 8.5. **Lower:** The change in the extreme high air temperature for the start-, mid-, and end of the century for three RCP scenarios of 2.6, 4.5, and 8.5.

The change in air temperature of [KLIMATL], reproduced in Figure 13-16, is in line with the findings from the ensemble of climate models of Figure 13-15, with some variance between the different RCP scenarios for the start- and mid of the century. In line with the results of the ensemble of climate change models, both the low- and high extreme air temperatures are predicted to increase for all of the evaluated RCP scenarios.

Following the analyses and discussion above, the site-specific quantitative analysis based on an ensemble of CMIP6 climate change models concludes that, for an indicative lifetime of the KG wind farm covering the period 2025-2055, the KG wind farm is unlikely to experience sea ice conditions more severe than those assessed by the present document during its lifetime. The analysis finds that the model

ensemble predicts mean-, extreme high- and extreme low temperatures all to increase, while the frequency of occurrence- and duration of low temperature events is predicted to decrease.

14. References

[BACC] **The BACC II Author Team.**
Second Assessment of Climate Change for the Baltic Sea Basin, Springer Open, DOI 10.1007/978-3-319-16006-1
Link: https://link.springer.com/book/10.1007/978-3-319-16006-1
(2015).

[BEK1773] **Energistyrelsen**
Bekendtgørelse om teknisk certificering og servicering af vindmøller m.v.
BEK nr. 1773 af 30/11/2020.

[C2WCC24] **Garza J., Hatfield D.W. and Gandoin R.**
Quantitative approach for climate model selection and application in WRA & EYA. Wind Europe Technology Workshop 2024 - Climate change session.
(2024-06-11).

[CHRSKO] **Christensen, F. T., Skourup, J.**
Extreme Ice Properties.
Journal of Cold Engineering, Vol. 5, No. 2, ASCE.
(1991-06).

[CMEMS] **Copernicus Marine Environment Monitoring Service**
Oceanographic SST data from the Copernicus Programme of the European Union.
Downloaded by C2Wind using the tool 'MyOcean Pro' for the '*Baltic Sea Physics Reanalysis*' product.
Link:
https://data.marine.copernicus.eu/product/BALTICSEA_MULTIYEAR_PHY_003_011/description

[DMIMET] **Dansk Meteorologisk Institut**
Meteorological measurements from the Danish meteorological institute. Downloaded by C2Wind using the DMI open data API for meteorological observations found at:
https://opendatadocs.dmi.govcloud.dk/en/Data/Meteorological_Observation_Data

[DMIOCE] **Dansk Meteorologisk Institut**
Oceanographic measurements from the Danish meteorological institute. Downloaded by C2Wind using the DMI open data API for oceanographic observations:
https://opendatadocs.dmi.govcloud.dk/Data/Oceanographic_Observation_Data

[DNV0437] **DNV**
Standard DNV-ST-0437 - Loads and site conditions for wind turbines.
Edition May 2024.
(2024-05).

[FUGLEM] **Thijssen, J., Fuglem, M.**
Methodology to evaluate sea ice loads for seasonal operations.
OMAE2015-42194, pp. 1-7.
(2015-06-05).

[GULF1] **Seager, R. et. al.**
Is the Gulf Stream responsible for Europe's mild winters?
Quarterly Journal of the Royal Meteorological Society 128, pp. 2563–2586.
(2002-04-19).

[GULF2] **Liu, W., et. al.**
Overlooked possibility of a collapsed Atlantic Meridional Overturning Circulation in warming climate. Science Advances 3.
(2017-01-04).

[GULF3] **Emma J.V. Smolders, et. al.**
Probability Estimates of a 21st Century AMOC Collapse.
Institude for Marine and Athmospheric research Utrecht, Utrecht University.
(2024-06).

[GULF4] **Peter Ditlevsen & Susanne Ditlevsen**
Warning of a forthcoming collapse of the Atlantic meridional overturning circulation.
Unitersity of Copenhagen. Published in Nature Communications.
(2023-07-25).

[HCCUDATA] **SWECO, Deltares**
Hydrodynamic hindcast datasets for three reference locations for the Kattegat OWF, documented in [MA] and provided as data files in nc format:
- KattegatHesseloSouthArea_56.3000N_11.1500E_3D_1979_2023.nc
- KattegatHesseloSouthArea_56.3700N_11.3300E_3D_1979_2023.nc
- KattegatHesseloSouthArea_56.4475N_11.4400E_3D_1979_2023.nc

[HCOM111] **Helsinki Commission**
Climate Change in the Baltic Sea Area - HELCOM Thematic Assessment in 2007.
Baltic Sea Environment Proceedings No. 111.
Helsinki Commission - Baltic Marine Environment Protection Commission.
(2007).

[HCOM137] **Helsinki Commission**
Climate change in the Baltic Sea Area - HELCOM thematic assessment in 2013.
Baltic Sea Environment Proceedings No. 137.
Helsinki Commission - Baltic Marine Environment Protection Commission.
(2013).

[HCWWDATA] **SWECO, Deltares**
Wind- and Spectral Wave hindcast dataset for three reference locations for the Kattegat OWF, documented in [MA] and provided as data files in nc format:
- KattegatHesseloSouthArea_KG-1_56.370227814N_11.330537796E_WavesWind_1979_2023.nc
- KattegatHesseloSouthArea_KG-2_56.300807953N_11.149958611E_WavesWind_1979_2023.nc
- KattegatHesseloSouthArea_KG-3_56.449584961N_11.439541817E_WavesWind_1979_2023.nc

[HEINO] **Heinonen, J.**
Constitutive Modelling of Ice Rubble in First-Year Ridge Keel.
VTT Technical Research Centre of Finland, VTT publications 536.
Doctoral dissertation.
(2004-06-28).

[HØY1999] **Høyland, K., Løset, S.**
Measurements of temperature distribution, consolidation and morphology of a first-year sea ice ridge.
Cold Regions Science and Technology 29 (1999), pp. 59–74.
(1999-01-19).

[HØY2005] **Høyland, K., Liferov, P.**
On the initial phase of consolidation.
Cold Regions Science and Technology 41 (2005), pp. 49–59.
(2004-09-13).

[IEC6131] **IEC**
IEC 61400-3-1: Wind energy generation systems – Part 3-1: Design requirements for fixed offshore wind turbines. Edition 1.0. International Electrotechnical Commission.
(2019-04-05).

[IECRE502] **IECRE**
IECRE OD-502 - Operational document
IEC System for Certification to Standards relating to Equipment for use in Renewable Energy applications (IECRE System)
Project Certification Scheme
(2018-10-11)

[IPCC_11] **Intergovernmental Panel on Climate Change**
Climate Change 2013 – The Physical Science Basis - Working Group I Contribution to the Fifth Assessment Report of the Intergovernmental Panel on Climate Change.
Chapter 11 – Near-term Climate Change: Projections and Predictability.
(2013).

[IPCC_12] **Intergovernmental Panel on Climate Change**
Climate Change 2013 – The Physical Science Basis - Working Group I Contribution to the Fifth Assessment Report of the Intergovernmental Panel on Climate Change.
Chapter 12 – Long-term Climate Change: Projections, Commitments and Irreversibility.
(2013).

[IPCC_AR6] **Intergovernmental Panel on Climate Change**
Climate Change 2021 – The Physical Science Basis – Working Group I contribution to the Sixth Assessment Report of the Intergovernmental Panel on Climate Change.
(2021-08-07).
Link: https://www.ipcc.ch/report/ar6/wg1/#FullReport

[IPCCBRO] **Intergovernmental Panel on Climate Change.**
Climate Change 2013 - The Physical Science Basis - Summary for Policymakers.
Working Group I Contribution to the Fifth Assessment Report of the Intergovernmental Panel on Climate Change.
(2013).

[ISBES] **Istjenesten.**
Is- og besejlingsforholdene i de danske farvande.
Collection of historical records of the sea ice conditions in Danish waters during the winter season. Available from 1931 to present.
Link:https://www.forsvaret.dk/da/organisation/soevaernet/civile-opgaver/istjeneste/ismeldetjenesten/is-og-besejlingsforhold-i-danske-farvande/

[ISO19906] **ISO**
EN ISO 19906:2019(E): Petroleum and natural gas industries - Arctic offshore structures.
(2019-08).

[ISO800002] **ISO**
ISO 80000-2:2019: Quatities and units – Part 2: Mathematics.
(2019-08).

[JUSS] **Jussila, V.**
General principles of the procedure for ice-structure-interaction (PSSII).
Proceedings of the Twenty-eighth (2018) International Ocean and Polar Engineering Conference.
pp. 1630-1637.
(2018-07-30).

[JYLHA] **Jylhä, K., et. al.**
Changes in frost, snow and Baltic Sea ice by the end of the twenty-first century based on climate model projections for Europe.
Climatic Change 86, pp. 441–462.
(2008-02).

[KANK] **Kankaanpää, P.**
Distribution, morphology and structure of sea ice pressure ridges in the Baltic Sea.
Fennia - International Journal of Geography, 175(2), pp. 139–240.
(1997-02-01).

[KARNA20] **Kärnä, T., et. al.**
Simulation of multi-modal vibrations due to ice actions.
20th IAHR International Symposium on Ice.
(2010-06-18).

[KLIMA6] **Olesen, M., et. al.**
Fremtidige klimaforandringer i Danmark.
Rapport nr. 6, Danmarks Klimacenter.
(2014-10-01).

[KLIMATL] **Dansk Meteorologisk Institut**
Climate Atlas derived by the National Center for Climate Change and published by DMI, see:
https://www.dmi.dk/klima-atlas/data-i-klimaatlas
Climate variable '*Temperature'* examined using '*Version: v2024a'*.
(2024-10).

[LEPP] **Leppäranta, M.**
Freezing of Lakes and the Evolution of their Ice Cover.
Springer Heidelberg New York Dordrecht London.
ISBN 978-3-642-29080-0.
(2015).

[LEPP1992] **Leppäranta, M.**
The structure and strength of first-year ice ridges in the Baltic Sea.
Cold Regions Science and Technology 20 (1992), pp. 295–311.
(1992).

[LUOM1] **A. Luomaranta, K. Ruosteenoja, K. Jylha, H. Gregow, J. Haapala, and A. Laaksonen.**
Multimodel estimates of the changes in the Baltic Sea ice cover during the present century,
Tellus A 66, 22617.
(2014-03-05).
Link: http://www.tandfonline.com/doi/full/10.3402/tellusa.v66.22617

[LUOM2]	**A. Luomaranta.** Multimodel estimates of the changes in the Baltic Sea ice cover during the present century, Presentation given at the 6th National Seminar on Snow on the day of Pyry, Finnish Meteorological Institute. (2015-11-02). Link: http://harmosnow.eu/workshops/02.11.2015,%20Helsinki/pyry02112015_baltic_sea_ice_luomaranta.pdf
[MA]	**SWECO, Deltares** Kattegat and Hesselø South, Site Metocean Conditions Assessment, Part B: Analyses and Design Parameters for Kattegat. Doc. No.: 41011328B (2024-08-30).
[MADSEN]	**Skovgaard Madsen, K.** PhD thesis, Recent and future climatic changes in temperature, salinity, and sea level of the North Sea and the Baltic Sea. University of Copenhagen. (2009-07-31).
[NEUMANN]	**Neumann, T.** Climate change effects on the Baltic Sea ecosystem: a model study. Journal of Marine Systems 81(3), pp. 213-224. (2010-05).
[OMNY]	**Omstedt, A., and Nyberg. L.** Response of Baltic Sea ice to seasonal, interannual forcing and climate change. Tellus 48(5), pp. 644-662. (1996-10).
[POAC11]	**Kärnä, T., Masterson, D. M.** Data for Crushing Formula. Proceedings of the 21st International Conference on Port and Ocean Engineering under Arctic Conditions, POAC11-064. (2011-07). Link: https://trid.trb.org/view/1335444
[POAC3]	**Gravesen, H., et. al.** Ice Forces to Wind Turbine Foundations in Denmark. Proceeding of the 17th International Conference on Port and Ocean Engineering under Arctic Conditions, POAC ’03. (2003-06-19).
[POAC9]	**Gravesen, H., Kärnä, T.** Ice Loads for Offshore Wind Turbines in Southern Baltic Sea. Proceedings of the 20th International Conference on Port and Ocean Engineering under Arctic Conditions, POAC09-3. (2009-07-09).
[SMHIAT]	**Sveriges meteorologiska och hydrologiska institut** Collection of archived historical sea ice charts and report. Link: https://www.smhi.se/oceanografi/istjanst/havsis_en.php

[SMHIOCE] **Sveriges meteorologiska och hydrologiska institut**
Oceanographic measurements from the Swedish meteorological institute. Downloaded by C2Wind using the data portal for download of oceanographic observation data found at:
Link:https://www.smhi.se/data/oceanografi/ladda-ner-oceanografiska-observationer#param=seatemperature,stations=core

[SPARRE] **Sparre, A.**
The Climate of Denmark, Summary of observations from light vessels III
Danish Meteorological Institute, Climatologocal Papers No. 10
Sea temperature
ISBN: 87 7478 215 0
(1984).

[STEFAN] **Stefan, J.**
Über die Theorie der Eisbildung, insbesondere über die Eisbildung im Polarmeere.
Ann. Phys.
(1891).

[VICE] **Christensen, F. T. and Graversen, H.**
Determination of extreme ice forces, Lecture notes.
(2003-02-27).

[WA] **EMD international A/S**
Kattegat – Site Wind Conditions Assessment.
Doc. No.: 241011_23406_B_KB

Appendices

This page is intentional left blank.

Appendix A. Sea ice observations

This appendix contains a reproduction of the recorded ice observation data in [ISBES] for a selected number of ice observation stations. A short guide on how to read the data is included in Table A-1 and Table A-2 is given next.

Table A-1 contains the recorded ice observations from [ISBES] for the winters from 1960 to 1983 in accordance with the Danish Sea ice code. Each of the rows contains observations from one winter (1960-1961 to 1982-1983). In addition, the '*Kuldesum*', a measure of the severity of the winter is stated for each winter. Each observation station takes up 13 columns, and the station name is stated at the top. Of the 13 columns, the first 9 columns contain the number of recorded days of a certain ice type in accordance with the Danish Sea ice code. The observation categories from *1, 2 … 8, 9* are detailed as part of Table 5-3. The 10th column is unused whereas the 11th column contains the maximum recorded ice thickness in cm for the winter – this is however unused in the present study and rarely noted in [ISBES]. The final two columns represent the first- and last dates of ice observations.

Table A-2 contains a reproduction of the sea ice observations recorded by use of the Baltic Sea ice code from [ISBES] for the winters from 1984 to 2023. Each group of 4 rows contain ice observations from one winter (1983-1984 to 2022-2023). Within each group of 4 rows, each individual row contains the number of days where ice is observed within a specific subcategory of the '*A', 'S','T',* or '*K'* category of the Baltic Sea ice code. As for the winters before 1983, the '*Kuldesum'* index is indicated for each winter.

A total of six winters are marked in light blue to indicate that the yearly sea ice observation records from [ISBES] are missing for these years. From the [ISBES] reports for wintes after 2001-2002, the severity of the missing winters can be found as indicated by the '*Kuldesum'* value. For the six missing winters the '*Kuldesum'* ranges from 11.6 to 80.8, indicating mild winters with no contribution to the results of this study. For reference, the minimum *Kuldesum* value of the winters contributing to the evaluated sheet ice of this study is 163.0. Thus, it is concluded that the six missing winters will not affect the conclusions of the present study.

Each observation station takes up 13 columns, and the station name is stated at the top. Of the 13 columns, the first 11 columns contain the number of recorded days of a certain ice type in accordance with the Baltic Sea ice code. The observation categories from *0, 1, 2 … 9, X* are detailed as part of Table 5-4. The 12th and 13th columns represent the first- and last dates of ice observations.

		Kuldesum	Fornæs Fyr (Kattegat)												
Winter		°C Days	# Days of ice type										Max	First ice observation	Last ice observation
Start year	End year		1	2	3	4	5	6	7	8	9	-	h		
1960	1961	23.9													
1961	1962	78.9													
1962	1963	300.3	1		26	6		13	2	15				11/01/1963	26/03/1963
1963	1964	82.9													
1964	1965	67.9													
1965	1966	163.0	3		5			5		4	1			19/01/1966	25/02/1966
1966	1967	31.5													
1967	1968	94.1													
1968	1969	116.2	1											17/02/1969	17/02/1969
1969	1970	208.4	2		10	2		4	1	1				20/01/1970	01/03/1970
1970	1971	83.9													
1971	1972	66.6													
1972	1973	10.6													
1973	1974	27.8													
1974	1975	7.2													
1975	1976	75.0													
1976	1977	62.4													
1977	1978	70.3	2											19/02/1978	20/02/1978
1978	1979	215.2	2		11	5		12	1	2				03/01/1979	02/03/1979
1979	1980	97.7													
1980	1981	75.6													
1981	1982	218.7			19			3					50	07/01/1982	28/01/1982
1982	1983	23.9													

		Hundested - Farvandet mod Nord (Isefjorden)												
Winter		# Days of ice type										Max	First ice observation	Last ice observation
Start year	End year	1	2	3	4	5	6	7	8	9	-	h		
1960	1961													
1961	1962													
1962	1963			13				2	50				10/01/1963	15/03/1963
1963	1964													
1964	1965			4									09/03/1965	18/03/1965
1965	1966	4		10			3						25/01/1966	01/03/1966
1966	1967													
1967	1968	1		1	2		1						13/01/1968	19/01/1968
1968	1969	2											04/03/1969	05/03/1969
1969	1970	5		4			6						08/01/1970	18/02/1970
1970	1971	3											03/01/1971	06/03/1971
1971	1972	1		2									19/01/1972	09/02/1972
1972	1973													
1973	1974													
1974	1975													
1975	1976	2										1	04/03/1976	18/03/1976
1976	1977													
1977	1978	1											19/02/1978	19/02/1978
1978	1979	9		17	2		4						07/01/1979	09/03/1979
1979	1980	1		1									04/02/1980	19/02/1980
1980	1981													
1981	1982	1		25			8		7			30	17/12/1981	06/03/1982
1982	1983													

		Anholt fyr - Farvandet mod SØ (Kattegat) (Anholt - Farvandet mod vest 1964 + 1965 + 1996 + 2010)												
Winter		# Days of ice type										Max	First ice observation	Last ice observation
Start year	End year	1	2	3	4	5	6	7	8	9	-	h		
1960	1961													
1961	1962													
1962	1963	6	4	19		21	3	18	1				07/01/1963	22/03/1963
1963	1964													
1964	1965	2											06/03/1965	07/03/1965
1965	1966	3		3			5	3	5				08/02/1966	26/02/1966
1966	1967													
1967	1968													
1968	1969	4	5	1									16/02/1969	25/02/1969
1969	1970	9	6	9	2	3	2	4	1				08/01/1970	28/02/1970
1970	1971													
1971	1972	1											02/02/1972	02/02/1972
1972	1973													
1973	1974													
1974	1975													
1975	1976													
1976	1977													
1977	1978	1											19/02/1978	20/02/1978
1978	1979	15	2	7	1		2						04/01/1979	04/03/1979
1979	1980			2								5	09/02/1980	10/02/1980
1980	1981													
1981	1982	6	6	27			3		2			30	06/01/1982	02/03/1982
1982	1983													

		Nakkehoved Fyr (Øresund)												
Winter		# Days of ice type										Max	First ice observation	Last ice observation
Start year	End year	1	2	3	4	5	6	7	8	9	-	h		
1960	1961	2											26/01/1961	27/01/1961
1961	1962													
1962	1963	6	7	19	1	3	6		27	1			07/01/1963	05/04/1963
1963	1964													
1964	1965	1	1	5		1	1						02/03/1965	12/03/1965
1965	1966	1	1	4			2	2	2				08/02/1966	22/02/1966
1966	1967													
1967	1968													
1968	1969													
1969	1970	3	1	16	4	2	5						29/01/1970	25/03/1970
1970	1971													
1971	1972													
1972	1973													
1973	1974													
1974	1975													
1975	1976													
1976	1977													
1977	1978	2											19/02/1978	23/02/1978
1978	1979	3	3	17	1		2						10/01/1979	28/02/1979
1979	1980													
1980	1981													
1981	1982	2	2	25		1	15					30	08/01/1982	28/02/1982
1982	1983													

		Sletterhage, farvand mod syd og øst (Kattegat)												
Winter		# Days of ice type										Max	First ice observation	Last ice observation
Start year	End year	1	2	3	4	5	6	7	8	9	-	h		
1960	1961													
1961	1962													
1962	1963	6	3	26			19	2	18	5			08/01/1963	01/04/1963
1963	1964													
1964	1965													
1965	1966	7		9	2		6	4					25/01/1966	05/03/1966
1966	1967													
1967	1968													
1968	1969													
1969	1970	1		19		1	2		6				29/01/1970	06/03/1970
1970	1971													
1971	1972			7	1								30/01/1972	11/02/1972
1972	1973													
1973	1974													
1974	1975													
1975	1976				1								16/02/1976	25/02/1976
1976	1977													
1977	1978	1			1		1						19/02/1978	21/02/1978
1978	1979	2		10	4	1	15	2	9	2			03/01/1979	07/03/1979
1979	1980													
1980	1981													
1981	1982	4		20				1				50	28/12/1981	28/01/1982
1982	1983													

Table A-1: Sea ice observations from the observation stations "Fornæs Fyr", "Hundested", "Anholt Fyr", "Nakkehoved Fyr", and "Sletterhage" for the winters of 1960 to 1983.

			Kuldesum	Fornæs Fyr (Kattegat)												
Baltic code	Winter		°C Days	# Days of ice type											First ice observation	Last ice observation
	Start year	End year		0	1	2	3	4	5	6	7	8	9	X		
A	1983	1984	48.8													
S																
T																
K																
A	1984	1985	273.4	3	12	9	7	5		2					10/01/1985	12/03/1985
S				3	4	5	23							3		
T				18	7	3	2	3	2					3		
K				10	21	5	3									
A	1985	1986	193.3		12	3	11	6	2	2	5				09/02/1986	21/03/1986
S				3	8	3	19	8								
T				24	4	2			4	6	1					
K				9	16	11	5									
A	1986	1987	266.3	21	3	10	5	6	11	3				9	12/01/1987	20/03/1987
S				1		5	30					2		30		
T				10	2	3	1	9	13					30		
K				22	12	25								9		
A	1987	1988	11.0													
S																
T																
K																
A	1988	1989	8.0													
S																
T																
K																
A	1989	1990	10.2													
S																
T																
K																
A	1990	1991	37.9													
S																
T																
K																
A	1991	1992	12.7													
S																
T																
K																
A	1992	1993	32.7													
S																
T																
K																
A	1993	1994	51.4													
S																
T																
K																
A	1994	1995	16.2													
S																
T																
K																
A	1995	1996	183.2	6	5	4	1		1						07/02/1996	25/02/1996
S				11	5											
T				8	8					1						
K				12	1	4										

			Hundested - Farvandet mod Nord (Isefjorden)												
Baltic code	Winter		# Days of ice type											First ice observation	Last ice observation
	Start year	End year	0	1	2	3	4	5	6	7	8	9	X		
A	1983	1984													
S															
T															
K															
A	1984	1985	14	11	14	1	1	1	4	4		7		09/01/1985	06/03/1985
S			10	9	6	7	11						14		
T			21	6			4	11	1				14		
K			30	11	1	15									
A	1985	1986	6	8	7	2	1	1	14					08/02/1986	18/03/1986
S			11	1	9	12							6		
T			11	7			7	7					7		
K			16	9	6	8									
A	1986	1987	5	23	16	3	10	10	7					09/01/1987	23/03/1987
S			18	4	16	20	16								
T			39	11	1	1	9	11		2					
K			21	18	12	15		6		2					
A	1987	1988													
S															
T															
K															
A	1988	1989													
S															
T															
K															
A	1989	1990													
S															
T															
K															
A	1990	1991													
S															
T															
K															
A	1991	1992													
S															
T															
K															
A	1992	1993													
S															
T															
K															
A	1993	1994													
S															
T															
K															
A	1994	1995													
S															
T															
K															
A	1995	1996	2	3	2									02/01/1996	07/02/1996
S			4	3											
T			5	2											
K			5	2											

			Anholt fyr - Farvandet mod SØ (Kattegat) (Anholt - Farvandet mod vest 1964 + 1965 + 1996 + 2010)												
Baltic code	Winter		# Days of ice type											First ice observation	Last ice observation
	Start year	End year	0	1	2	3	4	5	6	7	8	9	X		
A	1983	1984													
S															
T															
K															
A	1984	1985	12	3	3	2	6	11			6		16	09/01/1985	08/03/1985
S			5	8	6	12							28		
T			19	4	2		6						28		
K			15	12	10	6							16		
A	1985	1986		2	7	3	3	4	10					08/02/1986	08/03/1986
S			5	6	3	15									
T			5	7	4	3	2	8							
K			9	9	2	9									
A	1986	1987	25	6		8	6	19	6					15/01/1987	25/03/1987
S			5		1	32							32		
T			7	9	4	13			12				25		
K			30	5	4	31									
A	1987	1988													
S															
T															
K															
A	1988	1989													
S															
T															
K															
A	1989	1990													
S															
T															
K															
A	1990	1991													
S															
T															
K															
A	1991	1992													
S															
T															
K															
A	1992	1993													
S															
T															
K															
A	1993	1994													
S															
T															
K															
A	1994	1995													
S															
T															
K															
A	1995	1996		5	5	1	1							06/02/1996	18/02/1996
S			5	4	3					1					
T			7	4	1										
K			7	5											

			Nakkehoved Fyr (Øresund)												
Baltic code	Winter		# Days of ice type											First ice observation	Last ice observation
	Start year	End year	0	1	2	3	4	5	6	7	8	9	X		
A	1983	1984													
S															
T															
K															
A	1984	1985	1	31	7	11	1	1	16	8				07/01/1985	23/03/1985
S			1		53	21							1		
T			15	38	7		14		1				1		
K			27	31	4	14									
A	1985	1986		10	1	7	6	14					3	09/02/1986	21/03/1986
S			2	15	21								3		
T			9	29									3		
K			2	23	13								3		
A	1986	1987	2	2	6	7	4	7	18	18			9	12/01/1987	26/03/1987
S			2	2	9	49				1			10		
T			2	8	29	22	2						10		
K			3	4	19	38							9		
A	1987	1988													
S															
T															
K															
A	1988	1989													
S															
T															
K															
A	1989	1990													
S															
T															
K															
A	1990	1991													
S															
T															
K															
A	1991	1992													
S															
T															
K															
A	1992	1993													
S															
T															
K															
A	1993	1994													
S															
T															
K															
A	1994	1995													
S															
T															
K															
A	1995	1996		12	1	4								29/01/1996	15/02/1996
S				17											
T			6	11											
K			17												

			Sletterhage, farvand mod syd og øst (Kattegat)												
Baltic code	Winter		# Days of ice type											First ice observation	Last ice observation
	Start year	End year	0	1	2	3	4	5	6	7	8	9	X		
A	1983	1984													
S															
T															
K															
A	1984	1985	9	13	12	7	9	2					10	18/01/1985	20/03/1985
S			6	4	17	15					1		19		
T			27	12	2			4					17		
K			31	12	4								15		
A	1985	1986	58	4	11	5	8	4						16/12/1985	15/03/1986
S			3	15	7	7							58		
T			8	22	2								58		
K			61	13	12	4									
A	1986	1987	28	4	10	5	7	3	12				5	12/01/1987	26/03/1987
S			3	8	9	18	3						33		
T			7	10	24								33		
K			33	10	18	8							5		
A	1987	1988													
S															
T															
K															
A	1988	1989													
S															
T															
K															
A	1989	1990													
S															
T															
K															
A	1990	1991													
S															
T															
K															
A	1991	1992													
S															
T															
K															
A	1992	1993													
S															
T															
K															
A	1993	1994													
S															
T															
K															
A	1994	1995													
S															
T															
K															
A	1995	1996	11	8	3	2	2		2	1			1	30/01/1996	29/02/1996
S			2	5	4	5					2		12		
T			8	4	2		1	3					12		
K			17	8	4								1		

A	1996	1997	80.8																																																																
S																																																																	
T																																																																	
K																																																																	
A	1997	1998	21.0																																																																
S																																																																	
T																																																																	
K																																																																	
A	1998	1999	55.1																																																																
S																																																																	
T																																																																	
K																																																																	
A	1999	2000	11.6																																																																
S																																																																	
T																																																																	
K																																																																	
A	2000	2001	52.8																																																																
S																																																																	
T																																																																	
K																																																																	
A	2001	2002	26.6																																																																
S																																																																	
T																																																																	
K																																																																	
A	2002	2003	105.0																																				1									22/02/2003	22/02/2003													
S																																						1																									
T																																					1																										
K																																					1																										
A	2003	2004	39.8																																																																
S																																																																	
T																																																																	
K																																																																	
A	2004	2005	38.4																																																																
S																																																																	
T																																																																	
K																																																																	
A	2005	2006	72.2																																		1		1									14/03/2006	15/03/2006													
S																																						1									1														
T																																						1									1														
K																																					1	1																									
A	2006	2007	9.7																																																																
S																																																																	
T																																																																	
K																																																																	
A	2007	2008	6.8																																																																
S																																																																	
T																																																																	
K																																																																	
A	2008	2009	21.5																																																																
S																																																																	
T																																																																	
K																																																																	
A	2009	2010	162.8														5	14	13	2	3							06/01/2010	14/02/2010	3		10				12	3	3			21/01/2010	21/03/2010	5	2	3	2								26/01/2010	16/02/2010													
S																	32										5			8	4	15			1					3			2	4	1								5															
T																	32										5			3	7			18						3			3	4									5															
K																	37													6	9	1	15										7	5																							
A	2010	2011	151.3														15	62	14	1								17/12/2010	25/03/2011														7			4	1							29/12/2010	03/02/2011													
S																	74	8									10																4	3	1								4															
T																	4										88																4	4									4															
K																	76	12																									7	4	1																						
A	2011	2012	68.6															14	4	1								06/02/2012	24/02/2012														5	7	2	1	1		1					06/02/2012	24/02/2012													
S																	16	2	1																								5	8	3								1															
T																	14	4	1																								10	5		1							1															
K																	11	5	3																								5	9	3																						
A	2012	2013	106.0																																																																
S																																																																	
T																																																																	
K																																																																	
A	2013	2014	26.0																																																																
S																																																																	
T																																																																	
K																																																																	
A	2014	2015	10.4																																																																
S																																																																	
T																																																																	
K																																																																	
A	2015	2016	32.9																																																																
S																																																																	
T																																																																	
K																																																																	
A	2016	2017	42.7																																																																
S																																																																	
T																																																																	
K																																																																	
A	2017	2018	54.9																																																																
S																																																																	
T																																																																	
K																																																																	
A	2018	2019	8.3																																																																

S			
T			
K			
A	2019	2020	0.4
S			
T			
K			
A	2020	2021	45.3
S			
T			
K			
A	2021	2022	5.7
S			
T			
K			
A	2022	2023	13.8
S			
T			
K			

Table A-2: Sea ice observations from the observation stations "Fornæs Fyr", "Hundested", "Anholt Fyr", "Nakkehoved Fyr", and "Sletterhage" for the winters from 1983 to 2023.

Appendix B. Thermal ice growth model

This appendix describes the method used for deriving the thermal growth of ice. The growth rate of ice as a function of time is described in Eq. 1 in [STEFAN] as:

$$\frac{dh}{dt} = \frac{\kappa(T_\mathrm{f} - T_\mathrm{a})}{\rho_\mathrm{ice} L_\mathrm{f} h} \qquad \text{Eq. B-1}$$

Where:

h	Ice thickness.
t	Time.
κ	Thermal conductivity of ice.
T_f	Freezing temperature of water with the salinity at the site.
T_a	Surface temperature of air/ice boundary.
ρ_ice	Density of ice.
L_f	Latent heat of melting for ice.

For Eq. B-1 to be valid, the following is assumed:

1. Thermal inertia is ignored.
2. Penetration of solar radiation is ignored.
3. No heat flux from water to ice.
4. No isolating effect from a snow cover is included.
5. No effect from currents included.

Besides the points above, it is assumed that the surface temperature, T_a, is a known function of time. For this evaluation, it is assumed that T_a equals the air temperature. By separation of variables, Eq. B-1 can be written as:

$$h\,dh = \frac{\kappa(T_\mathrm{f} - T_\mathrm{a})}{\rho_\mathrm{ice} L_\mathrm{f}} dt \qquad \text{Eq. B-2}$$

Integrating Eq. B-2 from time t_1 to t_2 yields:

$$\int_{h_1}^{h_2} h\,dh = \frac{\kappa}{\rho_\mathrm{ice} L_\mathrm{f}} \int_{t_1}^{t_2} (T_\mathrm{f} - T_\mathrm{a})\,dt \qquad \text{Eq. B-3}$$

Where:

h_1	Ice thickness at time t_1.
h_2	Ice thickness at time t_2.

Solving for h_2:

$$h_2 = \sqrt{h_1^2 + \frac{2\kappa}{\rho_\mathrm{ice} L_\mathrm{f}} S_\mathrm{f}} \qquad \text{Eq. B-4}$$

where S_f is the cumulative freezing degree days (measured in units of temperature · time, e.g. in °C · days or °C · s, or if SI-units are used, in K · s) defined by the integral in Eq. B-3 as:

$$S_\mathrm{f} = \int_{t_1}^{t_2} (T_\mathrm{f} - T_\mathrm{a})\, dt \tag*{Eq. B-5}$$

where it is assumed that $T_\mathrm{f} > T_a$, i.e. the air temperature must be smaller than the freezing temperature for ice.

Given a time series of temperature, Eq. B-5 is solved numerically by:

$$\Delta S_\mathrm{f} = \left(T_\mathrm{f} - \frac{T_\mathrm{a1}}{2} - \frac{T_\mathrm{a2}}{2}\right)\Delta t \tag*{Eq. B-6}$$

Where:

T_f	Freezing temperature of water with the salinity at the site.
T_a1	Air temperature at time t_1.
T_a2	Air temperature at time t_2.
Δt	Time step $t_2 - t_1$.

When $T_\mathrm{a} > T_\mathrm{f}$, the ice is not growing, but will instead start to melt. This is not included in the thermal ice growth model shown in Eq. B-4 where $h_2 = h_1$ when $T_\mathrm{a} < T_\mathrm{f}$. This means that no melting is included in the accumulated ice thickness.

Appendix C. Thermal ice growth results

Sheet ice thickness, h, and ice ridge consolidated layer thickness, h_c.

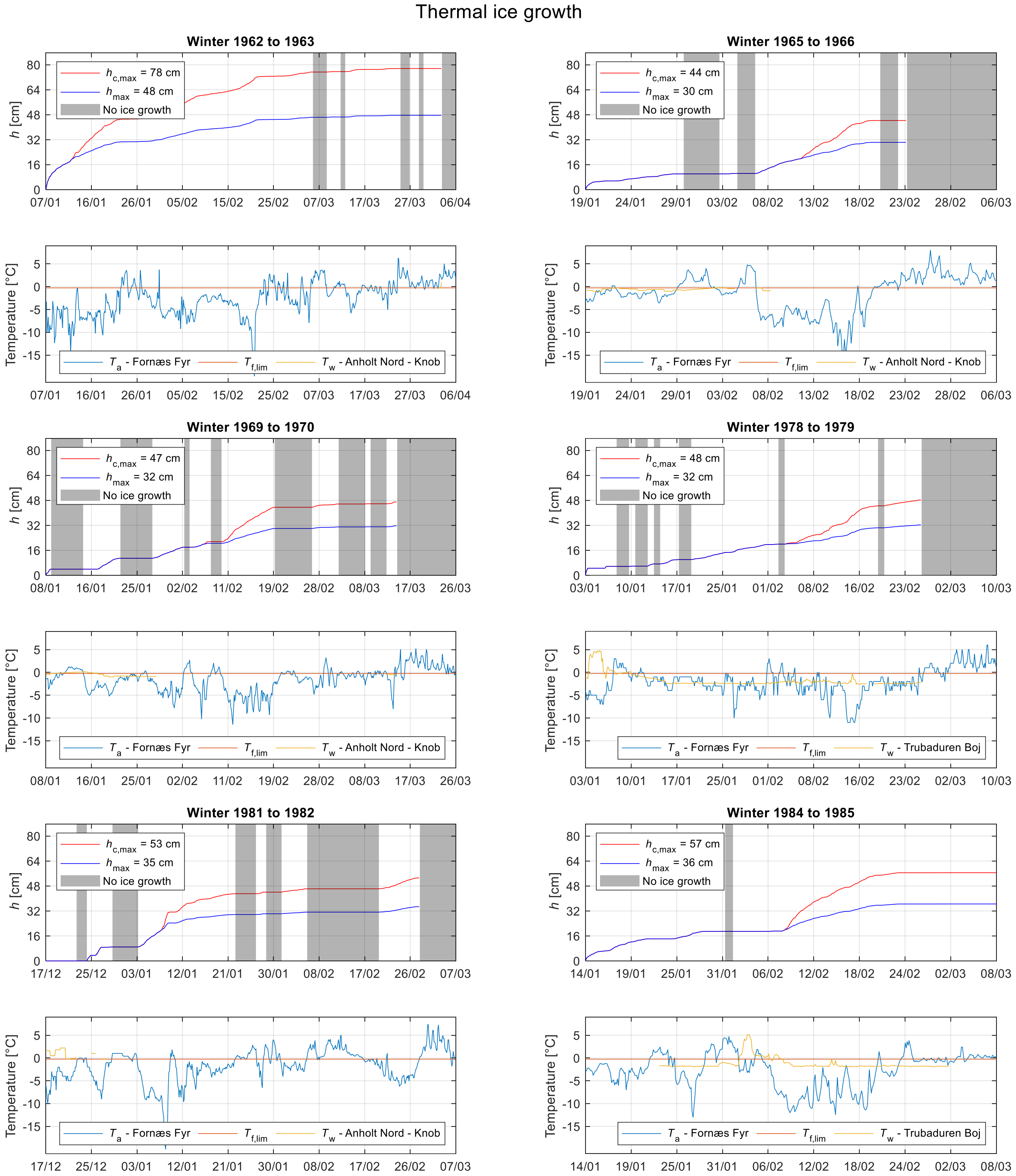

Figure C-1: Upper half of each pair of plots: Sheet ice thickness (dark blue curve), h, and consolidated layer thickness (red curve), h_c, as a function of time for winters 1962/1963 to 1984/1985. The bottom half of each pair of plots: The temperature curves shown in light blue are air temperatures, while the red lines are the freezing temperatures of the seawater at the site used in the modelling. SST temperatures are, when applied, shown by the yellow curve.

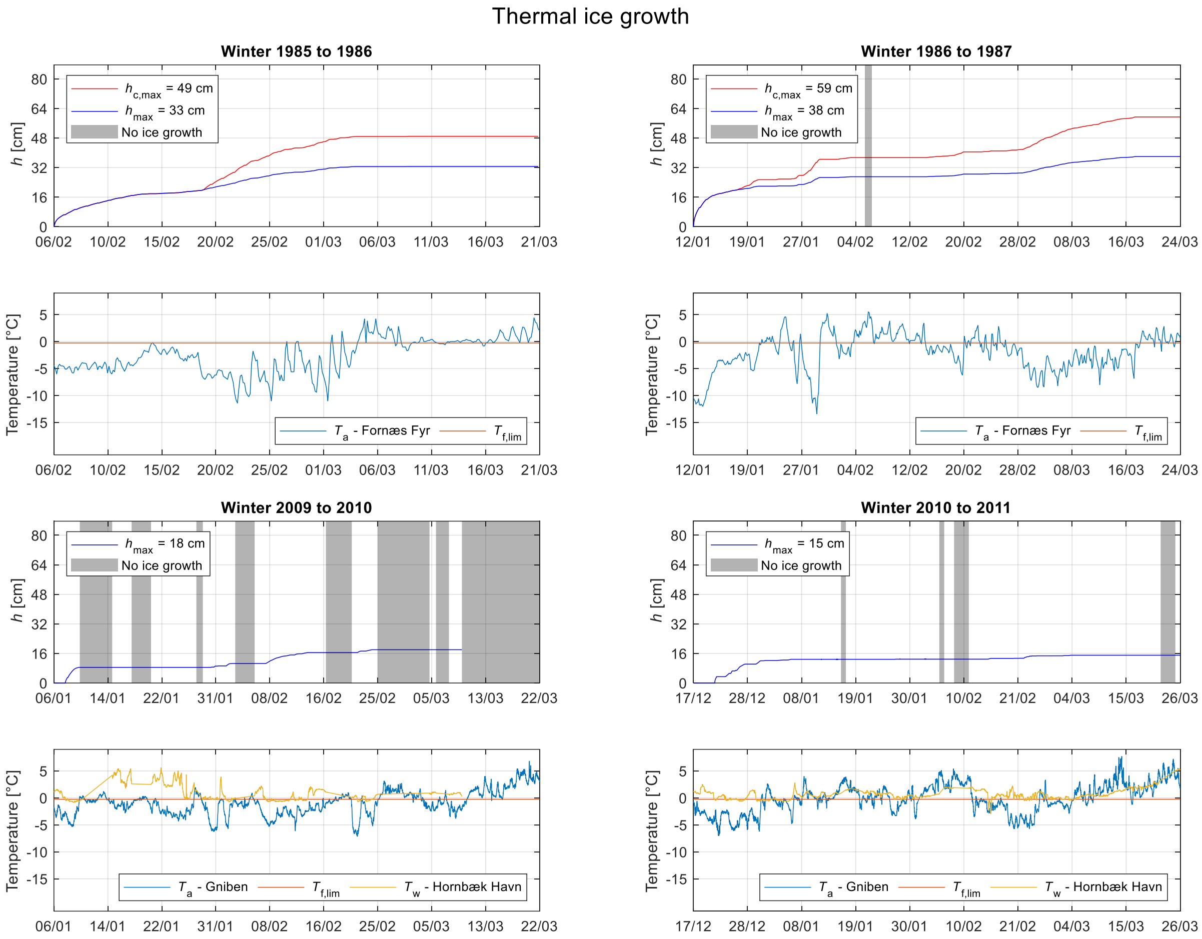

Figure C-2: Upper half of each pair of plots: Sheet ice thickness (dark blue curve), h, and consolidated layer thickness (red curve), h_c, as a function of time for winters 1985/1986 to 2010/2011. The bottom half of each pair of plots: The temperature curves shown in light blue are air temperatures, while the red lines are the freezing temperatures of the seawater at the site used in the modelling. SST temperatures are, when applied, shown by the yellow curve.

Appendix D. Supplementing ice atlasses

For the winters of 1984/1985, 1985/1986, and 1986/1987 ice atlases from [SMHIAT] are used to predict a more accurate date for the first- and last date of observed sea ice at the site to reduce the conservatism of the calculated sheet ice thickness. It is noted that the first date of observed sea ice is conservatively selected as the date of the last recording of ice-free waters before sea ice is recorded at the site. The last date of observed sea ice is conservatively selected as the date of the first recording of ice-free waters following the last recording of sea ice at the site.

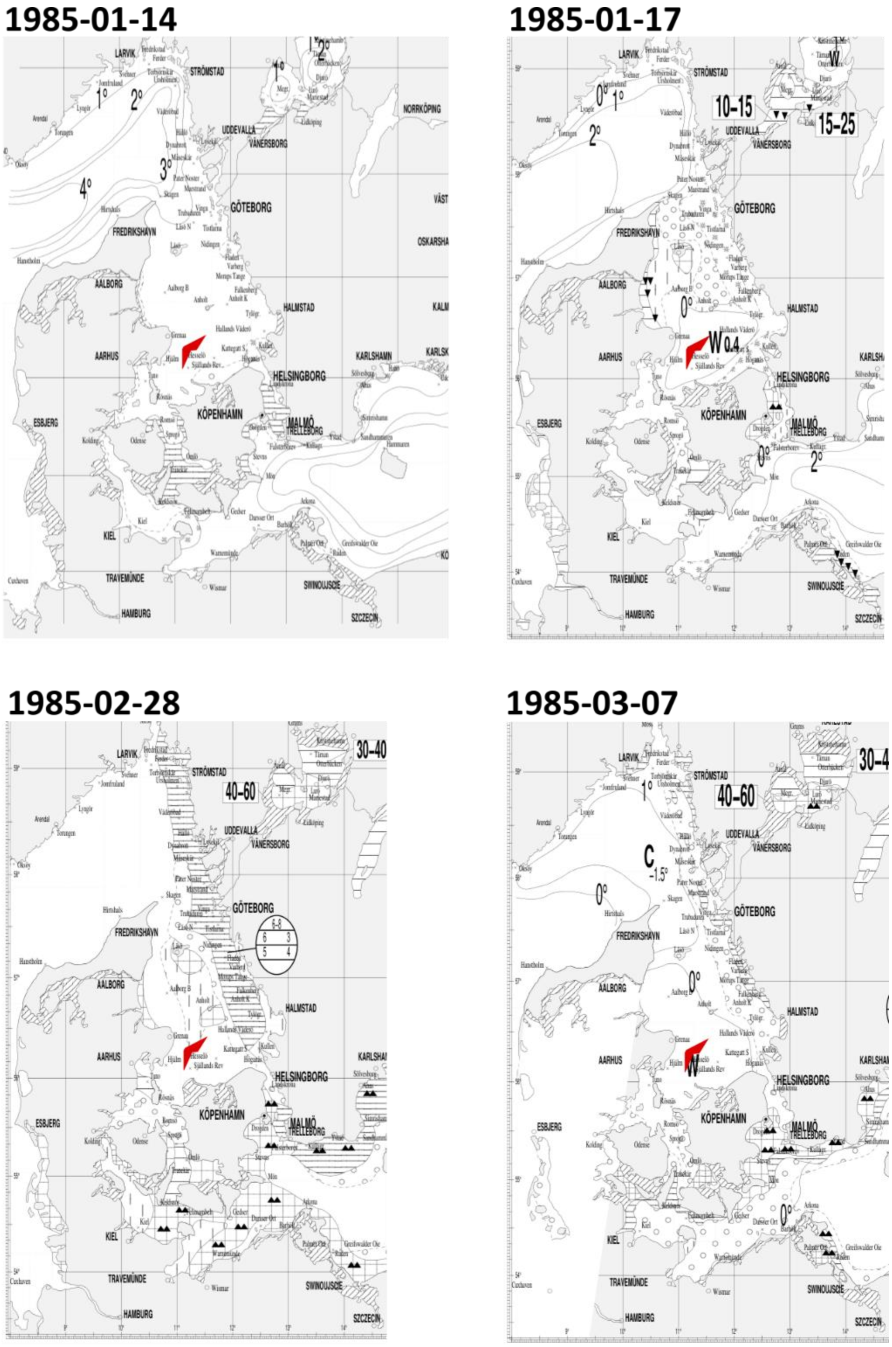

1985-01-14

1985-01-17

1985-02-28

1985-03-07

Figure D-1: Sea ice atlases of [SMHIAT] for the winter of 1984/1985. **Upper:** Selected first date of sea ice observation, 1985-01-14 and the following recording showing sea ice near the site. **Lower:** Last recording of sea ice at the site and the following observation showing ice-free waters selected as the last date of sea ice observation, 1985-03-07 at the evaluated site.

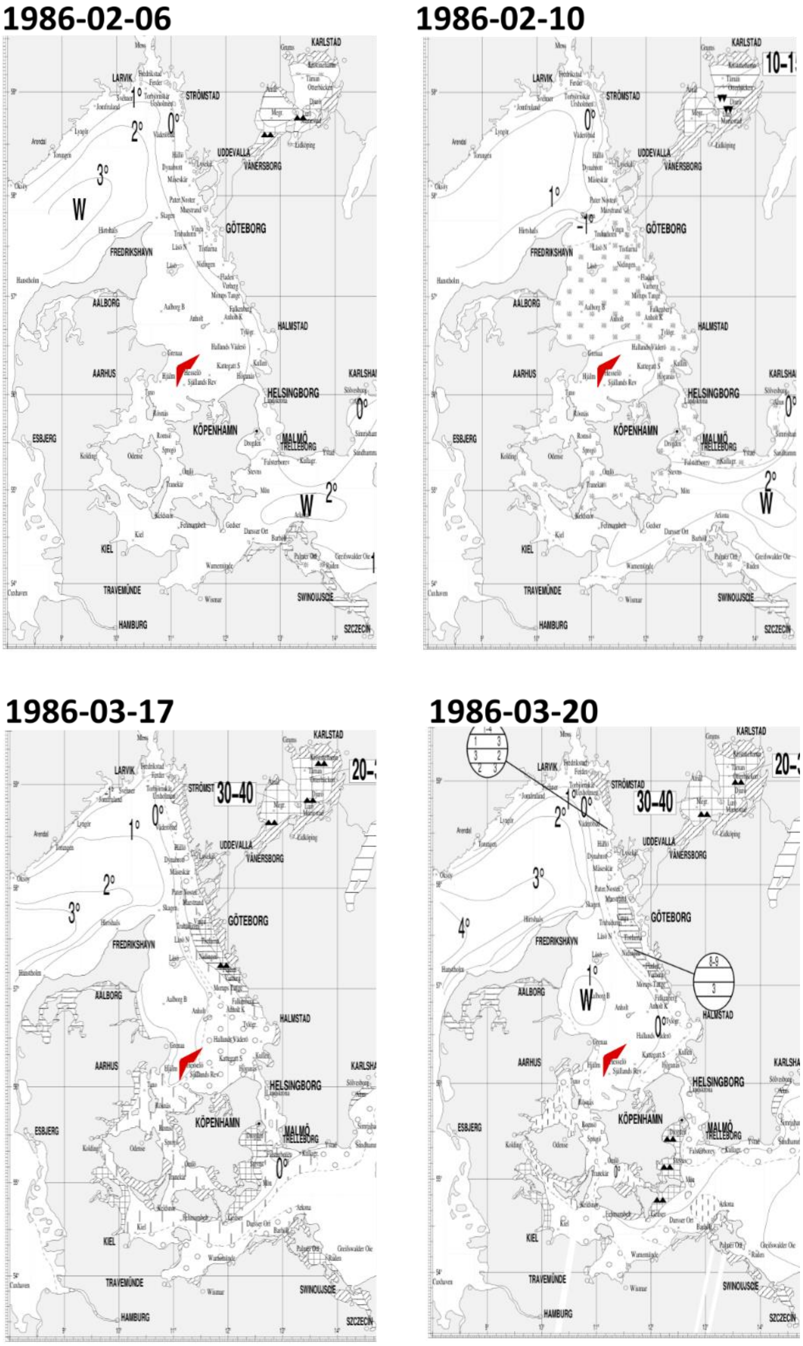

Figure D-2: Sea ice atlases of [SMHIAT] for the winter of 1985/1986. **Upper:** Selected first date of sea ice observation, 1986-02-06 and the following recording showing sea ice near the site. **Lower:** Last recording of sea ice at the site and the following observation showing ice-free waters selected as the last date of sea ice observation, 1986-03-20 at the evaluated site.

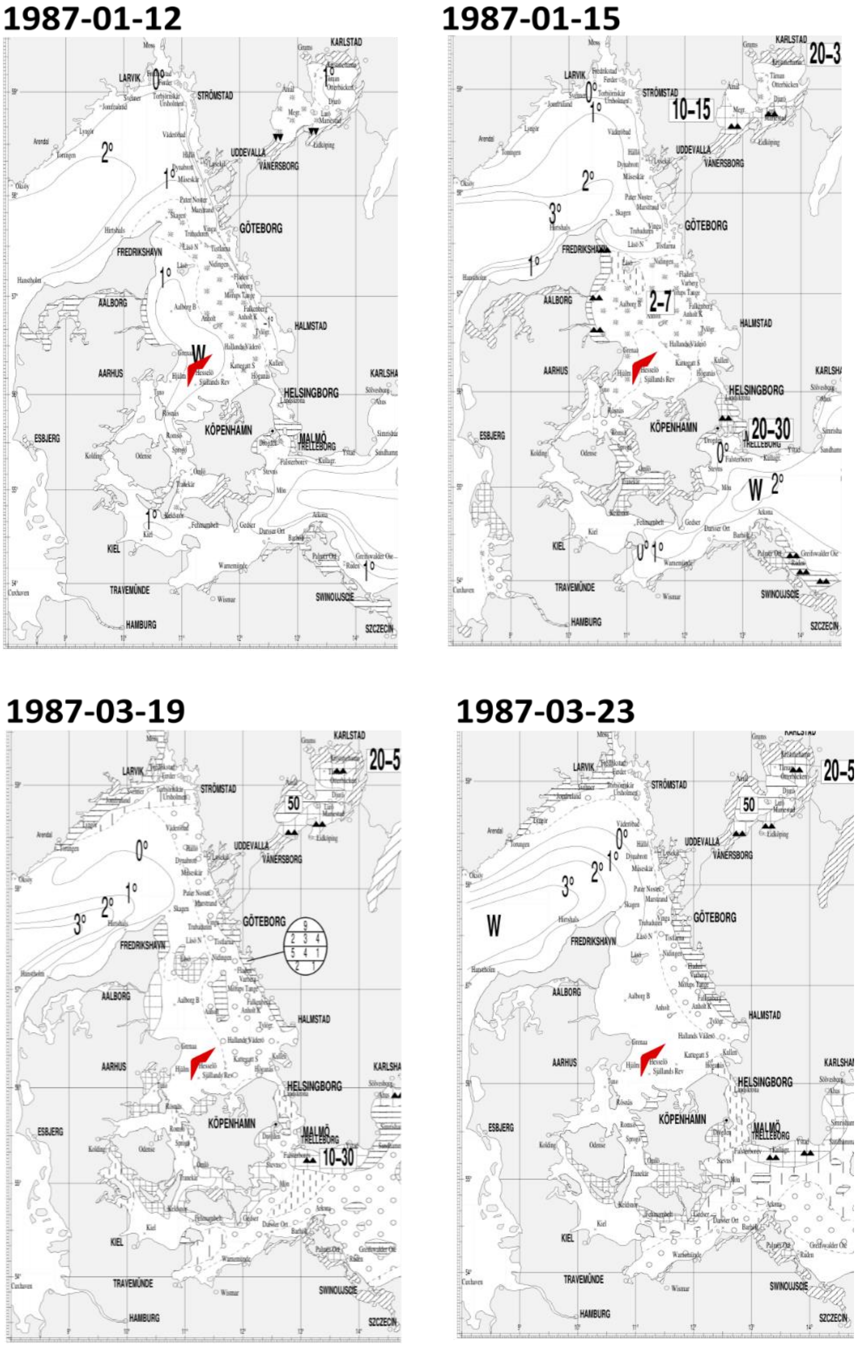

1987-01-12

1987-01-15

1987-03-19

1987-03-23

Figure D-3: Sea ice atlases of [SMHIAT] for the winter of 1986/1987. **Upper:** Selected first date of sea ice observation, 1987-01-12 and the following recording showing sea ice near the site. **Lower:** Last recording of sea ice at the site and the following observation showing ice-free waters selected as the last date of sea ice observation, 1987-03-23 at the evaluated site.